

Dissertation  
submitted to the  
Combined Faculties of the Natural Sciences and Mathematics  
of the Ruperto-Carola-University of Heidelberg, Germany  
for the degree of  
Doctor of Natural Sciences

Put forward by

*Florian Führer*

born in *Aachen*

Oral examination: *October 27, 2016*



# **Non-linear structure formation in standard and non-standard cosmology**

Referees: *Christof Wetterich*  
*Luca Amendola*



## Nichtlineare Strukturentstehung in Standard- und Nichtstandardkosmologien

Diese Arbeit beinhaltet Forschung über zwei Themen aus dem Bereich der kosmologischen Strukturentstehung auf großen Skalen. Ein Teil untersucht die Bildung von Neutrino-Klumpen in "Growing Neutrino Quintessence" (GNQ), einem Modell für die Dunkle Energie. Hierfür werden N-body-Simulationen mit relativistischen Teilchen und nichtlinearen skalaren Feldgleichungen benötigt. Die Bildung von Klumpen wird von einer Kopplung zwischen den Neutrinos und einem skalarem Quintessenzfeld verursacht. Die Neutrino-Klumpen erzeugen Rückwirkungseffekte, die möglicherweise GNQ als Modell für die Dunkle Energie disqualifizieren. Wir untersuchen ob trotz der Rückwirkungseffekte eine realistische Kosmologie möglich ist. Für eine konstante Kopplung ist dies schwer zu realisieren, während wir für eine variierende Kopplung eine realistische Kosmologie finden. GNQ kann mithilfe von kosmologischen Beobachtungen über den Nachweis der Gravitationspotentiale der Klumpen getestet werden. Der andere Teil untersucht effektive Flüssigkeiten als Modelle für die gewöhnliche Strukturentstehung von Dunkler Materie. Diese Modelle zielen darauf ab Störungsmethoden zu verbessern, indem über kleine Skalen gemittelt wird und Informationen über die Nichtperturbative Dynamik auf kleinen Skalen aus Simulationen entnommen wird. Dabei garantiert eine Renormierungsprozedur, dass physikalische Größen unabhängig von der Mittelungsskala sind. Wir untersuchen die Konsistenz der Renormierungsprozedur mit der Galilei-Invarianz der Theorie.

## Non-linear structure formation in standard and non-standard cosmology

This thesis comprises research on two topics of cosmological non-linear structure formation. One part investigates the formation of neutrino lumps in the Dark Energy model Growing Neutrino Quintessence (GNQ). Therefore N-body simulations with relativistic particles and non-linear scalar field equations are required. The formation of lumps is caused by a coupling between the neutrinos and a scalar Quintessence field. The neutrino lumps induce backreaction effects, possibly invalidating GNQ as a Dark Energy model. We investigate if despite the backreaction effects a realistic cosmology is possible. For a constant coupling this is hard to realize, while we find a realistic cosmology for a varying coupling. GNQ can be tested with cosmology by detecting the gravitational potentials of the lumps. The other part investigates effective fluid models for ordinary structure formation of Dark Matter. These models aim at improving perturbative methods by averaging over small scales and taking the information on the non-perturbative dynamics on small scales from simulations. Thereby, a renormalization procedure ensures that physical quantities are independent of the arbitrary smoothing scale. We investigate consistency of the renormalization procedure with the Galilean Invariance of the theory.



The cumulative thesis is based on the following publications

1. *Nonlinear growing neutrino cosmology*  
Y. Ayaita , M. Baldi, F. Führer, E. Puchwein, C. Wetterich  
Phys.Rev. D93 (2016) no.6, 063511
2. *Backreaction in Growing Neutrino Quintessence*  
F. Führer, C. Wetterich  
Phys.Rev. D91 (2015) no.12, 123542
3. *Renormalizing a viscous fluid model for large scale structure formation*  
F. Führer, G. Rigopoulos  
JCAP 1602 (2016) no.02, 032

The author of the thesis is the principal author of the publications 2 and 3. He performed the analytical and numerical calculations (only publication 2 ). For the publication 1 he contributed to the numerical work.



# Contents

<b>1</b>	<b>Introduction</b>	<b>1</b>
1.1	The cosmic history . . . . .	2
1.1.1	The cosmic inventory . . . . .	4
1.1.2	Dark Energy . . . . .	7
1.1.3	Inhomogeneities . . . . .	8
1.1.4	Averaging and backreaction . . . . .	11
1.1.5	Inflation . . . . .	13
1.2	Cosmological structure formation . . . . .	16
1.3	The dynamics of gravitational collapse . . . . .	17
1.3.1	Perturbation theory . . . . .	18
1.3.2	Effective fluids as models for large-scale structure formation .	26
1.3.3	N-body simulations . . . . .	27
1.4	Growing Neutrino Quintessence . . . . .	32
1.4.1	The Cosmological Constant problem . . . . .	32
1.4.2	(Growing Neutrino) Quintessence . . . . .	34
1.4.3	Structure formation and backreaction in Growing Neutrino Quintessence . . . . .	36
<b>2</b>	<b>Nonlinear growing neutrino cosmology</b>	<b>39</b>
<b>3</b>	<b>Backreaction in Growing Neutrino Quintessence</b>	<b>55</b>
<b>4</b>	<b>Renormalizing a viscous fluid model for large-scale structure formation</b>	<b>67</b>
<b>5</b>	<b>Summary, discussion and outlook</b>	<b>91</b>
5.1	Growing Neutrino Quintessence . . . . .	91
5.2	Effective fluids in large-scale structure formation . . . . .	96
	<b>Bibliography</b>	<b>99</b>



# Introduction

When talking about cosmology one usually talks about the expansion history of the universe, about its composition, and asks questions like: How much Dark Matter (DM) is there? And how much Dark Energy (DE)? All this refers to the overall cosmology, or as cosmologists say to the homogeneous background cosmology. However, to learn about the background cosmology observations of fluctuations and structures are crucial. Primarily, of course, the small temperature fluctuations in the cosmic microwave background (CMB), as first observed by the COBE satellite [1], but also the large-scale structure (LSS), i.e. the matter distribution in the universe, yields valuable information about the cosmic history. While the small temperature fluctuations in the CMB can be described by (simplified) linear equations, describing structure formation via gravitational collapse requires to solve non-linear equations. Needless to say, this is much more difficult. During the early stages, i.e. at early times and on large scales, one can use perturbation theory to calculate corrections to the linear dynamics, but to follow the formation of structures also on small scales one has to use simulations. From simulations of structure formation a lot of knowledge about the process could be gathered: DM virializes and forms gravitational bound structures, so called halos. Within halos a sub-structure with sub-halos exist, in which galaxies can form. All this happens hierarchically, i.e. small scales collapse first and the first halos are formed, these halos merge to form larger halos.

Although the technology evolved, simulations are still too slow to scan different cosmological models as required for a comparison with observational data. Suitable (semi-)analytical tools may allow to scan different cosmological models much faster. Effective fluid approaches to cosmological structure formation are one possibility, recently they attracted a lot of attention in form of the effective field theory of large-scale structure (EFToLSS) [2]. These hybrid approaches use insights into the dynamics of non-perturbative small scales obtained from simulations in order to improve achieve a higher accuracy of perturbative calculations on large scales and to extend their validity to smaller scales. In publication 3 we investigate the consistency of such models.

The publications 1 and 2 explore Growing Neutrino Quintessence (GNQ) as a possible Dark Energy (DE) model, i.e. as an explanation for the observed accelerated expansion of the universe. Due to a fifth attractive force between neutrinos, they cluster to form large structures, called lumps. In GNQ lumps can induce strong

backreaction effects on the cosmological background. Therefore, understanding structure formation in GNQ is not only important in view of future tests, but also to explore the viability as a DE model.

The outline for the thesis is as follows.

Section 1.1 sets the stage. Here the dynamics of a homogeneous and isotropic cosmos is reviewed and the notation is introduced. Furthermore, a brief overview over cosmic perturbation theory is given.

In section 1.2, we briefly review the dynamics of gravitational instability, responsible for the formation of the observed structures. We then describe the standard perturbative approach (SPT) and the numerical approach, via so called N-body simulations, to structure formation. Understanding the formation of neutrino lumps in GNQ only requires mild modifications to this picture.

In section 1.4, we describe the motivation for exploring alternative DE models. Furthermore, we describe the homogeneous limit of GNQ. We briefly discuss neutrino structures and how they differ from standard gravitational bound structures.

The sections 2, 3 and 4 contain the publications. Publication 1, “Nonlinear growing neutrino cosmology”, can be found in section 2. In Section 3 publication 2, “Backreaction in Growing Neutrino Quintessence” can be found. Publication 3, “Renormalizing a viscous fluid model for large scale structure formation”, can be found in section 4.

In section 5 we give a brief summary of the obtained results together with a conclusion and a discussion of possible future research directions.

## 1.1 The cosmic history

This section briefly reviews the cosmological standard model. The focus thereby lies on introducing the notation and concepts required to understand the rest of the thesis. The interested reader can find more details in text books on modern cosmology e.g. [3, 4, 5] or on General Relativity e.g. [6, 7].

Modern cosmology is built on two pillars: General Relativity (GR) as the theory of gravity and the homogeneity and isotropy of the universe. GR provides the mathematical framework, determining the space-time in which all matter in the universe lives. As a consequence of the weak equivalence principle is GR invariant under diffeomorphisms, i.e. invariant under arbitrary coordinate transformations.

The central quantity is the metric of the space-time  $g_{\mu\nu}$ . The metric is connected to the matter by the Einstein equation

$$G_{\mu\nu} + \Lambda g_{\mu\nu} = 8\pi G T_{\mu\nu}. \quad (1.1)$$

The two constants are the Gravitational constant  $G$  and the cosmological constant (CC)  $\Lambda$ . On the left hand side the Einstein tensor is defined as  $G_{\mu\nu} = R_{\mu\nu} - \frac{1}{2}g_{\mu\nu}R$ . The Ricci scalar  $R = R^\mu{}_\mu$  and the Ricci tensor  $R_{\mu\nu} = R^\lambda{}_{\mu\lambda\nu}$  are contractions of the Riemann curvature tensor  $R^\lambda{}_{\mu\nu\sigma} = \Gamma^\lambda{}_{\mu\sigma,\nu} - \Gamma^\lambda{}_{\mu\nu,\sigma} + \Gamma^\rho{}_{\mu\sigma}\Gamma^\lambda{}_{\rho\nu} - \Gamma^\rho{}_{\mu\nu}\Gamma^\lambda{}_{\rho\sigma}$ , where the Christoffel symbols are given by  $\Gamma^\lambda{}_{\mu\nu} = 1/2g^{\lambda\sigma}(g_{\sigma\mu,\nu} + g_{\sigma\nu,\mu} - g_{\mu\nu,\sigma})$ . The source  $T_{\mu\nu}$  is the matter energy momentum tensor. The energy momentum is most conveniently derived from the action

$$S[g_{\mu\nu}, \psi] = S_{\text{EH}}[g_{\mu\nu}] + S_{\text{m}}[\psi, g] = \frac{1}{16\pi G} \int d^3x \sqrt{-g} (R - 2\Lambda) + S_{\text{m}}[\psi, g], \quad (1.2)$$

with  $g = \det(g_{\mu\nu})$ .  $S_{\text{m}}$  is the action of the matter fields, denoted by  $\Psi$ . Varying the Einstein-Hilbert action  $S_{\text{EH}}$  with respect to the metric yields the Einstein tensor. Varying the matter action yields the Energy-momentum tensor

$$T^{\mu\nu} = -\frac{2}{\sqrt{-g}} \frac{\delta S_{\text{m}}}{\delta g_{\mu\nu}}. \quad (1.3)$$

Conversely to matter determining how the space-time is curved, the space-time determines how matter moves in it. For example, in the absence of other forces classical particles follow geodesics, determined by the geodesic equation

$$\frac{du^\mu}{d\eta} + \Gamma^\mu{}_{\nu\lambda} u^\nu u^\lambda = 0, \quad (1.4)$$

where  $u^\mu = dx^\mu/d\eta$  is the four-velocity of the particle and  $\eta$  is the proper time.

The second pillar is the homogeneity and isotropy of the universe. Testing homogeneity and isotropy directly is difficult if not impossible, but the cosmological standard model based on the assumption of homogeneity and isotropy has so far passed all tests: Therefore homogeneity and isotropy are fair assumptions. The metric of a homogeneous and isotropic universe is the Robertson-Walker metric

$$ds^2 = g_{\mu\nu} dx^\mu dx^\nu = -dt^2 + a^2(t) \left( \frac{dr^2}{1 - kr^2} + r^2 (d\theta^2 + \sin^2(\theta) d\phi^2) \right). \quad (1.5)$$

Here,  $k$  denotes the curvature of spatial hypersurface ( $t = \text{const.}$ ). They can be flat  $k = 0$  or curved with positive (negative) curvature corresponding to a closed (open) universe. All observations point towards a flat universe, which is assumed

in the following. The (cosmic) time dependent function  $a$  is the scale factor, whose dynamics is determined by the Friedmann equations

$$\begin{aligned} H^2 &= \frac{8\pi G}{3}\bar{\rho} - \frac{k}{a^2}, \\ \frac{\ddot{a}}{a} + \frac{1}{2}H^2 &= -4\pi G\bar{p} - \frac{k}{2a^2}, \end{aligned} \quad (1.6)$$

where the Hubble parameter is defined as  $H = \dot{a}/a$ . The CC has been absorbed into the homogeneous (energy) density  $\bar{\rho} = -\bar{T}_0^0 \rightarrow \bar{\rho} + 3\Lambda/(8\pi G)$  and the homogeneous pressure  $\bar{p} = \bar{T}_i^i/3 \rightarrow \bar{p} - 3\Lambda/(8\pi G)$ . Combining the two equations 1.6 one obtains the continuity equation, expressing the conservation of energy

$$\dot{\bar{\rho}} + 3H(\bar{\rho} + \bar{p}) = 0. \quad (1.7)$$

In the case of several non-interacting species the individual energy densities are conserved, i.e. one copy of equation 1.7 holds for each species.

Before discussing the matter content of the universe a few remarks on the homogeneity are in order. In section 1.1.4 a more detailed discussion will follow. Clearly the universe is not homogeneous, as for example the existence of black letters on a white background proofs. But the distribution of matter in the universe is *statistically* homogeneous and isotropic such that on larges scales the universe can be considered as being homogeneous and isotropic. The standard treatment of deviations from homogeneity and isotropy is to use the Robertson-Walker metric as a background and add small metric fluctuations to account for the inhomogeneities, see section 1.1.3.

### 1.1.1 The cosmic inventory

The evolution of the scalar factor depends on the matter content of the universe. To get some feeling on how the matter content effects the evolution of the universe, we first consider a universe containing only one species. It is convenient to define the equation of state parameter as

$$w = \frac{\bar{p}}{\bar{\rho}}. \quad (1.8)$$

For many species one has  $w = \text{const.}$ , but even if this is not the case,  $w$  still provides useful information about the expansion of the universe. In the case of a constant equation of state, one finds for the energy density as a function of the scale factor

$$\bar{\rho} \propto a^{-3(1+w)}. \quad (1.9)$$

For  $w > -1$  the energy density decreases, while for  $w < -1$  it increases. The latter violates the Null Energy Condition (NEC). For matter respecting the NEC  $T_{\mu\nu}n^\mu n^\nu \geq 0$  holds for any light like vector  $n^\mu$ , i.e. for any vector satisfying  $g_{\mu\nu}n^\mu n^\nu = 0$ . Constructing a healthy theory violating the NEC is difficult.  $w < -1$  will not be considered in the following. If  $w > -1$ , two cases are of special interest. First, dust or non-relativistic matter with  $w = 0$ : in this case the energy density is simply diluted with the expanding volume, hence  $\bar{\rho} \propto a^{-3}$ . Second, radiation or relativistic matter with  $w = 1/3$ , which loses in addition to the growing volume energy as  $a^{-1}$  by the gravitational redshift, hence  $\bar{\rho} \propto a^{-4}$ . For the special case of  $w = -1$  one finds a constant energy density, which corresponds to the CC. Consider now the Friedmann equations 1.6 and combine them to

$$\frac{\ddot{a}}{a} = -\frac{4\pi G}{3}(\bar{\rho} + 3\bar{p}). \quad (1.10)$$

From this equation one can read off that for  $w > -1/3$  the expansion of the universe is slowed down, this is in particular the case for dust and radiation. For  $w = -1/3$  the universe expands with a constant speed. For  $w < -1/3$  the expansion of the universe is accelerated, this includes in particular the CC.

Most of the preceding arguments about the expansion of the universe remain true if the universe is populated by several species. In this case, it is useful to quantify the amount of energy each species contributes to the total energy budget in terms of the critical energy density, defined as

$$\rho_{\text{crit}} = \frac{H^2}{8\pi G}. \quad (1.11)$$

Now, the energy density  $\rho_i$  of one species can be specified in units of the critical density, via

$$\Omega_i \equiv \bar{\rho}_i / \rho_{\text{crit}}. \quad (1.12)$$

In a flat universe the total energy density equals the critical one. The  $\Omega_i$  measure then the fraction each species contributes to the total energy of the universe. In the following we will briefly discuss the most important species populating the universe.

**Baryons** In cosmology the term baryon refers to “ordinary” matter, like protons, neutrons, electrons. . . Baryons are luminous, by observing stars and galaxies we observe the distribution of baryons in the universe. For most of the cosmic history baryons are non-interacting; only before recombination, see “Photons”, their interaction with photons is relevant. Baryons have non-relativistic velocities  $v \ll 1$ , so their pressure  $p \sim \rho v^2$  is negligible and we have  $w = 0$ . Although baryons are everywhere in our daily life, only around 5% of the total energy of the universe is baryonic.

**Dark Matter** Most of matter in the universe is made of an unknown matter species,  $\Omega_{\text{DM}} \sim 0.25$ , dubbed Dark Matter (DM). Although DM particles have so far not been observed directly, they must be non-relativistic and non-interacting, otherwise DM would not be able to form structures and attract baryons to form galaxies and stars. Evidence for the existence of a non-luminous matter species comes from different astrophysical length scales, see e.g. [8]. Also cosmological observations, as the measurement of the Cosmic Microwave Background (CMB), see “Photons”, have confirmed the existence of Dark Matter.

**Photons** Today, photons only make a very small fraction of the total energy density of the universe,  $\Omega_\gamma \sim 10^{-5}$ , but as radiation their energy density decreased faster than the one of matter, so the universe was radiation dominated in the past. In the early universe photons were interacting with protons and electrons. At a scale factor around  $a_{\text{rec}} \sim 10^{-3}$  the temperature of the universe dropped below  $T_{\text{rec}} \sim 345$  eV so that electrons got captured by protons, the process is known as recombination. The universe became opaque for photons, which can be observed today as the CMB. Acoustic oscillations in the photon-electron-proton plasma before recombination got frozen. They are imprinted in the CMB and are observed in the temperature fluctuations of the CMB [9, 10]. Their amplitude and angular scale provides important information on the composition of the universe at recombination. Note that these acoustic oscillations are also imprinted in the matter distribution. They can be observed in the matter correlation function in form of the Baryonic Acoustic Oscillation (BAO) peak, located at a characteristic scale.

**Neutrinos** Similar to photons, neutrinos contribute only little to the energy budget of the universe today,  $\Omega_\nu \sim 10^{-3}$ - $10^{-2}$ , the precise number depends on the unknown neutrino masses. But they were important at earlier times. The observation of neutrino oscillations has proven that at least two of the three neutrino species are massive. Together with measurements of the beta-decay endpoint spectrum the sum of the neutrino masses can be constrained to lie in the range [11]

$$0.06 \text{ eV} \lesssim \sum_i m_i \lesssim 6 \text{ eV}. \quad (1.13)$$

Due to the small mass they act as radiation in the early universe, but are non-relativistic in the late universe and participate, as hot dark matter, in structure formation. However, the origin of the neutrino mass is unknown and requires physics beyond the Standard Model, for example the existence of right handed neutrinos. In GNQ, see section 1.4, the mass scale of neutrinos is related to the energy scale of Dark Energy.

## 1.1.2 Dark Energy

In the discussion of energy content of the universe, so far, we skipped Dark Energy, which makes today around 70% of the total energy. Apart from being almost constant in time, the nature of DE is unknown. A CC is consistent with observations, but many alternatives have been proposed [12].

DE was discovered in [13, 14] by measuring the distance to super novae of type Ia (SN Ia). These measurements use the fact that a relation between the luminosity and the duration of the super nova exists. So, the luminosity can be considered as known. Using that the luminosity decreases with the distance of the source  $r$  as  $L \propto r^{-2}$ , the distance of a SN Ia can be inferred from the observed luminosity. On a cosmological space time modifications to this relation are necessary. First, as already mentioned, photons experience a gravitational redshift, so that a photon emitted with an energy  $E_s$  at a scale factor  $a_s$ , has today an energy  $E_0$

$$\frac{E_0}{E_s} = \frac{a_s}{a_0} \equiv 1 + z, \quad (1.14)$$

where we defined the redshift  $z$ , providing an alternative measurement of time or distance. Second, the distance is given by the distance travelled by the light

$$\chi = \int_{t_s}^{t_0} dt \frac{1}{a(t)} = \frac{1}{a_0} \int_0^{z_s} dz \frac{1}{H(z)}. \quad (1.15)$$

The measured luminosity  $L_0$  of a supernova is given by

$$L_0 = \frac{L_s}{4\pi^2 d_L^2(z)}, \quad (1.16)$$

where we defined the luminosity distance

$$d_L(z) = (1 + z) \int_0^z dz' \frac{1}{H(z')}. \quad (1.17)$$

Observing SN Ia at different redshifts (distances) allows to reconstruct the (recent) cosmic history. Either it allows for a *direct* measurement of the Hubble parameter as a function of time, by using

$$\frac{1}{H(z)} = \frac{d}{dz} \frac{d_L(z)}{1 + z} \quad (1.18)$$

or a measurement of the energy densities today,  $\Omega_{0,i}$ , the equation of state parameters and today's Hubble parameter, via

$$d_L = \frac{(1 + z)}{H_0} \int_0^z dz' \frac{1}{\sqrt{\sum_i \Omega_{0,i} (1 + z')^{3(1+w_i)}}}. \quad (1.19)$$

The observed SN Ia at larger redshifts had larger distances than expected from a matter dominated universe, which is consistent with the presence of a CC with  $\Omega_\Lambda \approx 0.7$ . Recent analyses of redshift measurements of SN Ia, with  $z \lesssim 1$ , together with measurements of the distance to the BAO Peak, found for a constant equation of state  $w = -1.027 \pm 0.057$  [15]. Assuming an equation of state of the form  $w = w_0 + w_a(1 - a)$ , the best fit values are  $w_0 = -0.957 \pm 0.124$  and  $w_a = -0.336 \pm 0.552$ . This is close to a CC, but the large errors leave still room for alternative explanations.

Independent evidence for DE is obtained from the CMB and structure formation, see [16] for the recent Planck results. We will not discuss all different effects DE has on the CMB and structure formation. We will only give a brief discussion on Early Dark Energy (EDE). This is of particular interest for dynamical DE models, in which the Dark Energy density increases with time. The presence of DE effectively changes the strength of gravity. The reason is that for fixed  $H$  the amount of matter is smaller if DE is present, reducing the amount of structures, affecting for example CMB lensing (the deflection of light by gravitational potentials). The presence of EDE is strongly constrained by the recent Planck results  $\Omega_{\text{EDE}} < 0.0036$  and  $w_0 < -0.93$  at 95% confidence level, if the time evolution of DE is parametrized as  $\Omega_{\text{DE}} = \frac{\Omega_{0,\text{DE}} + \Omega_{\text{EDE}}(1 - a^{-3w_0})}{\Omega_{0,\text{DE}} + (1 - \Omega_{0,\text{DE}})a^{-3w_0}} + \Omega_{\text{EDE}}(1 - a^{-3w_0})$ . If EDE is only present for a limited time the bounds are weaker,  $\Omega_{\text{EDE}} = O(1\%)$ . This challenges dynamical DE models. A realistic DE candidate, with  $w \geq -1$ , must mimic a CC for a large range of redshifts.

### 1.1.3 Inhomogeneities

A complete description of the universe requires to go beyond the homogeneous approximation. For small fluctuations this can be done by splitting the metric in a background part  $\bar{g}_{\mu\nu}$  and a perturbation part  $\delta g_{\mu\nu}$ . For small perturbations we can use cosmological perturbation theory, in which the Einstein equation is linearized around the background, for a review see for example [17]. Using the Robertson-Walker metric as the background metric, the perturbed metric can be written as

$$ds^2 = a^2(\tau) \left( -(1 + 2\Psi)d\tau^2 + 2w_i d\tau dx^i + h_{ij} dx^i dx^j \right), \quad (1.20)$$

where the conformal time  $ad\tau = dt$  has been introduced. The spatial indices  $i$  and  $j$  are raised (lowered) with  $\delta^{ij}$  ( $\delta_{ij}$ ). On an isotropic background it is convenient to decompose  $w_i$  and  $h_{ij}$  into scalar, vector and tensor modes, according to their transformation properties under  $SO(3)$ . For the vector  $w_i$  this is the usual decomposition into a divergence-free  $\tilde{w}_i$  and a curl-free part  $\partial_i w$

$$w_i = \partial_i w + \tilde{w}_i. \quad (1.21)$$

The tensor  $h_{ij}$  can be decomposed as follows

$$h_{ij} = -2\Phi\delta_{ij} + \left(\partial_i\partial_j - \frac{1}{3}\delta_{ij}\nabla^2\right)h + \frac{1}{2}(\partial_i h_j + \partial_j h_i) + \chi_{ij}, \quad (1.22)$$

with

$$\chi_i^i = 0, \quad \partial_i \chi_j^i = 0, \quad \partial_i h^i = 0. \quad (1.23)$$

In total, these are 10 degrees of freedom, distributed among the 4 scalar modes  $\Phi$ ,  $\Psi$ ,  $w$ ,  $h$ , the two vectors  $\tilde{w}_i$ ,  $h_i$ , each carrying two degrees of freedom, and the tensor mode  $\chi_{ij}$ , carrying two degrees of freedom. Not all of the 10 degrees of freedom are physical. The reason is that there is no unique choice of coordinates for the background. Consider an infinitesimal coordinate transformation of the form

$$\hat{x}^\mu = x^\mu + \zeta^\mu. \quad (1.24)$$

To first order in  $\zeta^\mu$  the metrics transforms as follows

$$\hat{g}_{\mu\nu} = g_{\mu\nu} - g_{\mu\lambda}\partial_\nu\zeta^\lambda - g_{\lambda\nu}\partial_\mu\zeta^\lambda - \partial_\lambda g_{\mu\nu}\zeta^\lambda. \quad (1.25)$$

By decomposing  $\zeta^\mu$  into scalar and vector parts

$$\begin{aligned} \zeta^0 &= \alpha, \\ \zeta^i &= \partial^i\beta + \beta^i, \quad \partial_i\beta^i = 0, \end{aligned} \quad (1.26)$$

we obtain the following transformation laws

$$\begin{aligned} \hat{\Psi} &= \Psi - \partial_\tau\alpha - \mathcal{H}\alpha, \\ \hat{\Phi} &= \Phi + \frac{1}{3}\nabla^2\beta + \mathcal{H}\alpha, \\ \hat{w} &= w + \alpha - \partial_\tau\beta, \\ \hat{h} &= h - 2\beta, \\ \hat{w}^i &= w^i - \partial_\tau\beta^i, \\ \hat{h}^i &= h^i + \beta^i, \\ \hat{\chi}^{ij} &= \chi^{ij}, \end{aligned} \quad (1.27)$$

where we defined the conformal Hubble parameter  $\mathcal{H} = aH = da/d\tau/a$ . We can now employ the freedom in choosing the coordinate system to gauge away two scalar modes and one vector mode. So we are left with 6 physical degrees of freedom. Note that the tensor mode is not affected by the gauge transformation, since the gauge transformation 1.24 is fully specified by two scalar and one vector mode.

In practice, it is sufficient to consider the scalar modes only, since at linear order scalar, vector and tensor modes decouple and vector and tensor sources vanish in most cosmological scenarios. We will therefore consider in the following only the scalar modes. We choose to work in the Newtonian gauge, in which the metric has the form

$$ds^2 = a^2 \left( -(1 + 2\Psi)d\tau^2 + (1 - 2\Phi)d\mathbf{x}^2 \right). \quad (1.28)$$

At linear order in the gravitational potentials  $\Phi$  and  $\Psi$  the Einstein equation becomes

$$\nabla^2\Phi - 3\mathcal{H}(\partial_\tau\Phi + \mathcal{H}\Psi) = 4\pi Ga^2\delta\rho, \quad (1.29)$$

$$\nabla^2(\partial_\tau\Phi + \mathcal{H}\Psi) = -4\pi Ga^2(\bar{\rho} + \bar{P})\theta, \quad (1.30)$$

$$\begin{aligned} & \partial_\tau^2\Phi + \mathcal{H}(\partial_\tau\Phi + 2\partial_\tau\Psi) \\ & + \left( 2\frac{d\mathcal{H}}{d\tau^2} + \mathcal{H}^2 \right) \Psi + \frac{1}{3}\nabla^2(\Psi - \Phi) = 4\pi Ga^2\delta P, \end{aligned} \quad (1.31)$$

$$\nabla^2(\Psi - \Phi) = 12\pi Ga^2(\bar{\rho} + \bar{p})\sigma, \quad (1.32)$$

where we decomposed the energy-momentum tensor as follows

$$\begin{aligned} T_0^0 &= -(\bar{\rho} + \delta\rho), \\ T_i^0 &= (\bar{\rho} + \bar{p})v_i, \\ T_j^i &= (\bar{p} + \delta p)\delta_j^i + \Sigma_j^i, \end{aligned} \quad (1.33)$$

with

$$\theta = \partial_i v^i, \quad \Sigma_i^i = 0, \quad (\bar{\rho} + \bar{p})\nabla^2\sigma = -\left( \partial_i\partial^j - \frac{1}{3}\delta_j^i\nabla^2 \right) \Sigma_j^i. \quad (1.34)$$

General Relativity enforces energy-momentum energy conservation. Therefore, additionally to the four equations 1.29-1.32 one has the continuity equation  $T_{\nu;\mu}^\mu = 0$ , whose scalar parts read to first order in metric and energy-momentum perturbations

$$\partial_\tau\delta\rho + 3\mathcal{H}(1+w)\delta\rho + (1+w)\bar{\rho}(\theta - 3\partial_\tau\Phi) + 3\mathcal{H}(c_s^2 - w)\delta\rho = 0, \quad (1.35)$$

$$\partial_\tau\theta + \mathcal{H}(1-3w)\theta + \frac{\partial_\tau w}{1+w}\theta + \frac{c_s^2}{(1+w)\bar{\rho}}\nabla^2\delta\rho - \nabla^2\Psi = 0, \quad (1.36)$$

where we defined the adiabatic sound speed  $c_s^2 = \delta p/\delta\rho$ . To close the set of equations further information is required. One possibility is to assume a perfect fluid  $\sigma = 0$  and fix  $w$  and  $c_s^2$ . For example for CDM, with  $w = 0$  and  $c_s^2 = 0$ , this a good approximation for most of the cosmic history. However, in most cases the linearized Einstein equation must be supplemented by equations of motion for matter, typically a Boltzmann equation. In any case for the gravitational potentials only two of the

equations 1.29-1.32 are required. A convenient choice is to work with equation 1.29 and 1.32.

Perturbation theory is applicable as long as the inhomogeneities are small. During structure formation  $\delta\rho \sim \bar{\rho}$  is reached at some point and perturbation theory for matter can not be applied. However, metric perturbations remain small. We can use the linearized Einstein equations together with appropriate matter equations, see section 1.3. On small scales we recover Newtonian gravity. Showing that the Newtonian limit holds is subtle, see [18] for a discussion of the correspondence between relativistic and Newtonian cosmologies. Instead of showing that the Newtonian approximation can be used, we rather try to motivate it. Most conveniently this is done in Fourier space. The Newtonian limit holds then for wave vectors  $k \gg \mathcal{H}$ . Combining equation 1.29 with equation 1.30 we obtain

$$-k^2\Phi = 4\pi G \left( \delta\rho + \frac{\mathcal{H}}{k} \bar{\rho}(1+w)\theta k \right). \quad (1.37)$$

Which reduces for  $k \gg \mathcal{H}$  to the Poisson equation. Also equation 1.35 assumes its Newtonian form. From equation 1.30 we have  $\partial_\tau\Phi \sim \frac{\mathcal{H}^2}{k^2}\theta \ll \theta$ , so that  $\partial_\tau\Phi$  can be neglected. For non-relativistic matter, we have  $\sigma \sim v^2 \ll 1$ , equation 1.32 tell us that  $\Phi = \Psi$  and gravity becomes fully Newtonian.

The Newtonian limit provides an enormous simplification. To implement it in practice one use for the gravitational potentials the Poisson equations

$$\begin{aligned} \nabla^2\Phi &= 4\pi G a^2 \delta\rho, \\ \nabla^2(\Psi - \Phi) &= 12\pi G a^2 (\bar{\rho} + \bar{p})\sigma \end{aligned} \quad (1.38)$$

and employs the quasi-static limit, by neglecting  $\partial_\tau\Phi$  and  $\partial_\tau\Psi$  in the matter equations. In non-standard cosmologies this requires further justification, in particular in modified gravity theories, but the applicability of the quasi-static approximations has been confirmed by simulations [19, 20].

#### 1.1.4 Averaging and backreaction

As discussed, the universe being homogeneous and isotropic with small fluctuations on large scales is usually used as an argument for the use of the Friedmann equations. Given that on small scales fluctuations are large the Friedmann equations can only hold after some coarse-graining procedure has been applied. The standard approach is correct if the averaged metric  $\bar{g}_{\mu\nu}$  obeys the Einstein equation

$$G_{\mu\nu}(\bar{g}_{\mu\nu}) = 8\pi G T_{\mu\nu}(\bar{g}_{\mu\nu}). \quad (1.39)$$

Since averaging and time evolution do not commute, i.e.  $\overline{G_{\mu\nu}(g_{\mu\nu})} \neq G_{\mu\nu}(\overline{g_{\mu\nu}})$ , the metric obtained in this way is in general different from the one obtained by *first* solving the Einstein equation and then averaging the metric. A correct treatment requires to account for these differences by adding backreaction terms, e.g. in the form of an effective energy-momentum tensor, and to replace the energy momentum by its average, such that the Einstein equation takes the form

$$G_{\mu\nu}(\overline{g_{\mu\nu}}) = 8\pi G \left( \overline{T_{\mu\nu}} + T_{\text{eff},\mu\nu} \right) = 8\pi G \tau_{\text{eff},\mu\nu}, \quad (1.40)$$

with the effective gravitational energy-momentum tensor  $T_{\text{eff},\mu\nu} = G_{\mu\nu}(\overline{g_{\mu\nu}}) - \overline{G_{\mu\nu}(g_{\mu\nu})}$ . From this one recovers the standard approach if  $\overline{T_{\mu\nu}} \gg T_{\text{eff},\mu\nu}$  and the energy-momentum tensor as calculated from the homogeneous matter fields approximates the averaged one  $\overline{T_{\mu\nu}}$ .

The effective theory for the averaged metric is only diffeomorphism invariant, if the coarse graining prescription is diffeomorphism invariant. Since tensors at different points can not be added, constructing such a prescription is difficult. One approach, aiming at constructing an effective scale factor and deriving the corresponding effective Friedmann equations, is to average only scalar quantities [21]. This approach does not assume the metric of the universe to be close to the FRW-metric, hence is able to construct an effective FRW-metric in a highly inhomogeneous universe. In contrast to that, the approaches of [22, 23] use the fact that metric perturbations are small,  $\Phi \sim 10^{-5}$ , everywhere except in the immediate vicinity of compact objects as black holes. Nevertheless, derivatives of the metric perturbations can still be large, since first derivatives are related to velocities and second derivatives are related to the density. In principle they can induce large backreaction effects, leading to speculations that backreaction effects could account for DE, see for example [21, 24].

In [22] it is shown that backreaction effects from virialized structures can not give rise to an accelerated expansion, instead they mimic dust. Since this is similar to the backreaction effects of neutrino lumps in GNQ, we will briefly describe the argument. The average is performed by smoothing fields using a window function  $W_\Lambda(|\mathbf{x}|)$ . Here  $\Lambda$  denotes the coarse-graining scale. Expanding in the small metric perturbations, but keeping the (spatial) derivatives, one finds

$$\rho_{\text{eff}} = \bar{\rho} \left( \frac{1}{2} \overline{(1 + \delta)v^2} + \frac{1}{2} \overline{\Phi \delta} \right), \quad (1.41)$$

$$p_{\text{eff}} = \bar{\rho} \left( \overline{(1 + \delta)v^2} - \frac{1}{2} \overline{\Phi \delta} \right). \quad (1.42)$$

As expected, the effective energy density is given by the sum of kinetic and potential energy within the averaging volume  $\Lambda^3$ . For virialized structures  $2E_{\text{kin}} + E_{\text{pot}} = 0$  holds, hence the pressure vanishes, as it is the case for dust. From the Irvine-

Layzer equation  $\partial_\tau \frac{E_{\text{kin}} + E_{\text{pot}}}{\bar{\rho}} + 2\mathcal{H} \frac{2E_{\text{kin}} + E_{\text{pot}}}{\bar{\rho}} = 0$  follows that for virialized structures  $\bar{\rho}_{\text{eff}} \propto \bar{\rho} \propto a^{-3}$ . Furthermore, it can be shown that the effective stress tensor can be written as

$$\tau_{\text{eff},ij} = \frac{1}{2} \partial_\tau^2 I_{ij}. \quad (1.43)$$

The inertia tensor associated with the averaging domain is defined as

$$I_{ij} = \int d^3x' W_\Lambda(|\mathbf{x} - \mathbf{x}'|) \rho(\mathbf{x}') x'_i x'_j. \quad (1.44)$$

Since we are interested in the effect of small scales on large scales, evolving on a long time scale, we average over a long time scale  $T$  and obtain

$$\tau_{\text{eff},ij} \rightarrow \frac{1}{T} \partial_\tau I_{ij}|_0^T \sim \rho v l \sim \rho v^2 \frac{t_s}{T} \ll \rho v^2, \quad (1.45)$$

where  $l$  denotes the typical size of the system and  $t_s$  its typical timescale. For virialized systems we have  $t_s \ll T$ . The effect of small (virialized) scales on large scales is, compared to the expectation  $\tau_{\text{eff},ij} \sim \rho v^2$ , suppressed by the ratio of the two time scales, hence backreaction effects are small. If we anticipate from the discussion in section 1.3.2, that the effect of small scales on large ones is described by the effective stress tensor. We can extend the decoupling property to the effect of small scale fluctuations on large scale fluctuations, which is small too. The conclusion that backreaction is negligible is in agreement with other quantitative estimates based on perturbation theory [25] and relativistic simulations in the weak-field limit [26].

All this refers to gravitational backreaction in General Relativity. In modified gravity theories backreaction can be important [27] and in principle can account for DE [28]. Independent of the gravity theory non-gravitational backreaction, on the matter side, is possible. This is the case in GNQ, but could also be relevant in viscous fluids [29, 30].

### 1.1.5 Inflation

Before we can discuss the details of cosmological structure formation, we need to briefly discuss inflation. Inflation is a phase of rapid expansion in the early universe. It has been proposed to solve the following problems within the standard Big Bang Cosmology. First, the *horizon problem*: the causal horizon at recombination corresponds today to an angular scales of about  $1^\circ$ , but the CMB temperature is, up to very small fluctuations, the same in every direction, even on scales larger than  $1^\circ$ . No causal process could have caused this. During inflation a tiny region, in causal contact, grows large enough to be the observed universe today. The second problem is that in a decelerated universe, a tiny initial curvature grows large, which

is in contrast with the observed almost flat universe. This is the *flatness problem*. The rapid accelerated expansion during inflation drives the curvature towards zero, leaving a flat universe at the end of inflation. The third problem, the *monopole problem*, is that many particle physics models predict the existence of stable relics, which are not observed in the universe. During inflation these are simply diluted away.

We will not discuss the details of the solutions to these problems. Important for us is that inflation generates initial conditions for structure formation. Loosely speaking, inflation reboots the universe, inhomogeneities are diluted away, at the same time quantum fluctuations generate new inhomogeneities in a predictable way. The simplest realization of inflation is a single scalar field

$$\mathcal{L} = -\frac{1}{2}\partial_\mu\phi\partial^\mu\phi - V(\phi). \quad (1.46)$$

The details of the self-interaction potential  $V$  are not important. A homogeneous scalar field has the energy density and pressure

$$\bar{\rho} = \frac{1}{2}\dot{\bar{\phi}}^2 + V(\bar{\phi}), \quad (1.47)$$

$$\bar{p} = \frac{1}{2}\dot{\bar{\phi}}^2 - V(\bar{\phi}). \quad (1.48)$$

If the time derivative is small the energy density is constant. The Friedmann equation  $H^2 \approx \frac{8\pi G}{3}V$ , tells us that the scale factor grows approximately exponential. The Klein-Gordon-equation for the homogeneous field is

$$\ddot{\bar{\phi}} + 3H\dot{\bar{\phi}} + V'(\bar{\phi}) = 0. \quad (1.49)$$

The solution is a slowly moving field if  $\ddot{\bar{\phi}} \ll 3H\dot{\bar{\phi}}$ . This constrains, together with  $\frac{1}{2}\dot{\bar{\phi}}^2 \ll V$ , the potential to be flat, as expressed by the slow roll conditions

$$\epsilon_1 = \frac{1}{128G\pi^2} \left(\frac{V'}{V}\right)^2 \ll 1 \quad (1.50)$$

$$\epsilon_2 = -\frac{1}{192G\pi^2} \frac{V''}{V} \ll 1. \quad (1.51)$$

Inflation ends when the slow roll parameters reach order unity.  $\epsilon_{1/2} \sim 1$ . At the end of inflation  $\phi$  decays into (beyond) Standard Model Particles and (re)populates the universe.

Now we consider quantum fluctuations by adding a perturbation  $\delta\phi$  to the homogeneous field  $\phi = \bar{\phi} + \delta\phi$ . It is sufficient to consider perturbations to linear order. The Klein Gordon equation in Fourier space becomes

$$\partial_\tau^2\delta\phi + 2\mathcal{H}\partial_\tau\delta\phi + k^2\delta\phi + V''(\bar{\phi})\delta\phi = 0. \quad (1.52)$$

Neglecting the mass term, the solutions have the form

$$\delta\phi_{\mathbf{k}} = \frac{H\tau}{\sqrt{2k}} e^{-ik\tau} \left(1 - \frac{i}{k\tau}\right). \quad (1.53)$$

Using this we can write

$$\delta\phi(\mathbf{x}) = \int \frac{d^3k}{(2\pi)^3} \alpha_{\mathbf{k}} e^{i\mathbf{k}\cdot\mathbf{x}} \delta\phi_{\mathbf{k}} + \alpha_{\mathbf{k}}^* e^{-i\mathbf{k}\cdot\mathbf{x}} \delta\phi_{\mathbf{k}}^*. \quad (1.54)$$

The field can be quantised by promoting the coefficients to ladder operators  $\alpha_{\mathbf{k}} \rightarrow a_{\mathbf{k}}$ , with the usual commutation relation  $[a_{\mathbf{k}}, a_{\mathbf{k}'}^\dagger] = (2\pi)^3 \delta_D(\mathbf{k} - \mathbf{k}')$ . The Power Spectrum of Gaussian vacuum quantum fluctuations is given by

$$P_{\delta\phi}(k)(2\pi)^3 \delta_D(\mathbf{k} + \mathbf{k}') = \langle 0 | \delta\phi(\mathbf{k}) \delta\phi(\mathbf{k}') | 0 \rangle = |\delta\phi_{\mathbf{k}}|^2 (2\pi)^3 \delta_D(\mathbf{k} + \mathbf{k}'). \quad (1.55)$$

Of interest are the modes leaving the horizon,  $-k\tau \ll 1$ . Note that  $\tau < 0$  and  $\tau = 0$  corresponds to the end of inflation. In this limit the Power Spectrum reads

$$P_{\delta\phi}(k) = \frac{H^2}{2} k^{-3}. \quad (1.56)$$

Qualitatively this can be understood as quantum fluctuations generated inside the horizon leave the horizon. Outside the horizon they freeze and reenter the horizon as *classical* fluctuations and provide *Gaussian* initial conditions for the further evolution of inhomogeneities.

A correct treatment also involves metric fluctuations, taking them into account the Power Spectrum for the metric perturbations reads

$$P_{\Phi}(k) = A_s k^{n_s - 4}, \quad (1.57)$$

with the spectral index  $n_s = 1 - 6(\epsilon_1 + \epsilon_2)$  and the amplitude  $A_s$  determined by the Hubble parameter at horizon crossing. Since we only know the statistic of initial conditions, we can only predict statistical properties of inhomogeneities. Typically one is interested in the density-density power spectrum, which using homogeneity and isotropy reads

$$P_{\delta}(k, \tau)(2\pi)^3 \delta_D(\mathbf{k} + \mathbf{k}') = \langle \delta(\mathbf{k}, \tau; \delta_i) \delta(\mathbf{k}', \tau; \delta_i) \rangle. \quad (1.58)$$

Where  $\delta(\mathbf{k}, \tau; \delta_i)$  denotes the density contrast at  $\tau$  with the initial conditions  $\delta_i$ . The average is understood to be taken over the initial conditions set by inflation. As long as the dynamics is linear the distribution remains Gaussian. The Power Spectrum can then be written as  $P_{\delta}(k) = T^2(k) P_{\delta_{\text{in}}} \propto T^2(k) k^4 P_{\Phi_{\text{in}}}$ , with the transfer function  $T$  carrying all information about the dynamics between the initial time and

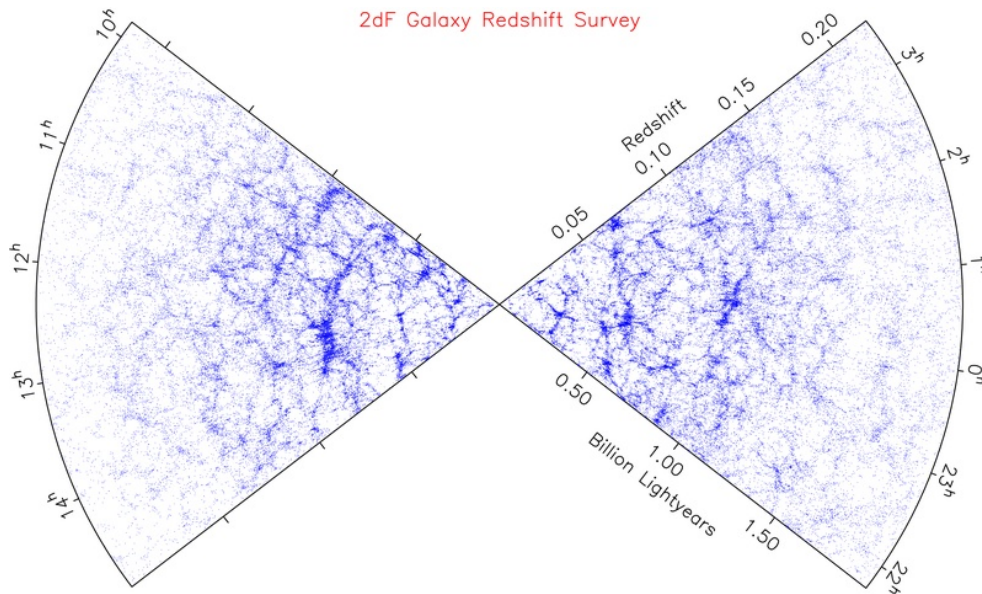


**Fig. 1.1:** The large-scale structure as seen by 2dF Galaxy Redshift Survey <sup>2</sup>. Observe the web-like structure, with galaxies concentrated in filaments and the large empty regions between, called voids.

$\tau$ . Observable is only one realization of the initial conditions<sup>1</sup>. The ergodicity of the distribution allows us to trade the ensemble average by a spatial average, so predictions can be compared to observations.

## 1.2 Cosmological structure formation

Although the universe is homogeneous and isotropic on large scales the observed structures range from cosmological scales, like galaxy clusters,  $\sim 2$  Mpc and larger, down to astrophysical scales as galaxies,  $\sim 30$  kpc, and solar systems,  $\sim 10^9$  km. By now it is accepted that the structures in the universe originate from the tiny fluctuations generated during inflation, see section 1.1.5. The initially small fluctuations in the distribution of Cold Dark Matter grow under the influence of gravity and form all the structures observed in galaxy surveys, see figure 1.1. Observing the cosmic large-scale structures became more and more important in the last years. Already running and upcoming surveys will increase the amount of available data even further [31, 32, 33, 34]. Observing the LSS is not only important to test the described picture of structure formation, e.g. to test DM properties, but it also provides a tool to test DE and modified gravity models. The evolution of structures is sensitive to the late time cosmic history. It is therefore expected that LSS observations can constrain properties of DE and deviations of general relativity relevant at late times much better than CMB measurements by the WMAP and PLANCK satellites [9,

<sup>1</sup>Similarly, simulations are performed with one realization of initial conditions

<sup>2</sup><http://www.2dfgrs.net/>

10]. Cosmology even allows us to “measure” the total neutrino mass, by observing a suppression of structures on small scales caused by neutrinos not being a cold dark matter species. In fact, the non-observation of this scale dependent effect and a similar effect in the CMB temperature autocorrelation spectrum<sup>3</sup> allowed us to constrain the total neutrino mass to  $\sum_i m_i \lesssim O(1 \text{ eV})$  [35, 36] in the standard  $\Lambda$ CDM model and variants thereof, the precise number depending on the cosmological model and the data combination used in the statistical analysis.

### 1.3 The dynamics of gravitational collapse

The mathematical model for structure formation is the Vlasov-Poisson system, consisting of the Vlasov equation 1.59 for the phase space distribution  $f(\mathbf{x}, \mathbf{p}, \tau)$  and the Poisson equation 1.60 for the gravitational potential  $\Phi(\mathbf{x}, \tau)$

$$\frac{\partial f}{\partial \tau} + \frac{\mathbf{p}}{ma} \cdot \nabla f - am \nabla \Phi \cdot \frac{\partial f}{\partial \mathbf{p}} = 0, \quad (1.59)$$

$$\nabla^2 \Phi = \frac{3}{2} \Omega_m(\tau) \mathcal{H}^2(\tau) \delta(\mathbf{x}, \tau). \quad (1.60)$$

Here  $\mathbf{x}$  denotes the comoving coordinate, meaning that coordinate distances must be multiplied by the scale factor  $a$  to obtain physical distances. The momentum is defined as  $\mathbf{p} = am\mathbf{u}$ , with  $\mathbf{u}$  denoting the peculiar velocity, i.e. the velocity relative to the overall Hubble flow. The density contrast  $\delta$  is defined by  $\bar{\rho}(1 + \delta) = \rho = \int d^3p f$ .

The use of the Vlasov-Poisson system relies on a few assumptions and approximations. First, DM is non-interacting except for gravity. So no additional force is present on large scales nor is equation 1.59 a Boltzmann equation with a collision term. Second, CDM particles have non-relativistic velocities, therefore the non-relativistic Vlasov equation can be used. Third, on scales much smaller than the horizon scale Newtonian gravity can be used instead of full general relativity. Finally, the system of equations 1.59+1.60 is valid for one (dark) matter species. In case of several species, for example in the presence of massive neutrinos, one copy of equation 1.59 is required for each species and equation 1.60 is sourced by all species<sup>4</sup>. At first these approximations seem to be very restrictive given that the nature of DM is unknown, but every viable DM candidate must effectively behave like non-interacting and non-relativistic particles, otherwise the observed structures would not have formed. An example for which it is not obvious that these criteria are fulfilled is ultra-light axion Dark Matter. Axion DM is described by a collective wave-function obeying a

<sup>3</sup>In the CMB neutrinos manifest as an enhancement of power in the temperature autocorrelation spectrum on small angular scales.

<sup>4</sup>Using an effective one-particle description in terms of the Vlasov equation is an additional approximation requiring that two particle correlations are negligible. This is the case since in a typical galaxy the number of DM particles is very high. This is true for all plausible DM candidates.

Schrödinger equation and may form a Bose-Einstein condensate [37]. Still, in the classical limit,  $\hbar \rightarrow 0$ , a correspondence between the wave function and the phase space distribution exists [38, 39]. This implies that axion DM behaves on scales larger than a characteristic scale like CDM. Other examples, requiring only mild modifications are coupled Quintessence models and some modified gravity models. Often, only the Poisson equation needs to be modified. Even in GNQ where, with neutrinos an extra species violating the first three conditions is present, it is still possible to understand the formation of neutrino lumps using a modified version of this framework.

To solve the Vlasov-Poisson system and its variants one has either to rely on numerical simulations, described in section 1.3.3, or on perturbative methods based on fluid equations, as described in the next section, for an extensive review see [40].

### 1.3.1 Perturbation theory

The Vlasov equation is impractical for analytical calculation and carries too much information. Observable is only the density (contrast) by measuring the gravitational potential or to some extent the velocity, e.g. by measuring the redshift of galaxies. It is tempting to derive a set of equations for the density  $\rho$  and the velocity  $\mathbf{u}$ . This is done by taking velocity moments as follows:

$$\rho(\mathbf{x}, \tau) = \int d^3p f(\mathbf{x}, \mathbf{p}, \tau), \quad (1.61)$$

$$\rho(\mathbf{x}, \tau)\mathbf{u}(\mathbf{x}, \tau) = \int d^3p \frac{\mathbf{p}}{am} f(\mathbf{x}, \mathbf{p}, \tau), \quad (1.62)$$

$$\rho(\mathbf{x}, \tau)\mathbf{u}(\mathbf{x}, \tau)\mathbf{u}(\mathbf{x}, \tau) + \boldsymbol{\sigma}(\mathbf{x}, \tau) = \int d^3p \frac{\mathbf{p}\mathbf{p}}{a^2m^2} f(\mathbf{x}, \mathbf{p}, \tau). \quad (1.63)$$

Taking the moments 1.61 and 1.62 of the Vlasov equation 1.59 one obtains the continuity equation 1.64 and the Euler equation 1.65

$$\partial_\tau \rho + 3\mathcal{H}\rho + \nabla \cdot (\rho\mathbf{u}) = 0, \quad (1.64)$$

$$\partial_\tau \mathbf{u} + \mathcal{H}\mathbf{u} + \mathbf{u} \cdot \nabla \mathbf{u} - \nabla \Phi = \frac{1}{\rho} \nabla \cdot \boldsymbol{\sigma}. \quad (1.65)$$

Taking higher moments one finds similar equations for the stress  $\boldsymbol{\sigma}$  and higher moments. This infinite hierarchy can be truncated by setting all moments higher than the velocity to zero. By setting  $\boldsymbol{\sigma} = 0$  the equations 1.64 and 1.65 reduce to those of a perfect pressureless fluid. This is the so called single-stream approximation, in which the distribution function is of the form

$$f(\mathbf{x}, \mathbf{p}, \tau) = \rho(\mathbf{x}, \tau) \delta_D(\mathbf{p} - a(\tau)m\mathbf{u}(\mathbf{x}, \tau)). \quad (1.66)$$

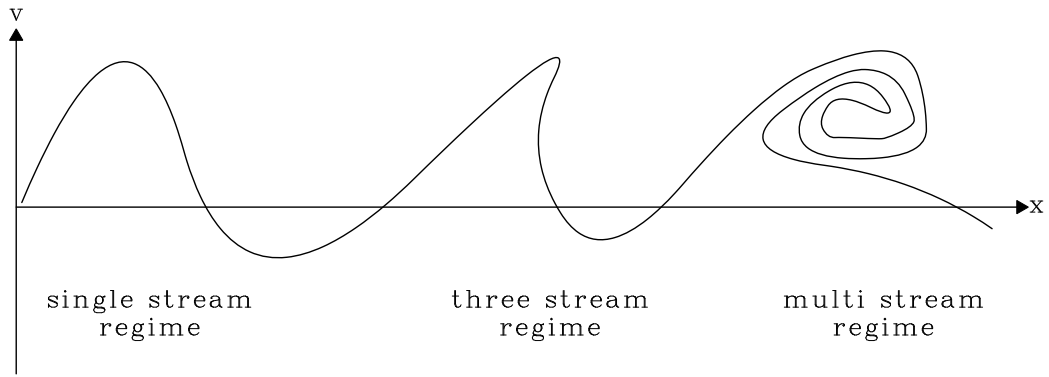


**Fig. 1.2:** A sketch of a possible phase space distribution, illustrating the breakdown of the single stream approximation

The single-stream approximation is a good approximation during the early stages of structure formation, but will fail at late time and small scales, even for perfect single stream initial conditions, see figure 1.2 for a sketch of a possible phase-space distribution. This happens when several characteristics of equation 1.59 cross in position space, c.f. 1.3.3. When this happens the velocity is not single-valued any more and the Vlasov equation has no solution of the form 1.66 anymore, see [41]. At points where this happens the solution of the fluid equations develops so-called shell-crossing singularities. This failure of the single-stream approximation is one of the motivations for studying effective fluid approaches, see section 1.3.2. For warm and hot DM species the velocity dispersion is non-negligible already initially. Often, a fluid approximation with an effective sound speed  $\sigma = c_s^2 \delta 1$  is invoked [42, 43], but at least for hot DM this is questionable [44].

The fluid equations can be simplified further. Taking the curl of the Euler equation, one finds an equation for the vorticity  $\mathbf{w} = \nabla \times \mathbf{u}$

$$\partial_\tau \mathbf{w} + \mathcal{H} \mathbf{w} - \nabla \times (\mathbf{u} \times \mathbf{w}) = 0. \quad (1.67)$$

This equation is solved by  $\mathbf{w} = 0$ . As a consequence a vanishing primordial vorticity remains zero until shell crossing. Even if a small initial vorticity is present, the vorticity decays away as  $\mathbf{w} \propto a^{-1}$ , as can be seen by linearizing 1.67. It is therefore justified to neglect the vorticity. The velocity is fully specified by the divergence  $\theta = \nabla \cdot \mathbf{u}$ .

Perturbation theory is most conveniently formulated in Fourier space. The equations 1.64 and 1.65 become in Fourier space

$$\partial_\tau \delta(\tau, \mathbf{k}) + \theta(\tau, \mathbf{k}) + \int d^3 k_1 d^3 k_2 \delta_D(\mathbf{k} - (\mathbf{k}_1 + \mathbf{k}_2)) \alpha(\mathbf{k}_1, \mathbf{k}_2) \delta(\tau, \mathbf{k}_1) \theta(\tau, \mathbf{k}_2) = 0, \quad (1.68)$$

$$\partial_\tau \theta(\tau, \mathbf{k}) + \mathcal{H} \theta(\tau, \mathbf{k}) + \frac{3}{2} \Omega_m \mathcal{H}^2(\tau) \delta(\tau, \mathbf{k}) + \int d^3 k_1 d^3 k_2 \delta_D(\mathbf{k} - (\mathbf{k}_1 + \mathbf{k}_2)) \beta(\mathbf{k}_1, \mathbf{k}_2) \theta(\mathbf{k}_1) \theta(\mathbf{k}_2) = 0, \quad (1.69)$$

where we used the Poisson equation to replace the potential by the density contrast, and defined

$$\alpha(\mathbf{k}_1, \mathbf{k}_2) = \frac{(\mathbf{k}_1 + \mathbf{k}_2) \cdot \mathbf{k}_1}{2k_1^2}, \quad \beta(\mathbf{k}_1, \mathbf{k}_2) = \frac{(\mathbf{k}_1 + \mathbf{k}_2)^2 \mathbf{k}_1 \cdot \mathbf{k}_2}{2k_1^2 k_2^2}. \quad (1.70)$$

## The linear theory

Let us first consider the linearized equations 1.68 and 1.69, formally  $\alpha = \beta = 0$ . They can be combined into an equation for  $\delta$

$$\partial_\tau^2 \delta + \mathcal{H} \partial_\tau \delta - \frac{3}{2} \Omega_m \mathcal{H}^2 \delta = 0. \quad (1.71)$$

The solution can be written in terms of the fastest growing mode  $D$  and the fastest decaying mode  $D_-$

$$\delta(\tau, \mathbf{k}) = D(\tau) A(\mathbf{k}) + D_-(\tau) B(\mathbf{k}). \quad (1.72)$$

The functions  $A$  and  $B$  are fixed by the initial conditions. In a matter dominated universe one finds

$$D = a, \quad D_- = a^{-3/2}. \quad (1.73)$$

Having the form of linear solution in mind we define

$$\varphi = \begin{pmatrix} \delta \\ -\frac{\theta}{f\mathcal{H}} \end{pmatrix}, \quad \eta = \ln(D), \quad f = \frac{d\eta}{d \ln a}. \quad (1.74)$$

In terms of these variable the fluid equations 1.68 and 1.69 become

$$\partial_\eta \varphi_a(\eta, \mathbf{k}) + \Omega_{ab}(\eta) \varphi_a(\eta, \mathbf{k}) = \gamma_{abc}(\mathbf{k}, -\mathbf{k}_1, -\mathbf{k}_2) \varphi_b(\eta, \mathbf{k}_1) \varphi_c(\eta, \mathbf{k}_2). \quad (1.75)$$

A summation over repeated indices and an integration over repeated wave vectors is implied. The non-vanishing elements of the vertex function are

$$\begin{aligned}\gamma_{121}(\mathbf{k}, \mathbf{k}_1, \mathbf{k}_2) &= \gamma_{112}(\mathbf{k}, \mathbf{k}_2, \mathbf{k}_1) = \delta_D(\mathbf{k} + \mathbf{k}_1 + \mathbf{k}_2) \frac{\alpha(\mathbf{k}_1, \mathbf{k}_1)}{2}, \\ \gamma_{222}(\mathbf{k}, \mathbf{k}_1, \mathbf{k}_2) &= \delta_D(\mathbf{k} + \mathbf{k}_1 + \mathbf{k}_2) \beta(\mathbf{k}_1, \mathbf{k}_2),\end{aligned}\quad (1.76)$$

and the time dependent matrix is defined as

$$\mathbf{\Omega} = \begin{pmatrix} 0 & -1 \\ -\frac{3}{2} \frac{\Omega_m}{f^2} & \frac{3}{2} \frac{\Omega_m}{f^2} - 1 \end{pmatrix}.\quad (1.77)$$

Using that in a  $\Lambda$ CDM cosmology  $\Omega_m \approx f^2$ ,  $\mathbf{\Omega}$  becomes time independent

$$\mathbf{\Omega} = \begin{pmatrix} 0 & -1 \\ -\frac{3}{2} & \frac{1}{2} \end{pmatrix}.\quad (1.78)$$

In order to recover the linear solution in terms of a growing and a decaying mode, we define the linear propagator by

$$\partial_\eta g_{ab}(\eta) + \Omega_{ac} g_{cb}(\eta) = \delta_{ab} \delta_D(\eta).\quad (1.79)$$

The solution is

$$\mathbf{g}(\eta) = \left( e^\eta \frac{1}{5} \begin{pmatrix} 3 & 2 \\ 3 & 2 \end{pmatrix} + e^{-3/2\eta} \frac{1}{5} \begin{pmatrix} 2 & -2 \\ -3 & 3 \end{pmatrix} \right) \theta(\eta).\quad (1.80)$$

Note that the growing mode  $e^\eta = D$  is not affected by the approximation  $\Omega_m \approx f^2$ , while the decaying mode is approximated by  $D_- \approx e^{-3/2\eta} = D^{-3/2}$ . Using the linear propagator we can write down the equal time Power Spectrum at linear order

$$P_{L,ab}(\eta, k) = g_{ac}(\eta - \eta_{\text{in}}) \langle \varphi_{\text{in},c}(\mathbf{k}) \varphi_{\text{in},d}(\mathbf{k}) \rangle g_{bd}(\eta - \eta_{\text{in}}) = D^2 u_a u_b P_{\delta_{\text{in}}}(k).\quad (1.81)$$

In the last step we used that the initial conditions are given by growing mode initial conditions  $\langle \varphi_{\text{in},a} \varphi_{\text{in},a} \rangle = u_a u_b P_{\delta_{\text{in}}}$ , with  $\mathbf{u} = (1, 1)^T$  and sent the initial time to the infinite past  $\eta_{\text{in}} \rightarrow -\infty$ .

### Higher-order perturbation theory

The linear solution we discussed so far is the lowest order in a systematic expansion in powers of the fields  $\delta$  and  $\theta$ . The corresponding expansion of correlation functions can be organized in terms of Feynman diagrams. To obtain the Feynman rules we first cast the equation 1.75 into a Martin-Siggia-Rose-Janssen-de Dominicis (MRSJD) path integral [45], for the MRSJD path integral in the context of cosmological structure

formation see for example [46, 47, 48]. From the associated MSRJD action the Feynman rules, corresponding to the linear Power Spectrum, propagator and vertex function, can be read off.

The expectation value of an observable  $O[\varphi]$ , with respect to the stochastic initial conditions can be written as

$$\langle O[\varphi] \rangle = \int D\varphi_{\text{in}} P[\varphi_{\text{in}}] \int D\varphi O[\varphi] \delta_D [\partial_\eta \varphi_a + \Omega_{ab} \varphi_a - \gamma_{abc} \varphi_b \varphi_c = \varphi_{\text{in}} \delta_D(\eta - \eta_{\text{in}})], \quad (1.82)$$

where here and in the following constant factors are absorbed into the measure. The  $\delta$ -functional picks out the solution of equation 1.75 with the initial conditions  $\varphi_{\text{in}}^5$ . The average is performed over the distribution of initial conditions

$$P[\varphi_{\text{in}}] \propto \exp \left( -\frac{1}{2} \varphi_{\text{in},a}(-\mathbf{k}) P_{\text{in},ab}^{-1}(k) \varphi_{\text{in},b}(\mathbf{k}) \right). \quad (1.83)$$

Expressing the delta-functional as a functional Fourier integral over an auxiliary field  $\chi_a$  and performing the Gaussian integral over the initial conditions, we obtain

$$\langle O[\varphi] \rangle = \int D\varphi D\chi O[\varphi] e^{iS[\chi, \varphi] + i\chi_a(\mathbf{k}) P_{\text{in},ab}(k) \chi_b(-\mathbf{k})}. \quad (1.84)$$

The action reads

$$S[\chi, \varphi] = \int d\eta \chi_a(\eta, -\mathbf{k}) (\delta_{ab} \partial_\eta + \Omega_{ab}) \varphi_a(\eta, \mathbf{k}) - \chi_a(\eta, -\mathbf{k}) \gamma_{abc}(\mathbf{k}, -\mathbf{k}_1, -\mathbf{k}_2) \varphi_a(\eta, \mathbf{k}_1) \varphi_b(\eta, \mathbf{k}_2). \quad (1.85)$$

From this we can read off the Feynman rules depicted in 1.3. The linear or free theory is recovered by formally setting  $\gamma = 0$ . The free two-point functions are given by

$$\begin{aligned} & \begin{pmatrix} P_L(\eta, \eta', k) & -iG^R(\eta, \eta', k) \\ -iG^A(\eta, \eta', k) & 0 \end{pmatrix} \\ & \equiv \begin{pmatrix} \langle \varphi_a(\eta, \mathbf{k}) \varphi_b^*(\eta', \mathbf{k}) \rangle' & \langle \varphi_a(\eta, \mathbf{k}) \chi_b^*(\eta', \mathbf{k}) \rangle' \\ \langle \chi_a(\eta, \mathbf{k}) \varphi_b^*(\eta', \mathbf{k}) \rangle' & \langle \chi_a(\eta, \mathbf{k}) \chi_b^*(\eta', \mathbf{k}) \rangle' \end{pmatrix} \\ & = -i \begin{pmatrix} 0 & -\delta_{ab} \partial_\eta + \Omega_{ba} \\ \delta_{ab} \partial_\eta + \Omega_{ab} & iP_{\text{in}ab}(k) \delta_D(\eta) \end{pmatrix}^{-1} \delta_D(\eta - \eta'), \end{aligned} \quad (1.86)$$

<sup>5</sup>Note that we implicitly used the  $\hat{\text{I}}\text{to}$ -discretization scheme, in which the determinant of the Jacobian  $\det \frac{\delta}{\delta \varphi_a} (\partial_\eta \varphi_a + \Omega_{ab} \varphi_a - \gamma_{abc} \varphi_b \varphi_c = \varphi_{\text{in}} \delta_D(\eta - \eta_{\text{in}}))$  is a constant.

$$\begin{aligned}
g_{ab}(\eta_1, \eta_2, k) &= \eta_1, a \text{ --- } \overset{k}{\text{---}} \text{ --- } \eta_2, b & P_{L,ab}(\eta_1, \eta_2, k) &= \eta_1, a \text{ --- } \overset{k}{\text{---}} \text{ --- } \eta_2, b \\
\gamma_{abc}(\mathbf{k}, \mathbf{k}_1, \mathbf{k}_2) &= \mathbf{k}, a \text{ --- } \left\langle \begin{array}{l} \mathbf{k}_1, b \\ \mathbf{k}_2, c \end{array} \right.
\end{aligned}$$

**Fig. 1.3:** The Feynman rules for the action 1.85. Similar to the in-in formalism in non-equilibrium quantum field theory, is the causal structure of the theory reflected by the different “propagators”: the retarded greens function  $g$  and the linear Power Spectrum  $P_L$ . The vertex implies wave vector conservation and an integration over time and internal momenta.

where the prime denotes that we omitted an overall  $(2\pi)^3 \delta_D(\mathbf{k} + \mathbf{k}')$ . The retarded and advanced Green functions are given by the linear propagator

$$G_{ab}^R(\eta, \eta', k) = G_{ba}^A(\eta', \eta, k) = g_{ab}(\eta - \eta') \quad (1.87)$$

and the linear Power Spectrum at unequal times is given by

$$\begin{aligned}
P_{L,a,b}(\eta, \eta', k) &= \int ds G_{ac}^R(\eta, 0, k) P_{in,cd}(k) G_{db}^A(0, \eta', k) \\
&= g_{ac}(\eta) g_{bd}(\eta') P_{in,cd}(k) = e^{\eta+\eta'} P_{\delta_{in}}(k) u_a u_b
\end{aligned} \quad (1.88)$$

As an example we give the expression for the 1-loop correction to the equal time density Power spectrum,

$$\begin{aligned}
P_{11}^{1\text{-loop}}(\eta, k) &= 8 \times \eta, \mathbf{k} \text{ --- } \overset{\mathbf{q}}{\text{---}} \overset{\mathbf{k}-\mathbf{q}}{\text{---}} \eta, -\mathbf{k} + 2 \times \eta, \mathbf{k} \text{ --- } \overset{\mathbf{k}-\mathbf{q}}{\text{---}} \overset{\mathbf{q}}{\text{---}} \eta, -\mathbf{k} \\
&= P_{13}(\eta, k) + P_{22}(\eta, k),
\end{aligned} \quad (1.89)$$

where

$$\begin{aligned}
P_{13}(\eta, k) &= 8 P_{\delta_{in}}(k) e^\eta \int_0^\eta d\eta_1 \int_0^{\eta_1} d\eta_2 g_{1c}(\eta, \eta_1) g_{fh}(\eta_1, \eta_2) e^{\eta_1+2\eta_2} \\
&\quad \times \int d^3q \gamma_{bef}(\mathbf{k}, -\mathbf{q}, \mathbf{q}-\mathbf{k}) u_e \gamma_{bgh}(\mathbf{k}, \mathbf{q}, -\mathbf{q}+\mathbf{k}) u_g u_b P_{\delta_{in}}(q) \\
&= D^4 P_{\delta_{in}}(k) \frac{k^2}{252} \frac{1}{(2\pi)^3} \int_0^\infty dq P_{\delta_{in}}(q) \\
&\quad \times \left( \frac{12k^2}{q^2} - 158 + 100 \frac{q^2}{k^2} - 42 \frac{q^4}{k^4} + \frac{3}{q^3 k^5} (q^2 - k^2)^3 (2k^2 + 7q^2) \ln \left( \frac{q+k}{q-k} \right) \right),
\end{aligned} \quad (1.90)$$

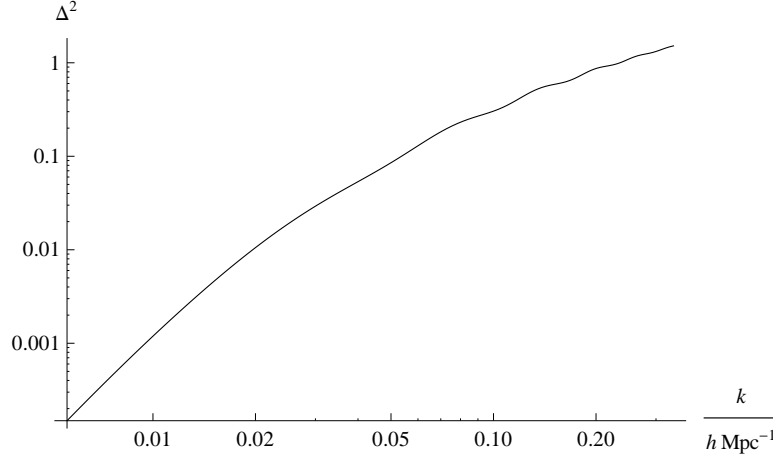


**Fig. 1.4:** The dimensionless Power Spectrum as a function of  $k$ , for an exemplary flat cosmology with  $\Omega_m = 0.3$ . The dimensionless Power Spectrum becomes order unity around  $k = 0.1 \text{ hMpc}^{-1}$ -  $0.2 \text{ hMpc}^{-1}$  indicating the breakdown of SPT.

$$\begin{aligned}
P_{22}(\eta, k) &= 2 \int_0^\eta d\eta_1 \int_0^\eta d\eta_2 g_{1c}(\eta, \eta_1) g_{1d}(\eta, \eta_2) e^{2(\eta_1 + \eta_2)} \\
&\quad \times \int d^3q \gamma_{bef}(\mathbf{k}, -\mathbf{q}, \mathbf{q} - \mathbf{k}) u_e u_f \gamma_{bgh}(\mathbf{k}, \mathbf{q}, -\mathbf{q} + \mathbf{k}) u_g u_h P_{\delta_{\text{in}}}(q) P_{\delta_{\text{in}}}(|\mathbf{q} - \mathbf{k}|) \\
&= D^4 \frac{k^2}{98} \frac{1}{(2\pi)^3} \int_0^\infty dq \int_{-1}^1 d\mu P_{\delta_{\text{in}}}(q) P_{\delta_{\text{in}}}(\sqrt{k^2 + q^2 - 2kq\mu}) \\
&\quad \times \left( \frac{3kq + 7\mu k^2 - 10qk\mu^2}{k^2 + q^2 - 2kq\mu} \right)^2. \tag{1.91}
\end{aligned}$$

The quadratic dependence of the 1-loop corrections on the initial Power Spectrum highlights that SPT is an expansion in powers of the initially small linear density Power Spectrum, but the density contrast grows with time, and so does the Power Spectrum. We should not expect that perturbation theory is valid at all scales for all times. As a rule of thumb, perturbation theory fails when the dimensionless Power Spectrum reaches order unity,  $\Delta^2 = k^3 P(k)/(2\pi^2) \sim 1$ , translating into the statement that SPT is valid today for  $k \lesssim 0.1 \text{ hMpc}^{-1}$ , see figure 1.4.

### Mode coupling and failure of perturbation theory

We finished the last section with a rough criteria for the validity of SPT. We will now try to give a more refined analysis of the performance of SPT. Ultimately, the failure of SPT is related to the coupling between modes of different wavelengths. As a starting point consider the 1-loop Power Spectrum in the limits of a soft, long-wavelength, and hard, short-wavelength, internal wave vector.

**Soft modes** First, consider the  $P_{13}$  contribution. In the limit  $q \ll k$  we find

$$P_{13}(k) = -k^2 P_{L,11} \frac{4\pi}{3} e^{2\eta} \int dq P_{\text{in},22}(q) + O(1) \equiv -k^2 \sigma_d^2(\eta) + O(1). \quad (1.92)$$

This contribution is finite for initial Power Spectra which decay in the IR faster than  $k^{-1}$ . For a realistic initial Power Spectrum  $P_{\text{in}} \sim k^{n_s}$  the integral is IR-finite, but still dominated by the soft modes. For the second diagram, summing over the two soft limits  $q \ll k$  and  $|\mathbf{q} - \mathbf{k}| \ll k$ , we find

$$P_{22}(k) = +k^2 \sigma_d^2(\eta) + O(1). \quad (1.93)$$

The sum of both contributions vanishes. Although the individual diagrams are dominated by soft modes, their sum is free of a large soft enhancement. The large leading soft contributions cancel among different diagrams at any order in perturbation theory for equal time correlation functions<sup>6</sup> [51, 52]. The cancellation is a consequence of the invariance of the fluid equations under time dependent boosts, often referred to as (Extended) Galilean Invariance. A long-wavelength velocity field moves short-wavelength modes coherently, due to the Galilean Invariance the short-wavelength modes are not affected by a coherent motion and hence not by the long-wavelength velocity field. However, subleading soft contributions can still have a sizable effect, e.g. they can lead to a broadening of the BAO peak [53].

**Hard modes** Now consider the opposite limit  $q \gg k$ , the dominant contribution is

$$P_{13}(k, \eta) = -\frac{61}{105} k^2 P_{L,11}(k, \eta) \frac{4\pi}{3} e^{2\eta} \int dq P_{L,22}(q) + O(1). \quad (1.94)$$

This integral is finite, if the initial Power Spectrum decays in the UV faster than  $P \sim q^{-1}$ . A realistic initial Power Spectrum has in the UV the asymptotic form  $P_{\text{in}} \sim k^{-3} \ln^2 \left( e + \frac{q}{k_0} \right)$ , hence the one loop integrals are UV-finite<sup>7</sup>. Generalizing to  $n$ -loop order one finds [50]

$$P_{n\text{-loop}} \sim -\frac{61}{105} C_n k^2 P_L(k, \eta) \frac{4\pi}{3} e^{2\eta} \int dq P_L(\eta, q) \sigma^{2n-2}(q, \eta) \quad (1.95)$$

where the  $C_n$  are unknown coefficients, while the expansion is controlled by

$$\sigma^2(k, \eta) = 4\pi \int_0^k dq q^2 P_L(\eta, q) \sim D^2 \ln^3 \left( e + \frac{k}{k_0} \right). \quad (1.96)$$

<sup>6</sup>For an accurate numerical evaluation of loop-integrals is important to make the cancellation between the different soft contributions explicit [49, 50]

<sup>7</sup>UV-divergences appear for a Power Spectrum  $P \sim k^{-m}$  at  $n$ -loop order, if  $m > 3 - 2/n$

The parameter  $\sigma$  is logarithmically divergent for  $k \rightarrow \infty$ , hence strongly depends on the UV-modes. For the  $n$ -loop integrals, in the limit  $k \ll q$  this translates into the finite asymptotic form

$$C_n \int dq P_L(\eta, q) \sigma^{2n-2}(q, \eta) \sim \frac{(3n-1)!}{2^{3n}} C_n D^{2n}. \quad (1.97)$$

The quickly growing numerical factor  $(3n-1)!2^{-3n}$  hinders the convergence of SPT. As the authors of [50] explicitly demonstrate the 3-loop contribution is larger than the one and two loop contribution, even on large scales. In SPT one expects the best approximation to the “true” answer to be the two loop approximation, which is a bad approximation compared to simulations [54].

### 1.3.2 Effective fluids as models for large-scale structure formation

The strong UV-sensitivity not only introduces a *large* parameter into the perturbative expansion, it also causes a strong dependence on scales which are neither described by perturbation theory nor by the perfect fluid approximation. The non-perfect fluid corrections have been quantified in [41] by measuring the velocity dispersion in simulations. At  $k \sim 0.1 h\text{Mpc}^{-1}$ , corrections to the linear Power Spectrum are small  $O(1\%)$ , but non-negligible in view of future surveys. On smaller scales they are even more important. Note, that independent of the size the velocity dispersion is important to regularize shell-crossing singularities, therefore in any consistent model the velocity dispersion must be taken into account.

A possibility to account for the complicated physics on small scales is to extract the relevant information from (small) simulations and to use it as an (external) input for perturbation theory. In practice this can be implemented by splitting fields into a long-wavelength part and a short-wavelength part, by smoothing over a scale  $\Lambda$ . For a well chosen averaging scale  $\Lambda$  the long-wavelength field will be in the perturbative regime. The long(short)-wavelength part of the density  $\rho_\Lambda$  ( $\rho_s$ ) is defined as

$$\begin{aligned} \rho_\Lambda(\mathbf{x}) &= \int d^3x' W_\Lambda(|\mathbf{x} - \mathbf{x}'|) \rho(\mathbf{x}'), \\ \rho_s(\mathbf{x}) &= \rho(\mathbf{x}) - \rho_\Lambda(\mathbf{x}). \end{aligned} \quad (1.98)$$

Instead of directly smoothing the velocity field it is convenient to smooth the momentum-density

$$\pi_\Lambda(\mathbf{x}) = \int d^3x' W_\Lambda(|\mathbf{x} - \mathbf{x}'|) \rho(\mathbf{x}') \mathbf{u}(\mathbf{x}') \quad (1.99)$$

and define the long-wavelength  $\mathbf{u}_\Lambda$  and short-wavelength velocity  $\mathbf{u}_s$  fields by

$$\begin{aligned}\rho_\Lambda(\mathbf{x})\mathbf{u}_\Lambda(\mathbf{x}) &= \pi_\Lambda(\mathbf{x}), \\ \rho(\mathbf{x})\mathbf{u}_s(\mathbf{x}) &= \rho(\mathbf{x})\mathbf{u}(\mathbf{x}) - \pi_\Lambda(\mathbf{x}).\end{aligned}\tag{1.100}$$

The fluid equations 1.64 and 1.65 for the long-wavelength fields become [22]

$$\partial_\tau \rho_\Lambda + 3\mathcal{H}\rho_\Lambda + \nabla \cdot (\rho_\Lambda \mathbf{u}_\Lambda) = 0,\tag{1.101}$$

$$\partial_\tau \mathbf{u}_\Lambda + \mathcal{H}\mathbf{u}_\Lambda + \mathbf{u}_\Lambda \cdot \nabla \mathbf{u}_\Lambda - \nabla \Phi_\Lambda = \frac{1}{\rho_\Lambda} \nabla \cdot \boldsymbol{\tau}_{\text{eff}}.\tag{1.102}$$

The coupling between small and large scales is taken into account by the effective stress tensor, given by

$$\begin{aligned}\boldsymbol{\tau}_{\text{eff}} &= \int d^3x' W_\Lambda(|\mathbf{x} - \mathbf{x}'|) \\ &\left( \boldsymbol{\sigma} + \rho \mathbf{u}_s \mathbf{u}_s + \frac{1}{8\pi G} \left( 2\nabla \Phi_s \nabla \Phi_s - \mathbf{1}(\nabla \Phi_s)^2 \right) \right) (\mathbf{x}') + O\left(\frac{\nabla^2}{\Lambda^2}\right).\end{aligned}\tag{1.103}$$

As we have seen in section 1.1.4 the contribution of virialized structures is suppressed, the UV-sensitivity is smaller than expected from SPT. Still, scales between  $\Lambda$  and the virialization scale can give sizable contributions. To improve perturbation theory, the strategy is to extract  $\boldsymbol{\tau}_{\text{eff}}$  from simulations and use it as an external input for a perturbative treatment of the left hand side of equation 1.102, along the lines of section 1.3.1.  $\boldsymbol{\tau}_{\text{eff}}$  can be either directly measured in simulations, as in the coarse-grained perturbation theory [55], or parametrized in terms of the long-wavelength fields as  $\partial_i \partial_j \tau_{\text{eff}}^{ij} / \bar{\rho} = J + c_s^2 \nabla^2 \delta_\Lambda - c_{\text{vis}}^2 \nabla^2 \theta_\Lambda / \mathcal{H} + \dots$ . The information on the small scale physics is encoded in the effective fluid parameters  $c_s$  and  $c_{\text{vis}}$  and the stochastic noise  $J$ . The ellipsis denote possible higher order terms, as in effective quantum field theories they are assumed to be suppressed by a high scale.

To respect the fact that the long-wavelength fields contain only modes  $k < \Lambda$  one has to introduce  $\Lambda$  as a UV-cutoff in the loop integrals of the perturbative expansion. The introduced  $\Lambda$ -dependence of the loops is canceled by the  $\Lambda$ -dependence of the effective stress, such that physical quantities are independent of the arbitrary smoothing scale  $\Lambda$ . In effective fluids models this can be realized by absorbing the cutoff dependence into the effective fluid parameters. Publication 3 studies the consistency of this renormalization procedure.

### 1.3.3 N-body simulations

To follow the growth of structures beyond the applicability of perturbative methods numerical simulations are required. For a detailed review see [56], for newer but shorter overviews see [57, 58, 59].

The Vlasov equation 1.59 is a conservation equation for the phase space density  $f(\mathbf{x}, \mathbf{p})$  along the trajectories or characteristics of fluid elements  $(\mathbf{x}(\tau), \mathbf{p}(\tau))$  as dictated by the Newtonian equations of motion

$$\begin{aligned}\frac{d\mathbf{x}}{d\tau} &= \frac{\mathbf{p}}{am}, \\ \frac{d\mathbf{p}}{d\tau} &= -am\nabla\Phi.\end{aligned}\tag{1.104}$$

By solving these equations one transports a fluid element initially at  $(\mathbf{x}_i, \mathbf{p}_i)$  to its position at later times. Therefore calculating the characteristics for all initial conditions  $(\mathbf{x}_i, \mathbf{p}_i)$  is equivalent to solving the Vlasov equation.

In principle one has to sample both the space and momentum dependence of the initial distribution function, but for CDM, which is initially single streaming, only the position dependence has to be sampled. In this case the characteristics obeying equation 1.104 are until shell crossing the same as those of the Euler equation 1.65.

A simulation is performed in a box of comoving volume  $V$ , typically  $V \sim (100 \text{ Mpc})^3 - (1000 \text{ Mpc})^3$ . The volume is filled with a homogeneous fluid with a density  $\bar{\rho}$ . By dividing the box into  $N$  cells the initial conditions are sampled by effective particles each with a mass  $m = \frac{\bar{\rho}V}{N}$ . These effective particles are evolved according to equations 1.104. The actual universe is infinite and has therefore no boundaries, to account for this one imposes periodic boundary conditions. This prevents particles of leaving the simulation box, since a particle leaving the volume on one side reenters on the opposite side. As a consequence mass, momentum . . . are conserved.

## Initial conditions

N-body simulations are typically initialized at  $z \sim 50-100$ . This is a compromise between the need of starting the simulation as late as possible, to reduce computation time, and the need of initializing the simulation while perturbations are still in the linear regime. Furthermore, at those times most particles of interest are non-relativistic.

Initial conditions are usually generated by displacing the homogeneously distributed particles using the Zel'dovich approximation. The Zel'dovich approximation assumes that particle velocities are proportional to gradients of the initial gravitational

potential  $\Phi_{\text{in}}$ . A particle initially at position  $\mathbf{q}$  is then displaced to its final position  $\mathbf{x}$  with the velocity  $\mathbf{u}$ , according to

$$\begin{aligned}\mathbf{x} &= \mathbf{q} - D\nabla_{\mathbf{q}}\Psi(\mathbf{q}), \\ \mathbf{u} &= -\partial_{\tau}D\nabla_{\mathbf{q}}\Psi(\mathbf{q}),\end{aligned}\tag{1.105}$$

with the displacement field  $\Psi = \frac{2}{3\Omega_m H^2}\Phi_{\text{in}}$ . The initial potential is a Gaussian random field determined by the initial Power Spectrum  $P_{\Phi_{\text{in}}}(k)$ . A simple procedure to generate the initial conditions is to decompose the initial potential in the box into a Fourier series

$$\Phi_{\text{in}}(\mathbf{q}) = \sum_{\mathbf{k}} \alpha_{\mathbf{k}} \sqrt{P_{\Phi_{\text{in}}}(k)} \cos(\mathbf{k} \cdot \mathbf{q}) + \beta_{\mathbf{k}} \sqrt{P_{\Phi_{\text{in}}}(k)} \sin(\mathbf{k} \cdot \mathbf{q}).\tag{1.106}$$

The Fourier coefficients  $\alpha_{\mathbf{k}}$  and  $\beta_{\mathbf{k}}$  are Gaussian random variables with mean 0 and width 1. Non-linear transients prevent reaching an accuracy of 1%, or better, as required for future observations. To avoid this, improvements of the Zel'dovich approximation based on Lagrangian Perturbation Theory should be used [60, 61].

As pointed out earlier, N-body simulations rely on the fact that for CDM only the position dependence of the distribution function must be sampled. For neutrinos this not possible, due to their large thermal motion. To account for this one adds a random thermal contribution to the velocity. The thermal velocity is drawn from the Fermi-Dirac distribution of the neutrinos.

## Calculating the force

At the heart of each simulation code lies the calculation of the interaction between particles. Most existing codes fall into two classes: particle-mesh (PM) codes and tree codes. None of them is superior to the other, both have their specific (dis)advantages with respect to accuracy, speed or the possibility of generalizing to other forces. Often, one uses a hybrid scheme, in order to obtain the best compromise between speed and accuracy. This is for example the case in the public available code GADGET2 [62].

**Particle-mesh codes** In PM codes the Poisson equation for the gravitational potential  $\Phi$  is solved numerically on a Cartesian grid, typically using Fast Fourier Transformations (FFT). Since they respect periodic boundaries automatically, PM codes are natural choices for cosmological simulations. PM codes can be generalized to situations where Fourier transformations can not be applied, by simply replacing the FFT based solver. For example to solve the non-linear scalar field equation in

GNQ we use a Newton-Gauß-Seidel multigrid relaxation method, described in the publications 1 and 2.

The force calculation proceeds as follows. First, the density field  $\rho(\mathbf{x})$  is calculated from the particle positions. This requires to project the position of every particle to a grid point. The simplest way to do this is to assign each particle to the nearest grid point. Summing up the mass of all particles at one grid point yields the density at that point. Higher accuracy can be achieved by treating the particle not as point-like. A first improvement is the cloud-in-cell scheme treating the particles as cubic. Here, each particle contributes to the density on eight cells. The next step solves the Poisson equation. Therefore the density field is Fourier transformed. The potential is obtained by transforming  $\Phi(\mathbf{k}) = -\frac{4\pi G}{k^2}\rho(\mathbf{k})$  back to real space. Similarly, the force field can be computed by transforming  $-4\pi G\frac{i\mathbf{k}}{k^2}\rho(\mathbf{k})$  to real space. Finally, the fields are interpolated back to the particle position, using the same prescription used to project the particles on the grid.

PM codes are fast. They scale with the number of particles  $N_p$  and grid points  $N_g$  as  $O(N_p) + O(N_g \ln(N_g))$ , but the force calculation becomes unreliable at distances of the order of the grid spacing.

**Tree codes** An alternative way of calculating the force uses that Newtonian gravity is a two-body force. The force acting on one particle at position  $\mathbf{x}_i$  can be written as the sum over all other particles

$$\mathbf{F}_i = G \sum_{j \neq i} m_i m_j \frac{\mathbf{x}_i - \mathbf{x}_j}{|\mathbf{x}_i - \mathbf{x}_j|^3}. \quad (1.107)$$

To avoid the singularity for  $\mathbf{x}_i = \mathbf{x}_j$  often a softening length  $\epsilon$  is added to the numerator, which determines the force resolution. However, the force resolution of tree codes is still better than the one of PM codes.

A direct summation for each of the  $N_p$  particles over all other  $N_p - 1$  particles would require  $O(N_p^2)$  operations, which is impractical. A more sophisticated treatment is implemented by Tree codes. The idea is to approximate particles far away by their monopole. Higher order generalizations are possible. As an illustration of the idea, consider one particle experiencing the force of a cloud of particles at a distance  $r$ . The particles belonging to the cloud are separated by a typical distance  $d$ . Now, consider  $\theta = d/r$ . If  $\theta$  is smaller than a predefined value, the force of the cloud particles is replaced by their monopole; if  $\theta$  is larger, the force is calculated by summing over the particles. In practice this is implemented by dividing the simulation box into subboxes and organizing the particle content in a tree structure, see figure 1.5. The force acting on a particle can be calculated by walking down the tree and adding whole branches or walking further down according to the selection criteria. This

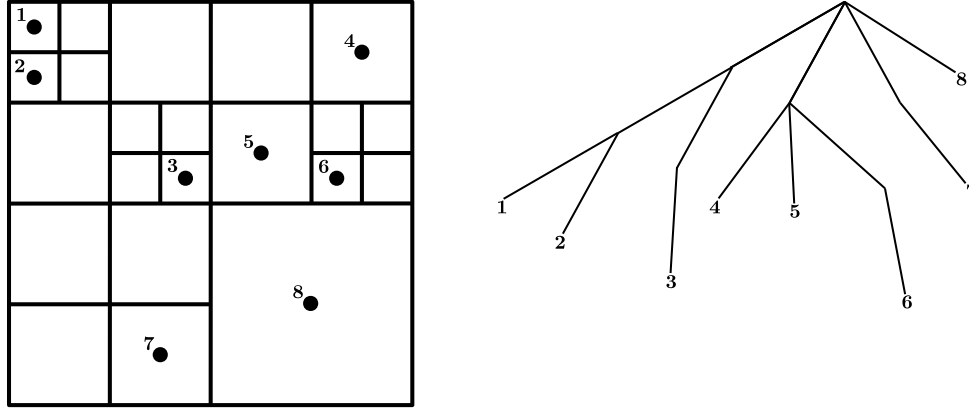


**Fig. 1.5:** Illustration of a tree code. *Left:* The particle distribution in a simulation box, dived into subboxes. *Right:* The corresponding tree structure, each leaf corresponds to one particle, indicated by the numbers.

scheme speeds up the force calculation to  $O(N_p \ln(N_p))$ . In contrast to PM codes periodic boundary conditions are not treated naturally in tree codes, but respecting periodic boundary conditions is possible by applying the Ewald summation [63].

## Leapfrog

The last piece missing is an integrator for the equation of motion of the particles 1.104. The standard method is the leapfrog scheme, in which the velocity and positions are update alternately after half a time step  $\Delta\tau/2$ , according to the following scheme:

$$\begin{aligned} \mathbf{p}\left(\tau + \frac{\Delta\tau}{2}\right) &= \mathbf{p}\left(\tau - \frac{\Delta\tau}{2}\right) + \mathbf{F}(\mathbf{x}(\tau), \tau) \Delta\tau, \\ \mathbf{x}(\tau + \Delta\tau) &= \mathbf{x}(\tau) + \frac{\mathbf{p}\left(\tau + \frac{\Delta\tau}{2}\right)}{a\left(\tau + \frac{\Delta\tau}{2}\right) m} \Delta\tau. \end{aligned} \quad (1.108)$$

This scheme is a second order scheme. Hence, it is more accurate than a simple Euler scheme, while requiring less memory than other second order schemes, since only one copy of the velocities and positions must be stored. Furthermore, leapfrog is a symplectic time-reversible scheme and as a consequence of that it conserves energy, angular momentum etc. Unfortunately, the leapfrog scheme can only be applied to velocity independent forces.

## 1.4 Growing Neutrino Quintessence

Although the CC provides a good fit to the cosmological data, a large amount of alternative DE models exists, see e.g. [12] for an overview. Questioning the standard paradigm and finding alternative explanations for the observed accelerated expansion of the universe is one motivation for the search for alternative DE models. The other motivation is the so called CC problem; a theoretical dissatisfaction with unpredictability of the CC, related to its size.

### 1.4.1 The Cosmological Constant problem

In this section, we describe several aspects of the CC problem. Hereby, we will follow the review [64]. General Relativity, including the CC, is the most general, local theory of a classical rank two tensor field with second order equations of motion [65]. However, even if the CC were classically absent the CC is generated by quantum effects, as the CC is consistent with the symmetries of gravity, namely diffeomorphism invariance. The Einstein-Hilbert action of gravity contains the term

$$S_{\text{EH}} \supset -\frac{1}{(8\pi G)} \int d^4x \sqrt{-g} \Lambda. \quad (1.109)$$

This term can be interpreted as a classical vacuum energy given by the minimum of the matter potential  $\Lambda = -8\pi G \rho_{\text{vac}} = -8\pi G V(\Phi_{\text{min}})$ . Such a term is irrelevant for non-gravitational physics. Furthermore, because the observed vacuum energy is small,  $\rho_{\text{vac,obs}} \sim 10^{-9} \text{ eV}^4$ , it is only relevant on cosmological scales.

The minimum of the potential changes during phase transitions, therefore also the classical vacuum changes during the cosmic history. In a given model the change is calculable for each phase transition, in the standard model of particle physics these are the electroweak phase transition with  $\Delta\rho_{\text{vac,EW}} \sim -10^{55} \rho_{\text{vac,obs}}$  and the QCD phase transition with  $\Delta\rho_{\text{vac,QCD}} \sim 10^{45} \rho_{\text{vac,obs}}$ . By choosing the minimum of the potential we are always able to set the vacuum energy to the observed value, but leaving us with a huge vacuum energy before the electroweak phase transition. Even if we set the vacuum energy to the observed value and “solve” classical CC problem the problem reappears at the quantum level.

In a quantum treatment of matter fields on a gravitational background the vacuum energy is the expectation value of the energy density

$$\rho_{\text{vac}} = \langle 0 | \hat{\rho} | 0 \rangle. \quad (1.110)$$

The mass dimension of the vacuum energy is 4, hence one expects that the vacuum energy is of the order of  $\rho_{\text{vac}} \sim M^4$ , with  $M$  being the highest scale of the theory.

Since gravity is involved it is plausible that  $M$  is of the order of the Planck scale. Hence, the quantum contribution to the vacuum is much larger than the observed value  $\rho_{\text{vac}} \sim M_{\text{pl}}^4 \sim 10^{120} \rho_{\text{vac,obs}}$ . This requires the classical contribution to be of the same order, with the opposite sign, such that the sum gives the observed value. This enormous amount of fine tuning is considered as being unnatural. Using a smaller cutoff, as the electroweak or QCD scale, the vacuum energy is still many orders of magnitude too large.

Let us now explain how to obtain a more trustworthy estimate. As an illustrative example consider a free scalar field  $\varphi$ , with the Lagrangian

$$\mathcal{L} = -\frac{1}{2}\partial_\mu\varphi\partial^\mu\varphi - \frac{1}{2}m^2\varphi^2. \quad (1.111)$$

The quantum contribution to the vacuum energy is dominated by UV-modes. These modes effectively see a Minkowski background. Therefore we can restrict the following considerations to flat space. A straightforward calculation yields

$$\rho_{\text{vac}} = \frac{1}{2(2\pi)^3} \int d^3k \sqrt{k^2 + m^2}. \quad (1.112)$$

This integral is divergent and must be regularized. As pointed out in [64] it is important to use a Lorentz invariant scheme e.g. dimensional regularization, yielding

$$\rho_{\text{vac}} = -\frac{m^4}{64\pi^2} \left( \frac{2}{\epsilon} + \frac{3}{2} - \gamma - \ln \left( \frac{m^2}{4\pi\mu^2} \right) \right) + O(\epsilon). \quad (1.113)$$

The  $1/\epsilon$ -pole can be absorbed into the CC, using a modified version of the  $\overline{\text{MS}}$ -scheme, also absorbing the  $3/2$ , the quantum contribution to the vacuum energy is

$$\rho_{\text{vac}} = \frac{m^4}{64\pi^2} \ln \left( \frac{m^2}{\mu^2} \right). \quad (1.114)$$

In this expression the UV-cutoff of the theory is not present. Instead the mass of the field together with the renormalization scale  $\mu$  determines the size of the vacuum energy. Although this is a toy model calculation, the result is similar to those obtained in more realistic situations. The same contribution can be found for each degree of freedom of massive vector and fermion fields, with a minus sign for fermions. Even in the presence of interactions, calculations based on non-perturbative variational methods reproduce this result, in particular the logarithmic term. To estimate the vacuum energy we choose the renormalization scale to be  $\mu \sim \sqrt{E_{\text{grav}}E_\gamma}$ . This choice combines the two relevant energy scales; the energy scale related to the expansion of the universe  $E_{\text{grav}} \sim H_0$  and the typical photon energy  $E_\gamma$ , determined by the typical wavelength of the photons travelling to us from

super novae,  $\lambda \sim 500$  nm. Plugging in the masses of the standard model particles the vacuum energy is estimated to be

$$\rho_{\text{vac}} \sim 10^{56} \rho_{\text{vac, obs}} \quad (1.115)$$

This is much smaller than the Planck scale estimate, but still many orders of magnitude larger than the observed one. This conclusion is not altered by varying the renormalization scale  $\mu$ .

Whether this estimate is more realistic than the Planck scale estimate or any other estimate is not important. What is important, is that any reasonable estimate gives, up to logarithmic corrections, an expression for the vacuum energy density of the form  $\rho_{\text{vac}} \sim M^4$ , with some mass scale  $M$ . For any plausible mass scale the quantum contribution to the vacuum energy is many orders of magnitude larger than the observed value. To avoid fine tuning the smallness of the vacuum energy density must be explained.

## 1.4.2 (Growing Neutrino) Quintessence

Popular alternatives to a CC as Dark Energy are dynamical Dark Energy models. Cosmologists' favorites are scalar field or Quintessence models, first proposed in [66, 67], and modified gravity theories. Dynamical DE models offer natural explanations for the smallness of the DE component. Typically its energy density decreases with time, as the density of matter and radiation. The DE density was larger in the past, its small value today is simply a consequence of the age of the universe. This reduces the amount of required fine tuning. However, many of those models still contain the CC therefore do not explain its absence. The publication [66] proposes to address the CC problem by classical scale free or dilatation invariant theories, in which the dilatation symmetry is anomalously broken in the quantum theory. The CC becomes an effective time dependent “cosmological constant” related to the pseudo-Goldstone mode of the broken dilatation symmetry.

In our discussion of inflation in section 1.1.5, we have seen that a minimally coupled scalar field can mimic a cosmological constant. However, every DE model must predict the correct amount of DE, preferably without fine tuning of initial conditions. Hereby, the form of the self interaction potential is crucial. If the potential allows for an attractor solution, the dynamics of the scalar field becomes independent of the initial conditions. The DE density and equation of state are specified in terms of the free parameters in the potential, see [68] for a discussion of requirements on the potential to allow for attractor solutions.

A possible choice, motivated by the dilatation invariant scenario, is an exponential potential

$$V(\varphi) = V_0 e^{-\alpha\varphi}. \quad (1.116)$$

The value of  $V_0$  is arbitrary. Changing  $V_0$  corresponds to shifting  $\varphi$  by a constant value. Effectively, the model possess only one free parameter  $\alpha > 0$ . The exponential potential has scaling solutions, in which the scalar field equation of state assumes the value of the dominant energy density present, i.e.  $w_\varphi = 0$  during matter domination and  $w_\varphi = 1/3$  during radiation domination. The energy density becomes for all initial conditions  $\Omega_\varphi = \frac{3(1+w_\varphi)}{\alpha^2}$ . However, an accelerated expansion is not possible, since the scaling regime will never end. An alternative choice possessing attractor solutions is a power law potential  $V(\varphi) \propto \varphi^{-\alpha}$ . The power law potential flattens out for large field values. A field rolling towards large field values will eventually reach negative  $w_\varphi$ . But, typically  $w_\varphi \rightarrow -1$  is only reached for  $\Omega_\varphi \rightarrow 1$ . Therefore it is difficult to find a model with  $\Omega_\varphi \approx 0.7$  and  $w_\varphi \approx -1$ , without fine-tuning of the potential.

### Growing Neutrino Quintessence

Let us consider a possible coupling of the scalar field, the cosmon, to matter. The energy scale in particle physics, which is closest to the DE energy scale is the neutrino mass. Therefore a coupling to neutrinos, via a cosmon dependent neutrino mass is plausible [69]. The coupling between neutrinos and cosmon allows the cosmon to exit the scaling regime, as soon as the cosmic neutrinos become non-relativistic. In this section we briefly discuss the homogeneous limit, for more details see for example [70].

The main ingredients are the equations of motion for the cosmon and the neutrinos

$$\ddot{\bar{\varphi}} + 3H\dot{\bar{\varphi}} + V'(\bar{\varphi}) = \beta(\varphi) (\bar{\rho}_\nu - 3\bar{P}_\nu), \quad (1.117)$$

$$\dot{\bar{\rho}}_\nu + 3(\bar{\rho}_\nu + 3\bar{P}_\nu) = -\dot{\bar{\varphi}}\beta(\varphi) (\bar{\rho}_\nu - 3\bar{P}_\nu). \quad (1.118)$$

The potential is the exponential. The  $\varphi$ -dependent coupling  $\beta < 0$  is related to the neutrino mass by

$$\beta(\varphi) = -\frac{d \ln(m_\nu(\varphi))}{d\varphi}. \quad (1.119)$$

Two regimes are of interest. First, a small mass variation with  $\varphi$ , corresponding to  $\beta = \text{const.}$  and  $m_\nu = m_i e^{-\beta\varphi}$ . Second, a scenario where the mass varies strongly near a formal pole  $m_\nu = m_i / (\varphi_{\text{crit}} - \varphi)$  corresponding to  $\beta = -1 / (\varphi_{\text{crit}} - \varphi)$ . We

will restrict our discussion to the technically simpler case of a constant coupling, the case of a varying coupling is analogous. The coupling between neutrinos and the cosmon vanishes for relativistic neutrinos. Hence, it is irrelevant at earlier times. The cosmon approaches its scaling solution. During matter domination we have

$$\bar{\rho}_\varphi \propto V(\bar{\varphi}) \propto a^{-3}, \quad m_\varphi \propto a^{-3\beta/\alpha}. \quad (1.120)$$

The scaling regimes ends when the neutrino mass has grown large enough so that the neutrinos become non-relativistic. At this point the interaction becomes important. The neutrinos act as an effective potential barrier, stopping the cosmon once  $\alpha V(\varphi) = -\beta\rho_\nu$  is reached. Both the cosmon and neutrino energy density are approximately constant. Today's DE is the combined cosmon-neutrino fluid. The DE density is  $\bar{\rho}_{\text{DE}} = \bar{\rho}_\varphi + \bar{\rho}_\nu$ . Using the relation between total neutrino mass and the energy density of non-relativistic neutrinos  $\Omega_{\nu,0} = m_{\nu,0}/(h^2 94 \text{ eV})$ , we can relate DE properties to the neutrino mass

$$\Omega_{\text{DE},0} = -\left(\frac{\beta}{\alpha} + 1\right) \frac{m_{\nu,0}}{h^2 94 \text{ eV}}, \quad w_{\text{DE},0} = -1 + \frac{m_{\nu,0}}{\Omega_{\text{DE}} h^2 94 \text{ eV}}. \quad (1.121)$$

For a fixed neutrino mass the late time cosmology is describe by a single free parameter  $\beta/\alpha$ . Demanding for the DE density  $\Omega_{\text{DE}} \sim 0.7$  and for the neutrino mass  $m_{\nu,0} \sim 1 \text{ eV}$  the equation of state is  $w \sim 0.9$  and the free parameters is  $\beta/\alpha \sim 5$ . Since bounds on EDE require  $\alpha \gtrsim 10$ , the coupling  $\beta \sim 50$  must be large and the attractive fifth force between neutrinos mediated by the cosmon is large.

### 1.4.3 Structure formation and backreaction in Growing Neutrino Quintessence

We have seen that GNQ provides a realistic homogeneous cosmology, this does not remain true once fluctuations are taken into account [71, 72, 73]. As a consequence of the required large coupling, linear perturbations become unstable and perturbation theory fails already on large scale,  $\sim 100 h\text{Mpc}$ , around  $a \sim 0.4$ . In the constant coupling model the instabilities are resolved by the formation of stable neutrino lumps, of a typical size  $\sim 30 h\text{Mpc}$ , to be compared with the size of *large* galaxy clusters  $\sim 10 h\text{Mpc}$ . Also in the varying constant coupling lumps form, but instead of being stable they periodically form and dissolve. The formation of neutrino lumps shares many similarities with the formation of gravitational structures, but in contrast to gravitational structures neutrino lumps induce large backreaction effects, invalidating the homogeneous analysis once structures have formed. Since, neutrinos became non-relativistic in the recent cosmic history, say at  $a \sim 0.2$ , lumps form late. Neutrino structure and backreaction is unimportant during most of the cosmic history, in particular the CMB and the large-scale structure formation remain

unaffected until lumps start to form. Afterwards, the lumps form and may leave observable effects. The differences to gravitational structure formation can be traced back to the field dependent mass, which does vary in time and space. A neutrino “falling” into a lump loses mass, to compensate the accompanied loss of energy the neutrino is accelerated to relativistic velocities. In the varying coupling model this process is so violent that structures form and dissolve periodically. In the constant coupling model the relativistic neutrinos form stable lumps. The small neutrino masses together with the relativistic velocities reduce the (volume) averaged trace of the energy momentum tensor, compared to the homogeneous estimate. Hence, reducing the stopping power. In the constant coupling model the stable lumps decouple [74], similar to gravitational bound structures, see section 1.1.4. The pressure of lumps vanishes when averaged over a sufficiently large scale,  $\Lambda \gtrsim 30 h\text{Mpc}$ , hence, on scales larger than  $\Lambda$  the lumps can be interpreted as an effective non-relativistic fluid interacting with a long-wavelength cosmon field, c.f. section 1.3.2. The weaker stopping effect is accounted for by a reduced effective coupling  $\beta_\Lambda < \beta$ .

The publications 1 and 2 investigate the possibility of a realistic cosmology. In publication 2 the constant coupling model is considered and in publication 1 the varying coupling model. In the constant coupling model, the strong backreaction effects induced by the stable lumps, seem not to allow for a realistic cosmology. In contrast, the oscillating lumps in the varying coupling model induce only small backreaction effects, the overall cosmology is close to the  $\Lambda\text{CDM}$  model.



# Nonlinear growing neutrino cosmology



**Nonlinear growing neutrino cosmology**Youness Ayaita,<sup>1,\*</sup> Marco Baldi,<sup>2,3,4</sup> Florian Führer,<sup>1</sup> Ewald Puchwein,<sup>5,6</sup> and Christof Wetterich<sup>1</sup><sup>1</sup>*Institut für Theoretische Physik, Universität Heidelberg, Philosophenweg 16,  
D-69120 Heidelberg, Germany*<sup>2</sup>*Dipartimento di Fisica e Astronomia, Alma Mater Studiorum Università di Bologna, viale Bertini Pichat,  
6/2, I-40127 Bologna, Italy*<sup>3</sup>*INAF-Osservatorio Astronomico di Bologna, via Ranzani 1, I-40127 Bologna, Italy*<sup>4</sup>*INFN-Sezione di Bologna, viale Bertini Pichat 6/2, I-40127 Bologna, Italy*<sup>5</sup>*Institute of Astronomy and Kavli Institute for Cosmology, University of Cambridge, Madingley Road,  
Cambridge CB3 0HA, United Kingdom*<sup>6</sup>*Heidelberger Institut für Theoretische Studien, Schloss-Wolfsbrunnenweg 35,  
69118 Heidelberg, Germany*

(Received 7 August 2014; published 11 March 2016)

The energy scale of dark energy,  $\sim 2 \times 10^{-3}$  eV, is a long way off compared to all known fundamental scales—except for the neutrino masses. If dark energy is dynamical and couples to neutrinos, this is no longer a coincidence. The time at which dark energy starts to behave as an effective cosmological constant can be linked to the time at which the cosmic neutrinos become nonrelativistic. This naturally places the onset of the Universe's accelerated expansion in recent cosmic history, addressing the *why-now* problem of dark energy. We show that these mechanisms indeed work in the *growing neutrino quintessence* model—even if the fully nonlinear structure formation and backreaction are taken into account, which were previously suspected of spoiling the cosmological evolution. The attractive force between neutrinos arising from their coupling to dark energy grows as large as  $10^6$  times the gravitational strength. This induces very rapid dynamics of neutrino fluctuations which are nonlinear at redshift  $z \approx 2$ . Nevertheless, a nonlinear stabilization phenomenon ensures only mildly nonlinear oscillating neutrino overdensities with a large-scale gravitational potential substantially smaller than that of cold dark matter perturbations. Depending on model parameters, the signals of large-scale neutrino lumps may render the cosmic neutrino background observable.

DOI: [10.1103/PhysRevD.93.063511](https://doi.org/10.1103/PhysRevD.93.063511)**I. INTRODUCTION**

The cosmological constant  $\Lambda$  has emerged as the standard explanation for the observed accelerated expansion of the Universe [1,2]. Together with the assumption of cold dark matter (CDM), it forms the remarkably successful concordance model  $\Lambda$ CDM [3]. The proposed alternatives to the cosmological constant are already many—more complicated and often a worse fit to observational data [4]. A new model should only be added to this list if it provides theoretical advantages or phenomenological aspects that neither the cosmological constant nor its most prominent competitors can offer. Growing neutrino quintessence (GNQ) was proposed in this spirit [5,6]. It addresses both the cosmological constant problem (why is the energy density of dark energy so small?) and the *why-now* problem (why has dark energy just started to dominate the energy budget of the Universe?) [7,8]. On the phenomenological side, it predicts a time-varying neutrino mass and the formation of large-scale neutrino overdensities that might be detectable by their gravitational potentials [9].

As a quintessence model [10,11], GNQ describes the dark energy by a dynamical scalar field, the cosmon  $\varphi$ . Analogous to the inflaton in inflationary theories of the early Universe, the cosmon can describe an accelerated expansion of the Universe at late times. The similarity of the mechanism even allows for a unified picture in which the same field is responsible for both the early and the late accelerating epochs [12,13]. Quintessence models address the cosmological constant problem: the energy density of dark energy decays, during most of the cosmological evolution, just like that of radiation and matter. Its small size today is then simply a consequence of the large age of the Universe.

In contrast to the simplest quintessence models, GNQ includes a mechanism for a natural crossover to the accelerated phase. No fine-tuning of the self-interaction potential is needed. Instead, a coupling between the cosmon and the neutrinos affects the dynamics of dark energy. The event of the cosmic neutrinos becoming nonrelativistic—which, due to their small masses, happens in relatively recent cosmic history—triggers the onset of dark energy domination. The present dark energy density is correlated to the present value of the neutrino mass [5].

\*ayaita@thphys.uni-heidelberg.de

Within a quantum gravity setting the change in the ratio between neutrino masses and the electron mass may be associated to a crossover between two fixed points [14].

A substantial effect of neutrinos on the overall cosmic evolution requires a coupling between the cosmon and the neutrinos, which is substantially larger (say a factor  $10^2$ ) than the gravitational coupling. A cosmon coupling to neutrinos, rather than to electrons or nucleons can have a natural explanation in a particle physics setting [6]. Such a coupling has, however, a decisive impact on the evolution of perturbations in the neutrino density. The perturbations become nonlinear even on very large scales [9]. Furthermore, the expansion history can be affected by a nonlinear backreaction effect [15]. These technical complications motivated a comprehensive simulation technique [16]. The technique has by now matured and allows us to obtain full cosmological evolutions of the model. In the technically simpler case of a constant coupling parameter, its preliminary results already inspired a consistent physical picture and an approximation scheme for the nonlinear evolution [17]. In this work, we will turn to the more natural yet technically challenging case of a field-dependent coupling. Again, a coherent (though fundamentally different) physical picture of the cosmological evolution will emerge. Our results for the first time show the full cosmological evolution of GNQ until redshift zero.

A relation between dark energy (in the form of a scalar field) and the neutrino masses has earlier been studied in models of “mass-varying neutrinos” (MaVaNs) [18]. These models share certain features with GNQ, in particular the instability problem of neutrino perturbations [19–21]. The cosmon-neutrino coupling, once strong enough, can lead to the formation of large nonlinear neutrino lumps. These lumps would, as a backreaction effect, influence the expansion dynamics of the Universe. They could even prevent the Universe from entering a phase of accelerated expansion. For GNQ, the strong backreaction effect of stable neutrino lumps on the expansion dynamics has been shown in a simulation [16]. Our results, however, provide a counterexample in which—in spite of the instability of perturbations—the backreaction effect remains small and the expansion dynamics is affected only marginally. We anticipate this numerical result in Fig. 1. Although we will encounter sizable backreaction effects in the interaction of dark energy and neutrinos, the backreaction effect on the combined cosmon-neutrino fluid is hardly visible. The evolution of the energy density of this fluid is very similar to that of a cosmological constant. The main distinction is the presence of a small fraction of early dark energy.

This work is organized as follows. The next section covers a brief overview of the fundamentals of the model and the most important insights into its cosmological evolution that preceded this work. Section III will explain the main ideas of the simulation method. The numerical results in Sec. IV are followed by a physical interpretation

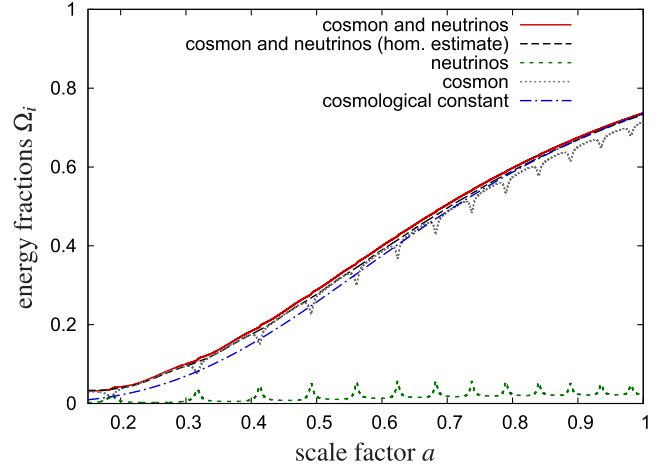


FIG. 1. The transition to dark energy domination in nonlinear growing neutrino cosmology. The figure shows the energy fraction of the coupled cosmon-neutrino fluid as obtained in a nonlinear simulation (red solid) and a purely homogeneous computation (black dashed). The two lines almost coincide, demonstrating the smallness of the “backreaction”. The individual components are the cosmon (gray dotted) and the neutrinos (green dotted). The cosmological evolution of the dark energy fraction is compared to a cosmological constant normalized to the same present-day dark energy density (blue dot-dashed).

in Sec. V sketching a coherent physical picture of the evolution. The work concludes in Sec. VI.

## II. GROWING NEUTRINO QUINTESSENCE

### A. Basic concepts

In this section, we briefly collect and explain the main ingredients that make up the GNQ model. In a nutshell, these are the cosmon  $\varphi$  described as a scalar field with a canonical kinetic term and a self-interaction potential  $V(\varphi)$  and the neutrinos whose masses are assumed to depend on  $\varphi$ . The field dependence of the neutrino mass defines an interaction between the cosmon and the neutrinos whose coupling parameter  $\beta$  is a measure of how strong this field dependence is.

Let us take the time to go through this in more detail. The Lagrangian of the cosmon alone is of standard form

$$-\mathcal{L}_\varphi = \frac{1}{2} \partial^\lambda \varphi \partial_\lambda \varphi + V(\varphi). \quad (1)$$

Here and in the following, we use the metric signature  $(-, +, +, +)$  and units where the reduced Planck mass is unity, implying  $8\pi G = 1$ . We assume an exponential potential  $V(\varphi) \propto \exp(-\alpha\varphi)$  [22]. The details of the potential do not matter as long as it gives rise to suitable scaling solutions ensuring—for a wide range of initial conditions—that dark energy decays just as the dominant component (radiation and later matter). In our case, the constraints on early dark energy require  $\alpha \gtrsim 10$  [23–25]. The scaling

solution should hold as long as neutrino masses play no role.

The second ingredient is the dependence of the neutrino masses on  $\varphi$  [6]. For simplicity, we only consider the average neutrino mass  $m_\nu$  instead of the full mass matrix  $M_\nu$  of the three light neutrinos. A dependence  $m_\nu = m_\nu(\varphi)$  occurs if a fundamental mass scale  $M$  in the mechanism of neutrino mass generation depends on  $\varphi$ . For example, in the *cascade* or *induced triplet* mechanism [26–29], the neutrino masses are proportional to  $M_t^{-2}$  where  $M_t$  denotes the mass of a heavy  $SU(2)_L$  triplet. If  $M_t$  depends on  $\varphi$  such that it reaches a small value near  $\varphi = \varphi_{\text{crit}}$ , the average neutrino mass can be approximated, in the range of interest, by the ansatz

$$m_\nu(\varphi) = \frac{\bar{m}}{\varphi_{\text{crit}} - \varphi} \quad (2)$$

with a parameter  $\bar{m}$  [6]. The formal pole at  $\varphi_{\text{crit}}$  is never reached by the cosmological solution and may be considered as an artifact of the approximation. Also the behavior far away from this pole is not important for our considerations as, in this case, the cosmon-neutrino coupling is negligible. We can thus employ the relation given by Eq. (2) for the full cosmological evolution.

The cosmon-neutrino coupling  $\beta$  quantifies the strength of the field dependence of  $m_\nu$ . It is defined as

$$\beta(\varphi) \equiv -\frac{d \ln m_\nu(\varphi)}{d\varphi} = -\frac{1}{\varphi_{\text{crit}} - \varphi}, \quad (3)$$

where, in the last step, we have used the explicit dependence of Eq. (2). When  $\varphi$  approaches  $\varphi_{\text{crit}}$ , the coupling becomes strong and successfully stops the evolution of the cosmon. However, other functional shapes for  $\beta$  are possible as well. For instance, a technically simple choice is a constant coupling  $\beta = \text{const}$  implying an exponential mass dependence  $m_\nu(\varphi) \propto \exp(-\beta\varphi)$ . A growing neutrino mass requires a negative coupling parameter  $\beta < 0$ . We assume that only neutrinos have a sizable coupling to the cosmon. This is motivated in particle physics by a cross-over in the flow of couplings within the beyond standard model sector, which first manifests itself in the neutrino sector through the dependence of neutrino masses on some heavy scale [30].

The coupling between the cosmon and the neutrinos manifests itself as an energy-momentum exchange between the two components. This energy-momentum transfer is proportional to the coupling parameter  $\beta(\varphi)$  and reads

$$\nabla_\lambda T_{(\varphi)}^{\mu\lambda} = +\beta(\varphi)T_{(\nu)}\partial^\mu\varphi, \quad (4)$$

$$\nabla_\lambda T_{(\nu)}^{\mu\lambda} = -\beta(\varphi)T_{(\nu)}\partial^\mu\varphi, \quad (5)$$

where  $T_{(\nu)} \equiv T_{(\nu)\lambda}^\lambda = -\rho_\nu + 3p_\nu$  denotes the trace of the neutrino energy-momentum tensor. Quintessence

couplings of this simple type are discussed in early works on coupled dark energy [31,32].

Inserting the cosmon's energy-momentum tensor in Eq. (4) yields the field equation

$$\nabla^\lambda \nabla_\lambda \varphi - V_{,\varphi}(\varphi) = \beta(\varphi)T_{(\nu)}. \quad (6)$$

It shows that the cosmon-neutrino coupling becomes only effective once the right-hand side  $\beta T_{(\nu)}$  is comparable to or larger than the potential derivative  $V_{,\varphi}$ . As long as the neutrinos are relativistic with  $w_\nu \approx 1/3$ , the trace  $T_{(\nu)} = -\rho_\nu(1 - 3w_\nu)$  and thereby the effect of the coupling is negligible. In this sense, the neutrinos becoming non-relativistic serves as a trigger event. On the other hand, also  $\beta(\varphi)$  grows towards large negative values as  $\varphi$  rolls down its potential towards  $\varphi_{\text{crit}}$ . This ensures that, eventually, the effect of the coupling cancels the effect of the potential derivative. In that case, the evolution of the cosmon is essentially stopped, and the dark energy approximately acts as a cosmological constant with vacuum energy  $V(\varphi_{\text{crit}})$ . We will find that  $\varphi$ , and therefore the neutrino masses, oscillate around a slowly increasing value.

For a neutrino particle on a classical path, the coupling implies the equation of motion [16]

$$\frac{du^\mu}{d\tau} + \Gamma_{\alpha\beta}^\mu u^\alpha u^\beta = \beta(\varphi)\partial^\mu\varphi + \beta(\varphi)u^\lambda\partial_\lambda\varphi u^\mu, \quad (7)$$

where  $u^\mu$  is the four-velocity and  $\tau$  denotes the proper time. The left-hand side is simply the motion under gravity, whereas the right-hand side includes the effects of the cosmon-neutrino coupling. For the (spatial) velocities  $u^k$ , the first term  $\beta\partial^k\varphi$  is similar to a potential gradient in Newtonian gravity and can be interpreted as an attractive force between the neutrinos. In the limit of small velocities, it is about  $2\beta^2$  stronger than gravity [33]. For relativistic velocities, it becomes negligible as the other contributions grow quadratically with components of the four-velocity  $u^\mu$ . In this case, the coupling is only important in the second term on the right-hand side, which, however, cannot change the direction of motion of the particle. Thus, the cosmon-mediated attraction of neutrinos is only effective in the nonrelativistic case.

A second important ingredient is the replacement of the Hubble damping by ‘‘cosmon acceleration.’’ Neglecting the (spatial) gradients  $\partial^k\varphi$  (and, similar, for the metric), Eq. (7) becomes ( $u^0 = \gamma$ )

$$\frac{du^k}{dt} = [\beta(\varphi)\dot{\varphi} - 2H]u^k, \quad (8)$$

$$\frac{d\gamma}{dt} = [\beta(\varphi)\dot{\varphi} - H]\frac{\gamma^2 - 1}{\gamma}. \quad (9)$$

(This is consistent with the defining relation  $\gamma^2 = 1 + a^2 u^k u_k$ .) For an expanding universe, the positive

sign of  $H$  induces a damping of all motions. We will find that the contribution  $\propto \beta \dot{\varphi}$  overwhelms the Hubble damping for important periods in the formation of nonlinear neutrino structures. The acceleration of all neutrino motions for  $\dot{\varphi} < 0$  will play a crucial role for the dissolution of previously formed neutrino lumps.

### B. Cosmon-neutrino structure formation for constant coupling

Understanding structure formation in GNQ is not only important to make contact with various observational constraints such as from the cosmic microwave background (CMB) or galaxy surveys. It even is a prerequisite for obtaining reliable estimates of the expansion dynamics. This is because, as we will review in this section, nonlinear perturbations in the cosmon-neutrino fluid can lead to strong backreaction effects. They alter cosmological averages of the neutrino mass and equation of state, which, in turn, influences the evolution of dark energy at the background level. We explain this by briefly reviewing the main steps undertaken by previous works that have shed light on the issue [9,15–17,21,33–36]. These works focused on the constant coupling model where  $\beta$  does not depend on  $\varphi$ . It is technically simpler and may be regarded as a useful approximation in the case where  $\beta(\varphi)$  does not vary much in late cosmology. Obtaining a realistic accelerated expansion requires couplings of order  $\beta \sim -10^2$  if the potential is exponential with  $\alpha \gtrsim 10$ .

The large value of the coupling implies a fast growth of linear neutrino perturbations. The transition to the nonlinear regime can be associated roughly with the moment at which the dimensionless power spectrum  $\Delta_\nu^2(k) = k^3 P_\nu(k)/(2\pi^2)$  reaches order unity. In contrast to the CDM case, this transition occurs even on very large scales leading to a breakdown of linear perturbation theory [9]. Let  $a_{\text{nl}}(k)$  denote the cosmic scale factor at which  $\Delta_\nu^2(k)=1$  in linear perturbation theory. Figure 2 shows the transition to nonlinearity (in the Newtonian gauge) for  $\beta = -52$ ,  $\alpha = 10$ , and a relatively large present-day average neutrino mass  $m_\nu^0 \approx 2.3$  eV. Although the details depend on the precise parameters chosen, the qualitative finding is generic and has its origin in the instability of linear perturbations (cf. Sec. II A).

The first scales to enter the nonlinear regime are of comoving size  $\lambda \sim 100h^{-1}$  Mpc (cf. Fig. 2). The overdensities at this scale evolve into massive neutrino lumps that are stable for constant  $\beta$ . Although the picture will be different for the varying (i.e. cosmon-dependent) coupling  $\beta(\varphi)$  investigated in this work, cf. Eq. (3), it is worthwhile to discuss the main effects in the technically simpler setting of a constant coupling  $\beta \sim -10^2$ . They will reappear, albeit in a weaker form, in the varying coupling model and play a role in the physical interpretation of our results.

Two properties of the lumps were identified that imply a backreaction effect altering the expansion dynamics [35]. They both lead to a suppression

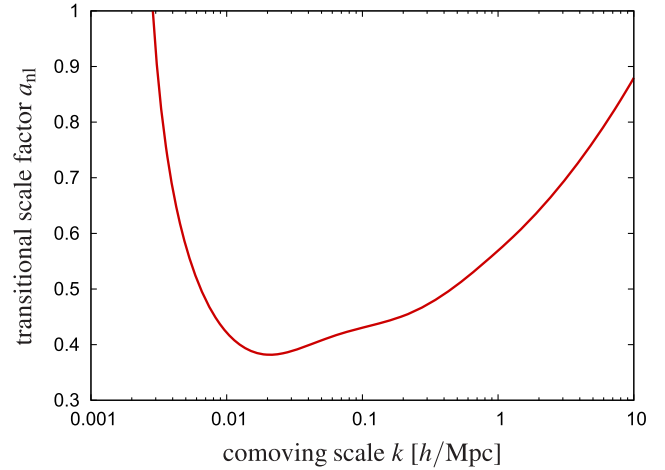


FIG. 2. Onset of nonlinearity for neutrino fluctuations. We show the scale factor  $a_{\text{nl}}$  at which different scales enter the nonlinear regime. Compare with the corresponding figure in Ref. [9].

$$|\overline{T_{(\nu)}}| < |T_{(\nu)}^{\text{hom}}| \quad (10)$$

of the actually averaged trace of the neutrino energy-momentum tensor as compared to the trace obtained in a purely homogeneous computation that neglects the nonlinear perturbations. It is, however, this trace  $T_{(\nu)}$  that enters the cosmon field equation, Eq. (6). The more severely the trace is suppressed, the less effective is the coupling in stopping the evolution of the cosmon.

First, during the lump formation, the neutrinos are accelerated to higher velocities. This can lead, in particular close to the lumps' centers, to relativistic neutrino velocities. Those neutrinos no longer contribute to  $\overline{T_{(\nu)}}$  as the energy-momentum tensor of relativistic particles is approximately traceless. Second, similar to a gravitational potential well, the local cosmon perturbation  $\delta\varphi$  is negative in lumps, leading to neutrino masses  $m_\nu(\bar{\varphi} + \delta\varphi)$  that are smaller inside the lumps than expected for the cosmological average field  $\bar{\varphi}$ . As  $T_{(\nu)} \propto m_\nu$ , this substantially weakens the effect of the coupling as most neutrinos will be located in lumps. The effect can be physically understood as an approximate mass freezing within lumps—the nonlinear lumps approximately decouple from the background; the local value  $\varphi_l$  of the cosmon within the lumps no longer follows the evolution of the homogeneous component  $\bar{\varphi}$  [35]. We illustrate this schematically in Fig. 3. In this illustration, a stable lump is located at  $r = 0$ ; within some time interval  $\Delta t$ , the cosmon evolves by  $\Delta\varphi_l$  within and by  $\Delta\bar{\varphi}$  far outside the lump. The figure tells us that  $\varphi_l < \bar{\varphi}$  and  $\Delta\varphi_l < \Delta\bar{\varphi}$ . Stated differently, the background component  $\bar{\varphi}$  feels a smaller neutrino mass  $\overline{m_\nu(\varphi)} < m_\nu(\bar{\varphi})$ , which, in addition, depends more weakly on  $\bar{\varphi}$  [15]. This weaker dependence can be expressed as a weaker effective coupling

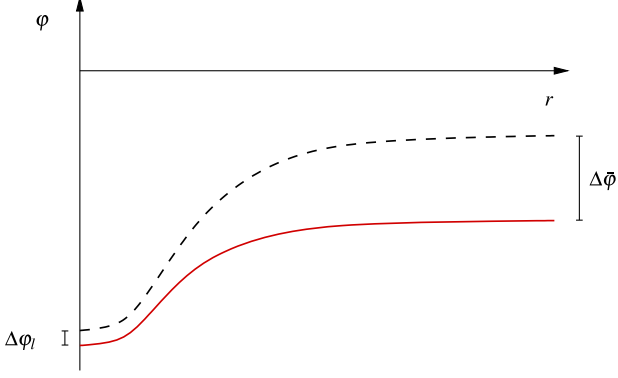


FIG. 3. The local value of the cosmon effectively decouples from the background evolution leading to an approximate mass freezing within lumps. We use arbitrary units in this schematic plot, where the core of the potential well is typically of the size of several megaparsecs and the depth of the potential well is of order  $\bar{\varphi} - \varphi(0) \sim 10^{-2}$  [16].

$$\beta_{\text{eff}} \equiv -\frac{d \ln \overline{m_\nu(\varphi)}}{d\bar{\varphi}}, \quad |\beta_{\text{eff}}| < |\beta|. \quad (11)$$

It postpones the onset of the accelerated expansion [16].

For constant  $\beta$ , a clear physical picture and a resulting approximation scheme have emerged that describe the cosmological evolution after the formation of lumps [17]. Despite relativistic neutrino velocities in the lumps' cores, the total lumps—also including the local cosmon perturbation—behave like nonrelativistic objects. This is because the negative pressure contribution of the local cosmon perturbation just cancels the positive neutrino pressure. The mutual attraction between these cosmon-neutrino lumps and the interaction between the nonrelativistic cosmon-neutrino lump fluid and the background cosmon  $\bar{\varphi}$  are governed by effective couplings weaker than the fundamental coupling  $\beta$ .

In this work, we investigate a field-dependent  $\beta$  given by Eq. (3). We will find that important features behave qualitatively different since lumps turn out to be no longer stable.

### III. METHOD

#### A. An $N$ -body approach

Usually,  $N$ -body simulations are employed to understand the nonlinear small-scale dynamics of a cosmological model whereas the evolution of the homogeneous background and of large-scale linear perturbations can be obtained by simpler means. Not so in GNQ: The effects of nonlinear perturbations have an impact on all scales including the homogeneous background (cf. Sec. II B). As a consequence, a nonlinear method is bitterly needed in order to understand the cosmological dynamics of the model.

The first step towards an  $N$ -body simulation of GNQ was to incorporate the cosmon-mediated attraction between neutrinos in the Newtonian limit [36]. In this setting, the attractive force is analogous to gravity but stronger by a factor  $2\beta^2$ . The simulation was capable of describing the first stages of the nonlinear evolution in which large neutrino lumps started to form. However, the simplifying assumptions of the approach subsequently broke down. First, the approach is only valid for nonrelativistic neutrino velocities, but the neutrinos reached, due to the attractive force, the relativistic regime. Second, the neutrino masses were assumed to only depend on the background cosmon  $\bar{\varphi}$  rather than on the local cosmon value  $\varphi$ ; this is a good approximation as long as the local cosmon perturbations are sufficiently small, i.e.  $m_\nu(\varphi) \approx m_\nu(\bar{\varphi})$ . Inside neutrino lumps, this no longer holds.

These issues were addressed by a comprehensive simulation method specifically designed for GNQ [16]. The latter allows for relativistic neutrinos whose motion is described by the full equation of motion, Eq. (7). The local neutrino mass variations are included by actually solving the nonlinear field equation for the local cosmon perturbation  $\delta\varphi$  (cf. Sec. III B). The backreaction effects (explained in Sec. II B) are accounted for by solving the equations for the homogeneous background simultaneously with the nonlinear perturbations.

Every neutrino particle  $p$  with four-velocity  $u^\mu$ , proper time  $\tau$ , and trajectory  $x_p^\mu$  gives rise to an energy-momentum contribution

$$T_{(p)}^{\mu\nu}(x) = \frac{1}{\sqrt{-g}} \int d\tau m_\nu(\varphi(x_p)) u^\mu u^\nu \delta^4(x - x_p) \quad (12)$$

with the determinant  $g$  of the metric and the Dirac delta function. From this, not only the perturbations of the energy density  $\delta\rho_\nu$  and of the pressure  $\delta p_\nu$ , the anisotropic shear  $\Sigma^i_j$ , but also the background quantities  $\bar{\rho}_\nu = -\bar{T}^0_{(\nu)0}$  and  $\bar{p}_\nu = \bar{T}^i_{(\nu)i}/3$  can be calculated as sums over particle contributions [16]. These are the actual cosmological averages

$$\bar{T}^{\mu\nu}_{(\nu)} = \frac{\int_V d^3x \sqrt{g_{(3)}} T^{\mu\nu}_{(\nu)}}{\int_V d^3x \sqrt{g_{(3)}}} \quad (13)$$

that appear in the background equations. Here,  $g_{(3)}$  is the determinant of the spatial metric, and  $V$  is the comoving simulation volume. In this way, the background quantities are directly linked to the perturbed quantities, thereby including the backreaction effects.

The anisotropic shear  $\Sigma^i_j$  is no longer negligible once the neutrinos reach relativistic velocities. Assuming the Newtonian gauge

$$ds^2 = -(1 + 2\Psi)dt^2 + a^2(1 - 2\Phi)d\mathbf{x}^2, \quad (14)$$

it implies a difference  $\Psi \neq \Phi$  between the two gravitational potentials. This is accounted for by solving the well-known Poisson equation for  $\Phi - \Psi$ .

The simulation includes also CDM as nonrelativistic particles accelerated by the Newtonian gravitational potential  $\Psi$ . In GNQ, also the neutrino perturbations contribute to  $\Psi$  such that additional forces act on CDM particles potentially increasing their peculiar velocities [37].

The  $N$ -body simulation is specified by a number of physical and numerical parameters [16]. The most important numerical parameters are the comoving box volume  $V = L^3$ , the number  $N_\nu$  of neutrino and  $N_m$  of effective CDM particles, the initial scale factor  $a_i$ , and the resolution, i.e. the number  $N_c$  of cells. A fixed, equilateral cubic lattice is used. This is sufficient as cosmon-neutrino structures form on relatively large scales. On this lattice, the gravitational potentials  $\Psi$ ,  $\Phi$ , and the cosmon perturbation  $\delta\varphi$  are calculated.

The initial conditions at  $a_i$  are taken from linear perturbation theory [9]. The evolution of CDM particles in the  $N$ -body simulation starts even earlier than  $a_i$  since nonlinearities in CDM perturbations occur at much smaller scale factors than in the neutrino perturbations. The simulation is governed by a global time parameter for which we use the scale factor  $a$ . As the dynamical time scale of the cosmon-neutrino interaction varies with the coupling  $\beta$ , it is adequate to let the time steps depend on  $\beta$ , i.e.  $\Delta a = \Delta a(\beta)$ .

## B. The cosmon field equation

A technical difficulty lies in nonlinearities in the field equation for cosmon perturbations  $\delta\varphi$ . Whereas the perturbation  $\delta\varphi$  generally remains rather small, the steepness of the mass function  $m_\nu(\varphi)$  expressed by the large values of  $\beta$  can invalidate the linear approximation

$$m_\nu(\varphi) \approx m_\nu(\bar{\varphi}) - \beta(\bar{\varphi})m_\nu(\bar{\varphi})\delta\varphi. \quad (15)$$

This can arise for two reasons. First, if stable cosmon-neutrino lumps form, the local neutrino mass within lumps effectively freezes while the mass far outside the lumps continues to grow (cf. Fig. 3). Second, for very large coupling parameters, e.g. for  $\varphi$  close to  $\varphi_{\text{crit}}$  in Eq. (3), the linear approximation of the mass function can even break down without a mass-freezing effect.

The nonlinear mass function enters the field equation for  $\delta\varphi$  by virtue of the trace  $T_{(\nu)} \propto m_\nu(\varphi)$ . The equation for  $\delta\varphi$  is obtained from the fundamental field equation for  $\varphi$ , Eq. (6), which we split into a homogeneous and a perturbative part. The homogeneous part reads

$$\ddot{\bar{\varphi}} + 3H\dot{\bar{\varphi}} + V_{,\varphi}(\bar{\varphi}) = -\overline{\beta(\varphi)T_{(\nu)}}. \quad (16)$$

In the perturbative part, we neglect the time derivatives of  $\delta\varphi$  and the nonlinearities in  $\delta\varphi$  except for the coupling parameter and the mass function [16]:

$$\frac{1}{a^2}\Delta\delta\varphi - V_{,\varphi\varphi}(\bar{\varphi}) + 2\Psi(\ddot{\bar{\varphi}} + 3H\dot{\bar{\varphi}}) = \delta(\beta(\varphi)T_{(\nu)}). \quad (17)$$

Here, the right-hand side is defined as the perturbation

$$\delta(\beta(\varphi)T_{(\nu)}) = \beta(\varphi)T_{(\nu)} - \overline{\beta(\varphi)T_{(\nu)}} \quad (18)$$

and can be highly nonlinear in  $\delta\varphi$ . The solution of Eq. (17) by an iterative Fourier-based method broke down once the nonlinearities became severe; for the constant coupling model, this happened at  $a \gtrsim 0.5$  [16]. We have implemented a Newton-Gauß-Seidel (NGS) multigrid relaxation method recently developed for modified gravity [38] to overcome these difficulties. Thereby, stable solutions of the cosmological evolution can be obtained.

We write Eq. (17) schematically as

$$\mathcal{L}[\delta\varphi] \equiv \Delta\delta\varphi - F[\delta\varphi] = 0 \quad (19)$$

with nonlinear functionals  $\mathcal{L}$  and  $F$ . The NGS solver applies an iterative prescription which, similar to Newton's method, is based upon finding the root of the linearized functional in each iteration step. However, the linearization is done at every lattice point  $\mathbf{x}$  individually; no functional derivative is performed. The main step of the iteration is thus

$$\delta\varphi^{(n+1)}(\mathbf{x}) = \delta\varphi^{(n)}(\mathbf{x}) - \frac{\mathcal{L}[\delta\varphi^{(n)}](\mathbf{x})}{\partial\mathcal{L}[\delta\varphi]/\partial\delta\varphi(\mathbf{x})}, \quad (20)$$

where the derivative in the denominator is just a usual partial derivative with respect to the value  $\delta\varphi(\mathbf{x})$ . The coupling between neighboring cells is accounted for by the iterative procedure. We split the derivative as follows:

$$\frac{\partial\mathcal{L}[\delta\varphi]}{\partial\delta\varphi(\mathbf{x})} = \frac{\partial(\Delta\delta\varphi(\mathbf{x}))}{\partial\delta\varphi(\mathbf{x})} - \frac{\partial F[\delta\varphi]}{\partial\delta\varphi(\mathbf{x})}. \quad (21)$$

Approximating the Laplacian by a seven-point stencil gives us  $-6/\Delta x^2$  for the first term on the right-hand side if  $\Delta x$  is the comoving lattice spacing. In the second term, the crucial  $\delta\varphi$  dependence comes from the product  $\beta m_\nu$ ,

$$\frac{\partial[\beta(\varphi)m_\nu(\varphi)]}{\partial\delta\varphi} = \beta_{,\varphi}(\varphi)m_\nu(\varphi) - \beta^2(\varphi)m_\nu(\varphi). \quad (22)$$

For the varying coupling model investigated in this work, Eq. (3), the coupling  $\beta(\varphi)$  and the mass function  $m_\nu(\varphi)$  grow large for  $\varphi \rightarrow \varphi_{\text{crit}}$ . When the background cosmon  $\bar{\varphi}$  is very close to the barrier  $\varphi_{\text{crit}}$ , the perturbation  $\delta\varphi$  has to be calculated very accurately. A small numerical error might lead to exceeding the barrier,  $\bar{\varphi} + \delta\varphi > \varphi_{\text{crit}}$ , which gives unphysical results. If this is an issue, a change of variables is appropriate that automatically enforces the barrier  $\varphi < \varphi_{\text{crit}}$ . This is achieved by solving the field equation for the variable  $u(\mathbf{x})$  defined by

$$e^{u(\mathbf{x})} \equiv \varphi_{\text{crit}} - \varphi(\mathbf{x}). \quad (23)$$

Regardless of which values  $u(\mathbf{x})$  obtains in the NGS solver, calculating back to  $\delta\varphi(\mathbf{x})$  will give a value respecting the barrier. The resulting term  $\Delta e^{u(\varphi(\mathbf{x}))}$  is represented by finite differences as proposed by Ref. [39]. The NGS solver uses multigrid acceleration and the so-called full approximation scheme, which is suited for highly nonlinear problems. Full details are given in Ref. [38].

#### IV. RESULTS

The generic finding of our simulations is a strong oscillatory behavior of the neutrino perturbations—mildly nonlinear neutrino overdensities continuously form and dissolve. In contrast to the stable neutrino lumps in the constant coupling model (cf. Sec. II B), these short-lived overdensities never reach high density contrasts. So, neither do they induce a large gravitational potential comparable to that of cold dark matter nor do they decouple from the evolution of the homogeneous background. The expansion dynamics is only slightly affected, cf. Fig. 4. In particular, the effective average cosmon-neutrino coupling differs only mildly from the microscopic coupling  $\beta$ . A standard epoch of accelerated expansion results from the effective stop of the cosmon evolution.

The numerical method (cf. Sec. III), however, is not yet sufficiently fast and robust to explore the parameter space of the field-dependent coupling model, Eq. (3). A crucial parameter is the normalization  $\bar{m}$  of the average neutrino mass defined in Eq. (2). For large  $\bar{m}$ , the cosmological evolution becomes more similar to the constant coupling case. The short-lived overdensities are more concentrated and massive, and a reliable numerical treatment of the violent oscillatory behavior in combination with these

concentrated lumps has not yet succeeded. For small  $\bar{m}$ , the neutrinos are lighter and accelerate to highly relativistic velocities in the process of the formation and dissolution of the short-lived overdensities. Our method is not yet capable of accurately resolving the collective motion of neutrinos very close to the speed of light.

The results presented at this stage are thus obtained for an exemplary set of parameters. They will be followed by more comprehensive studies once the numerical methods are sufficiently refined. The neutrino mass parameter  $\bar{m}$  is chosen as  $\bar{m} = 0.5 \times 10^{-3}$  eV corresponding to a present-day neutrino mass  $m_\nu(t_0) \approx 0.2$  eV. In the exponential potential of the cosmon, we choose  $\alpha = 10$ . The comoving box of size  $V = (600h^{-1} \text{ Mpc})^3$  is divided into  $N_c = 128^3$  cells. The number of effective neutrino and matter particles is chosen equal to the number of cells,  $N_\nu = N_m = N_c$ . The simulation starts for matter at  $a_{\text{ini},m} = 0.02$  and adds neutrinos at  $a_{\text{ini},\nu} = 0.15$ . The initial perturbations are characterized by a nearly scale invariant spectrum,  $n_s = 0.96$ , with scalar amplitude  $A_s = 2.3 \times 10^{-9}$  at the pivot scale  $k_{\text{pivot}} = 0.05 \text{ Mpc}^{-1}$ .

The form of the coupling  $\beta(\varphi)$  is not restricted to the one in Eq. (3). As long as it is increasing steeply with the field, we expect a cosmology similar to the one discussed in this paper. In particular we expect oscillating neutrino perturbations. The constant coupling model and the presented field-dependent coupling model can be seen as two extreme cases. Between these two cases we expect models with a moderate field dependence of the coupling, in which the lumps are more stable than in the varying coupling model, but not as concentrated as in the constant coupling model. Those models might still have a realistic overall cosmology, but also interesting and observable deviations from a  $\Lambda$ CDM-like cosmology.

#### A. Cosmic neutrinos

One cycle of disappearance and reappearance of mildly nonlinear neutrino overdensities is shown in Fig. 5. Large-scale neutrino lumps have formed at  $a = 0.45$ . At the intermediate scale factor  $a = 0.475$ , however, the neutrino distribution again is almost homogeneous. Shortly afterwards, the overdensities appear again. Even in their centers, neutrino lumps hardly reach density contrasts above order 10. The number of structures within the whole  $600h^{-1}$  Mpc simulation box is very small. The overdensities thus form on a scale of roughly  $\lambda \sim 100h^{-1}$  Mpc. This is similar to the constant coupling model in which, however, the lumps subsequently shrink to the size of several megaparsecs and subhalos form [16]. In order to guarantee that the simulation box is a representative cosmological volume and to generally avoid box size effects, a larger simulation box would be desirable. Due to the corresponding loss of resolution or, if more cells are used, the increased numerical effort, this analysis is postponed to future work. Our

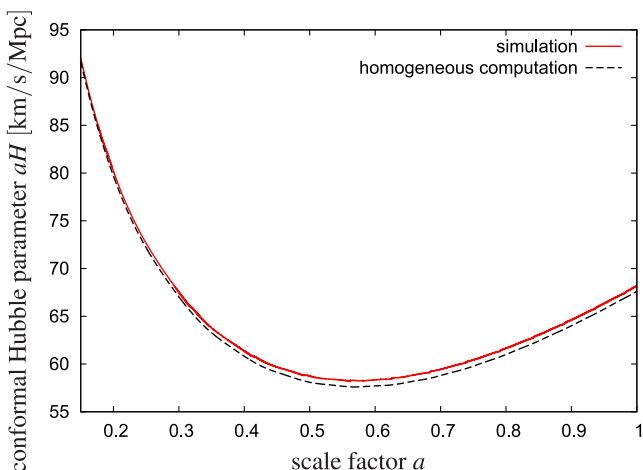


FIG. 4. The conformal Hubble parameter  $aH$  calculated using the simulation (red solid line) compared to the homogeneous computation (black dashed line). The backreaction effects of the neutrino lumps on the expansion history are small.

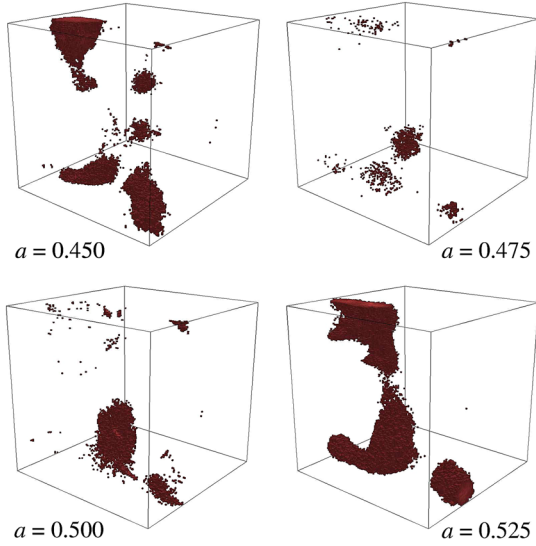


FIG. 5. Forming and dissolving mildly nonlinear neutrino overdensities. Simulation cells with a neutrino number density contrast  $n_\nu/\bar{n}_\nu \geq 5$  are marked red.

preliminary tests indicate that our findings are robust with respect to box size.

A period of overdensity formation is initiated by a low neutrino equation of state  $w_\nu \approx 0$ . As discussed in the context of the neutrino equation of motion, Eq. (7), the bending of neutrino trajectories and therefore the formation of neutrino overdensities is most effective in this case. The effect is strengthened when the cosmon  $\bar{\varphi}$  has come close to the critical value  $\varphi_{\text{crit}}$  implying large neutrino masses by Eq. (2) and according to Eq. (3) a strong coupling. During the formation of lumps the coupling is enhanced compared to other periods by a factor of about  $6^2$ , where both the mass and the coupling contribute the same factor. This adds to the effect of vanishing pressure.

After the stage of neutrino lump formation, the cosmon “bounces” against the barrier, and  $\dot{\bar{\varphi}}$  switches sign becoming negative. The cosmon acceleration  $\propto \beta\dot{\bar{\varphi}} - 2H$  in Eq. (8) becomes then positive. Rather than as a damping, it acts as an accelerant and leads to relativistic neutrino velocities high enough such that the neutrinos fly out of the lumps. Consequently, a period of lump formation is followed by a period of lump dissolution. Subsequently,  $\dot{\bar{\varphi}}$  turns again positive due to the gradient of the cosmon potential and a new period of lump formation begins.

These cycles of slowdown and speedup are visualized in Fig. 6. None of these oscillatory features are visible in a purely homogeneous calculation, which would predict a neutrino equation of state very close to zero. It is the proper treatment of nonlinear perturbations that uncovers why the instability of neutrino perturbations is not “catastrophic” [19]. The instability, only present for nonrelativistic neutrinos and leading to the formation of neutrino lumps, is counteracted by the neutrinos

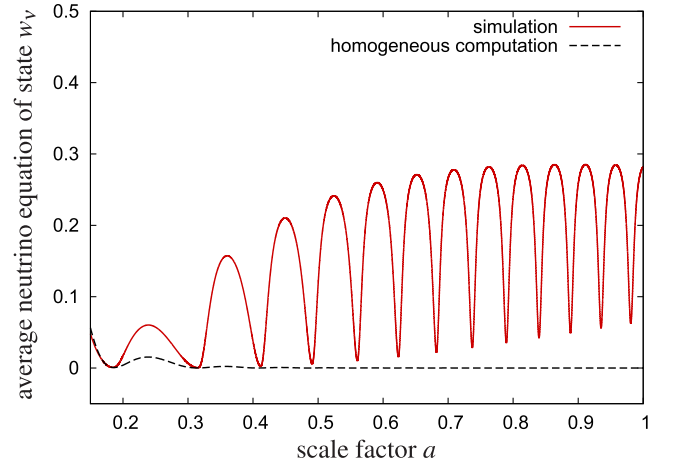


FIG. 6. Evolution of the average equation of state  $w_\nu$  of neutrinos in the simulation (red solid line) as compared to a purely homogeneous computation (black dashed line).

turning relativistic again. This constitutes a nonlinear stabilization mechanism.

## B. Dark energy

The periods of nonrelativistic neutrino velocities  $w_\nu \approx 0$  are essential for stopping the evolution of the cosmon and ensuring a phase of accelerated expansion (cf. Sec. II A). The periodically reached relativistic neutrino velocities render the stopping mechanism slightly less effective as they suppress the coupling term  $\propto T_{(\nu)\lambda}^\lambda$  in Eq. (6). This is visible in the evolution of the cosmon equation of state  $w_\varphi$ , cf. Fig. 7. The equation of state  $w_\varphi$  approaches the cosmological constant value  $w_\Lambda = -1$  although the full simulation taking the effect of periodically relativistic neutrino velocities into account approaches this value a

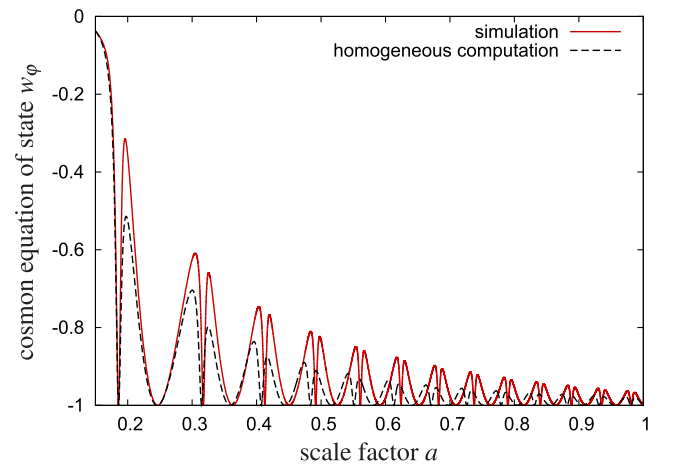


FIG. 7. Evolution of the equation of state  $w_\varphi$  of dark energy in the simulation (red solid line) and in a homogeneous computation (black dashed line). The double peak structure reflects the oscillation of  $\varphi$  in an effective potential.

bit more slowly. Albeit clearly visible, this backreaction effect does not significantly postpone the onset of the accelerated expansion as seen in Fig. 1.

The oscillations in Fig. 7 show a simple pattern. Repeatedly,  $w_\varphi$  reaches the value  $-1$ . These are turning points where  $\bar{\varphi}$  switches sign and thus encounters a zero where  $w_\varphi = -1$  holds exactly. Narrow and wide minima alternate. The narrow minima occur when  $\bar{\varphi}$  bounces against the steep barrier at  $\varphi_{\text{crit}}$ . The wide minima are related to the other turning point when  $\bar{\varphi}$  has climbed the gently inclined scalar self-interaction potential  $V(\bar{\varphi})$ . The decay of the oscillation amplitude for growing  $a$  is a consequence of the damping term  $3H\dot{\bar{\varphi}}$  in Eq. (16).

The evolution of the cosmon  $\bar{\varphi}$  is reflected in the evolution of the coupling parameter  $\beta(\bar{\varphi})$  and the average neutrino mass  $m_\nu(\bar{\varphi})$ , cf. Fig. 8. They are both proportional to the inverse of  $\varphi_{\text{crit}} - \bar{\varphi}$  (which is the distance to the barrier), Eqs. (3) and (2), and reach extrema at the turning points of  $\bar{\varphi}$ . As the cosmon perturbations  $\delta\varphi$  remain small,

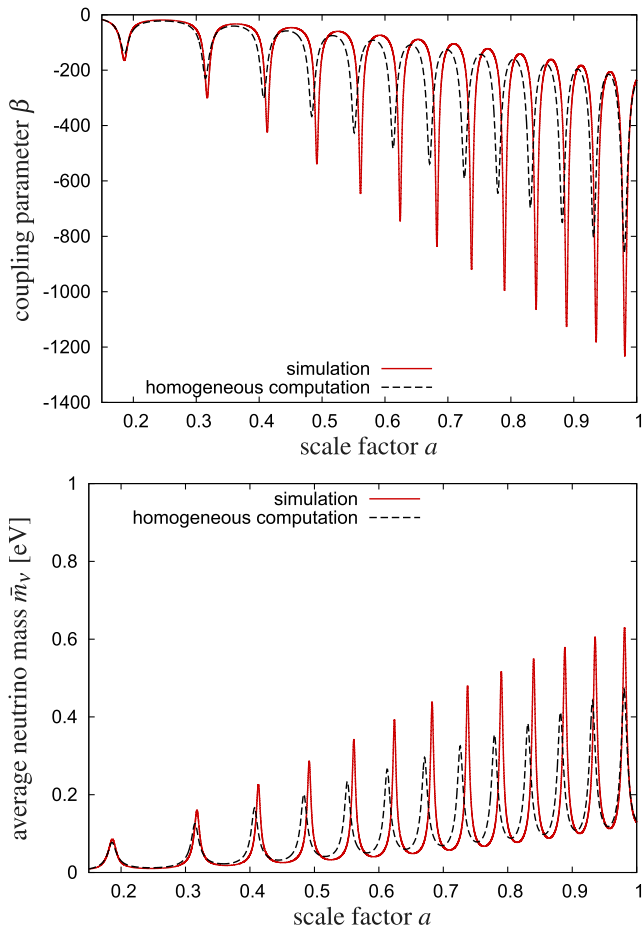


FIG. 8. Evolution of the coupling parameter  $\beta(\varphi)$  and the average neutrino mass  $\overline{m_\nu(\varphi)}$  in the simulation (red solid line) as compared to a purely homogeneous computation (black dashed line). The nonlinear effects (backreaction) enhance the peaks and lead to a small shift.

it is justified to assume  $\overline{\beta(\varphi)} \approx \beta(\bar{\varphi})$  and  $\overline{m_\nu(\varphi)} \approx m_\nu(\bar{\varphi})$  for the averages; this is different from the constant coupling case, cf. Sec. II B. Figure 8 tells us that the backreaction effect is most pronounced at the cusps of the plots. The coupling reaches values  $\beta \approx -1.2 \times 10^3$ , and the highest average neutrino mass is  $m_\nu \approx 0.6$  eV. At the opposite point of the oscillation, the coupling parameter is around  $\beta \approx -2 \times 10^2$ , and the mass is at  $m_\nu \approx 0.1$  eV. As the precise oscillatory pattern will sensitively depend on the chosen model parameters, we conclude that the varying coupling model will not predict a precise value for the present-day neutrino mass but rather a range.

### C. Neutrino lump gravitational potential

The only way for cosmological observations to detect the large neutrino overdensities is via the effects of their gravitational potentials. These gravitational potentials have an impact on the evolution of CDM perturbations, in particular on the peculiar velocity field [37]. More important, they can leave direct observational traces on the cosmic microwave background via the Integrated-Sachs-Wolf effect. The quantitative results on these gravitational potentials will thus ultimately decide whether the GNQ model will prove viable in light of various observational constraints. Although answering this question is beyond the scope of this work as it requires an exploration of the model's parameter space, we show the results obtained for the exemplary set of parameters employed here in Fig. 9. The neutrino-induced gravitational potential  $\Phi_\nu$  is subdominant, by 2 orders of magnitude, compared to the CDM potential  $\Phi_m$ . More precisely, the figure shows the dimensionless spectra  $\Phi_\nu(k)$ ,  $\Phi_m(k)$  (cf. also Ref. [16]).

Between the different comoving scales, we observe a phase shift. During the dissolution process, small scales are washed out more rapidly than large scales. Inversely, during the formation process, small-scale perturbations build up faster.

Even though the neutrino-induced gravitational potential is small at late time the neutrinos could have a more substantial effect on the density perturbations over time. For example such a cumulative effect happens for standard massive neutrinos which suppress the growth of density perturbations on small scales [40,41]. We do not expect an effect of similar size in GNQ from the neutrino perturbations. Before the neutrinos become nonrelativistic the only difference to  $\Lambda$ CDM with relativistic neutrinos is the presence of a dynamical early dark energy component which suppresses the growth of matter perturbations compared to  $\Lambda$ CDM. This is small for a large enough parameter  $\alpha$  in the cosmon potential. Neutrino perturbations are only important at late times after neutrinos became nonrelativistic. Since the formation of neutrino structures is dominated by the cosmon-neutrino interaction, we can get an estimate of the effect of neutrino perturbations on the matter perturbations by running a simulation in which the

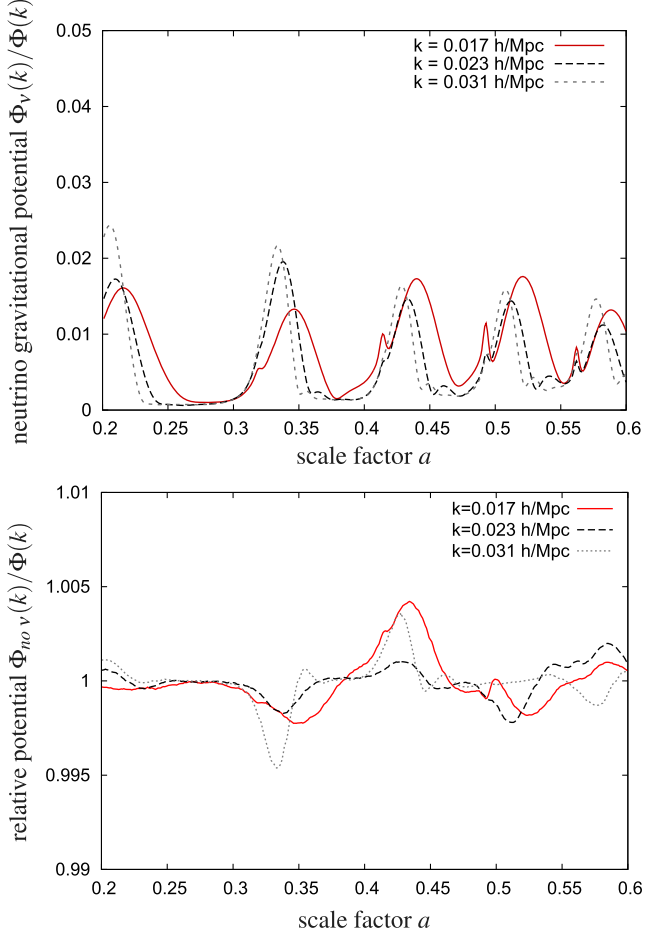


FIG. 9. Top: Comparison between the neutrino-induced gravitational potential  $\Phi_{\nu}$  and the total gravitational potential  $\Phi$  during the first oscillations at three large comoving scales. Bottom: Comparison of the total gravitational potential obtained from a simulation in which the Poisson equation is not sourced by the neutrinos, with the one obtained from the full simulation. The overall effect of the varying neutrino masses on the gravitational potential remains on the subpercent level.

neutrinos do not source the Poisson equation for the gravitational potential. As the lower plot of Fig. 9 shows, the effect of the neutrinos on the matter is on the subpercent level.

We find that, for most of the cosmic history, the cosmon-induced gravitational potential is one order of magnitude smaller than the one induced by neutrinos. Only around  $a = 1$  on large scales, it becomes comparable to the one induced by neutrinos.

## V. PHYSICAL PICTURE

### A. Effective cosmon dynamics

Our aim is an analytic understanding of the time evolution of the average cosmon field  $\bar{\varphi}$  in the presence of inhomogeneous and possibly rapidly moving neutrinos. For this purpose, we employ an effective potential  $V_{\text{eff}}(\bar{\varphi})$

which depends, in addition to  $\bar{\varphi}$ , also on a characteristic neutrino momentum  $p$  and the average neutrino density  $\bar{n}_{\nu}$ . Both  $p$  and  $\bar{n}_{\nu}$  may depend on the scale factor  $a$  or other cosmological quantities, but are assumed to show no explicit dependence on  $\bar{\varphi}$ . The time evolution of  $\bar{\varphi}$  will then be governed by the equation of motion

$$\ddot{\bar{\varphi}} + 3H\dot{\bar{\varphi}} + V_{\text{eff},\bar{\varphi}}(\bar{\varphi}) = 0. \quad (24)$$

The derivative  $V_{\text{eff},\bar{\varphi}}$  is composed of the self-interaction part  $V_{,\bar{\varphi}}$  and a contribution from the cosmon-neutrino interaction given by the right-hand side of Eq. (16),

$$V_{\text{eff},\bar{\varphi}}(\bar{\varphi}) = V_{,\bar{\varphi}}(\bar{\varphi}) + \overline{\beta T_{(\nu)}}. \quad (25)$$

For an estimate of the coupling term, we assume that it can be written in the form

$$\overline{\beta T_{(\nu)}} = \frac{\partial \bar{m}_{\nu}(\bar{\varphi}) \bar{n}_{\nu}}{\partial \bar{\varphi} \bar{\gamma}}, \quad (26)$$

with  $\bar{m}_{\nu}(\bar{\varphi})$  the average neutrino mass and  $\bar{n}_{\nu}(a) \propto a^{-3}$  the (known) average neutrino number density. The exact formula would be a sum over individual particle contributions, where the right-hand side for each particle is just as in Eq. (26) if we replace  $\bar{\gamma}$  by the usual Lorentz factor  $\gamma$  (cf. Ref. [16]). The effective Lorentz factor  $\bar{\gamma}$  is assumed to depend on  $\bar{\varphi}$  only through  $\bar{m}_{\nu}(\bar{\varphi})$ . Then, dimensional analysis implies that  $\bar{\gamma}$  is a function of the combination  $p^2/\bar{m}_{\nu}^2(\bar{\varphi})$ , where  $\mathbf{p}$  is some appropriate characteristic momentum for the neutrinos and  $p = \sqrt{\mathbf{p}^2}$ . In principle, the difference between the average of  $\partial m_{\nu}/\partial \varphi$  and  $\partial \bar{m}_{\nu}/\partial \bar{\varphi}$  is included in the factor  $\bar{\gamma}$ . For the present scenario, our numerical simulations show that these two quantities are approximately equal since the neutrino density perturbation sourcing the cosmon perturbation  $\delta\varphi$  never reaches large values during the cosmic evolution.

The effective potential can now be defined as

$$V_{\text{eff}}(\bar{\varphi}) = V(\bar{\varphi}) + \bar{n}_{\nu} \bar{m}_{\nu}(\bar{\varphi}) \hat{\gamma}, \quad (27)$$

with  $\hat{\gamma}$  related to  $\bar{\gamma}$  by

$$\hat{\gamma} + \frac{\partial \hat{\gamma}}{\partial \ln \bar{m}_{\nu}} = \frac{1}{\bar{\gamma}}. \quad (28)$$

Employing that  $\hat{\gamma}$  is a dimensionless function of  $p^2/\bar{m}_{\nu}^2$ , Eq. (28) follows directly from Eq. (24) and the definition of  $\bar{\gamma}$  by Eq. (26). For the case of a free particle with

$$\bar{\gamma}^2 = 1 + \frac{p^2}{\bar{m}_{\nu}^2(\bar{\varphi})}, \quad (29)$$

one obtains  $\hat{\gamma} = \bar{\gamma}$ . For more general momentum distributions of neutrinos, the functions  $\bar{\gamma}(p^2/\bar{m}_{\nu}^2)$  and  $\hat{\gamma}(p^2/\bar{m}_{\nu}^2)$

may be somewhat more complicated, but the qualitative relation remains similar.

We next need to understand the time evolution of the characteristic neutrino momentum  $p$ . We distinguish for each oscillation period two stages. The first stage is characterized by the importance of inhomogeneities in the cosmon field, occurring when  $\bar{\varphi}$  is close to the critical value  $\varphi_{\text{crit}}$ . There, the neutrino mass is close to its maximum, and  $p^2 \ll \bar{m}_\nu^2(\bar{\varphi})$  such that  $\bar{\gamma} \approx \hat{\gamma} \approx 1$ . The spatial cosmon gradients in the neutrino equation of motion, Eq. (7), lead to the growth of  $p^2$  and to the formation of neutrino overdensities. We identify a second stage when  $\bar{\varphi}$  is no longer close to  $\varphi_{\text{crit}}$ . Here, inhomogeneities in the cosmon field are no longer decisive, and the overall dynamics is dominated by cosmon acceleration. We will argue that, for this second stage,  $p^2$  is (almost) conserved. The effective potential  $V_{\text{eff}}(\bar{\varphi})$  then only depends on the value of  $p^2$  that has been reached during the first stage.

For a single particle in a homogeneous background, the combination  $\mathbf{p}/a$  is conserved due to translation symmetry. In the absence of gravity (for constant  $a$ ), this follows directly from the neutrino equation of motion, Eq. (7), in the case where spatial gradients of  $\varphi$  can be neglected,

$$\frac{d\mathbf{u}^k}{dt} = \beta(\bar{\varphi})\dot{\bar{\varphi}}\mathbf{u}^k. \quad (30)$$

This equation of motion conserves the relativistic momentum  $\mathbf{p} = m_\nu(\bar{\varphi})\mathbf{u}$ . Beyond small effects from the expanding scale factor, any additional change of  $p$  has to arise from inhomogeneities. These are small during the second stage.

We plot, in Fig. 10, the effective potential given by Eq. (29), taking the parameters from the simulation around

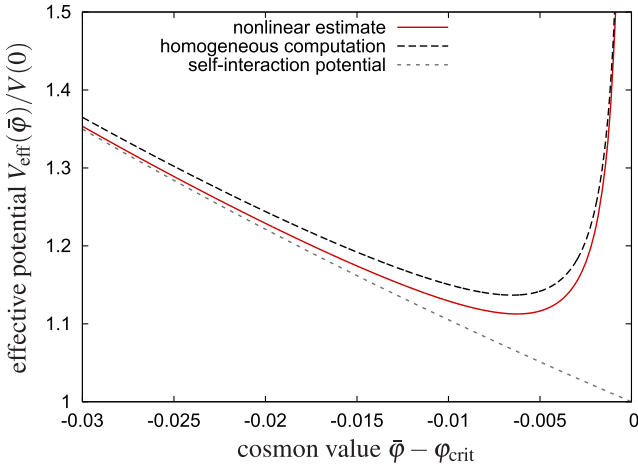


FIG. 10. Effective cosmon potential  $V_{\text{eff}}(\bar{\varphi})$  for the nonlinear (red solid) and the homogeneous case (black dashed). For comparison, we also show the self-interaction potential  $V(\bar{\varphi})$  (gray dotted) without the effects of the cosmon-neutrino coupling. Units of  $V$  are set by the normalization factor  $V(0) = 1.06 \times 10^{-7} \text{ Mpc}^{-2}$ .

the oscillation at  $a \approx 0.5$ . The homogeneous computation that we show as a comparison employs  $p = 0$ . The cosmon  $\bar{\varphi}$  oscillates around the minimum of the effective potential according to the effective equation of motion, Eq. (24). The asymmetry of the effective potential explains the double peak structure discussed in Sec. IV B.

The identification of the characteristic neutrino momentum  $p$  as the decisive parameter for the cosmon dynamics opens the door to effective descriptions no longer relying on a full cosmological simulation. For example, the momentum buildup during overdensity formation might be estimated in a suitable spherical collapse approach [42] or even with an adaption of linear perturbation theory. A detailed investigation of these routes is beyond the scope of this paper and left for future work.

## B. Effective neutrino dynamics

Within the structure formation cycle, we consider first the period of approximate homogeneity for which the cosmon acceleration has violently disrupted the previously formed overdensities. During this period, the effects of the mutual attraction of the neutrinos are suppressed due to their relativistic velocities. The decisive conserved quantity is the relativistic momentum  $p$  whose value is determined by the preceding period of overdensity formation. Of course,  $p$  shrinks due to the ordinary Hubble damping, but this effect is small because it is linked to a much larger time scale,  $1/H$ , as compared to the dynamic time scale of the cosmon-neutrino coupling, which is  $1/|\beta\dot{\bar{\varphi}}|$ . During this approximately homogeneous phase, the neutrinos influence the cosmon evolution via the effective potential  $V_{\text{eff}}(\bar{\varphi}; p)$  according to Eq. (24). For large enough  $\varphi_{\text{crit}} - \bar{\varphi}$ , there will be a turnaround with  $\bar{\varphi}$  increasing subsequently until a new phase of lump formation sets in.

The cosmon and the neutrinos can exchange energy. As a consequence the cosmon energy density is slightly decreasing. This is compensated by a slightly increasing neutrino energy density (cf. Fig. 1), so that the total energy density of the cosmon-neutrino fluid is constant. This effect can be taken into account by an increasing effective potential. This increase happens on a time scale of the order of  $1/H$  and has only a small quantitative influence.

We next discuss the phase of lump formation. During this phase, the influence of neutrino inhomogeneities on the effective potential  $V_{\text{eff}}(\bar{\varphi}; p)$  is small, and we may use the homogeneous computation ( $p = 0$ ). Indeed, when  $\bar{\varphi}$  comes close to  $\varphi_{\text{crit}}$  (where overdensities form), the neutrinos become nonrelativistic due to their rapidly growing masses, and the homogeneous computation of  $V_{\text{eff}}$  is fairly accurate. In principle, the validity of the homogeneous computation could be spoiled by the type of backreaction effects encountered in the constant coupling model, cf. Sec. II B, where the local cosmon value effectively freezes and no longer follows the homogeneous component. We do not

observe these effects, here, since the neutrino overdensities never become large.

Taking things together, we end with a rather simple qualitative understanding of the role of nonlinearities. The evolution of the cosmon average field  $\bar{\varphi}$  is rather independent of the details of the lump formation process. We only need to understand the small increase of the characteristic neutrino momentum  $p$  during each phase of lump formation. On the other hand, for the stages of lump formation, the cosmon field dynamics can be approximated by neglecting the backreaction effects (e.g.  $p = 0$  in  $V_{\text{eff}}$ ).

The details of the stages of lump dissolution are not crucial because the overall picture there is just given by the conservation of the momentum distribution  $f(\mathbf{p})$ . The latter provides an explanation for some of the observations made in Sec. IV A. Not only did the lumps periodically appear and disappear—they occurred roughly in a similar shape as in the preceding period. Furthermore, the periodic minima in the neutrino equation of state  $w_\nu$ , cf. Fig. 6, reach higher values every time rather than always shrinking to  $w_\nu = 0$ . This cannot be explained by the spatial distribution of the neutrino density which is, to a very good approximation, homogeneous after each dissolution phase. It is the conservation of the neutrino momentum distribution  $f(\mathbf{p})$  during the dissolution process that tells us that the overdensity formation process does not start from a clean state. When the overdensities are just to form again, the neutrino velocities are already pointing to the—previous and next—overdensities' centers. The momentum buildup during overdensity formation then adds up with the preceding momentum. In each iteration, the momentum thus takes on larger values, and the equation of state after overdensity formation has increased compared to the last iteration.

Rather than describing the process of overdensity formation in an adapted linear perturbation theory or spherical collapse scheme, we content ourselves here with a brief qualitative discussion explaining the main effects. This will make plausible our finding that the neutrino-induced gravitational potentials remain small compared to those of CDM (cf. Fig. 9). A refined analysis will be the subject of future work. The overdensities form when the cosmon comes close to  $\varphi_{\text{crit}}$ , the barrier in the effective potential  $V_{\text{eff}}$ . The spatial cosmon gradients become important compared to the time derivative. The coupling parameter  $\beta$  reaches order  $-10^3$ , cf. Fig. 8.

Although the resulting forces on the neutrinos are  $2\beta^2 \sim 10^6$  times stronger than gravity, several factors hinder the formation of highly concentrated lumps. First, the period of time during which the cosmon is close to  $\varphi_{\text{crit}}$  and the neutrinos are nonrelativistic is limited to roughly  $\Delta a \sim 10^{-2}$ , cf. Figs. 6 and 7. The nonrelativistic neutrinos are not fast enough to form overdensities beyond roughly  $\delta_\nu \sim 10^{-2}$  as seen in the simulation. After the cosmon has bounced against the barrier and  $\dot{\bar{\varphi}}$  is negative, the cosmon acceleration increases all neutrino velocities along their

respective directions of motion. At first, the overdensities continue to grow as the neutrino velocities were on average, during the nonrelativistic period, targeting towards the centers of the forming overdensities. This explains why the maxima of the neutrino-induced gravitational potential occur at later times than the bouncing of  $\bar{\varphi}$  against the barrier, cf. Fig. 9. However, during the cosmon acceleration, the neutrino masses rapidly decrease. Consequently, although the number overdensities grow, the effect on the gravitational potential is only moderate. At its maxima, the large-scale gravitational potential induced by neutrinos is only at the percent level compared to the CDM potential.

For small scales, the neutrinos form even less overdensities compared to  $\delta_m$ . The relative importance of the neutrino gravitational potential therefore decreases towards smaller length scales.

## VI. CONCLUSION

The growing neutrino quintessence model with a field-dependent coupling  $\beta(\varphi)$  shows violent nonlinear dynamics of the coupled cosmon-neutrino fluid, and yet an overall phenomenology similar to the standard  $\Lambda$ CDM picture. The accelerated expansion is almost the same as for  $\Lambda$ CDM (cf. Fig. 1), while large-scale neutrino overdensities remain small enough so that their induced gravitational potentials are subdominant to those of cold dark matter. At the fundamental level, however, the model is not anywhere near  $\Lambda$ CDM. Rather than being a parameter, the present dark energy density results from the stop of a scaling solution by a cosmological trigger event, namely neutrinos becoming nonrelativistic. In the process, the coupling parameter between the neutrinos and dark energy dynamically reaches order  $\beta(\varphi) \sim -10^3$  (cf. Fig. 8), inducing an attraction between neutrinos  $10^6$  times stronger than gravity. This may serve as an example that a standard overall phenomenology still leaves room for new physics, without unnaturally small parameters.

The average neutrino mass  $m_\nu$  is small in the early Universe. For most of the cosmological evolution, the dark energy scalar field rolls down steadily its potential towards larger values, and the average neutrino mass grows with time. In the recent epoch, however, the cosmon field value oscillates and so do the neutrino masses. For the investigated parameters,  $m_\nu$  oscillates between about 0.15 and 0.6 eV (cf. Fig. 8). Nonrelativistic neutrinos experience an attractive force due to the coupling  $\beta(\varphi)$  substantially stronger than gravity. Furthermore, Hubble damping is replaced by cosmon acceleration.

The violent nonlinear behavior of neutrino perturbations manifests itself in the repeated rapid formation and dissolution of large-scale overdensities (cf. Fig. 5). Rather than becoming nonrelativistic once and for all, the neutrinos are accelerated to relativistic velocities periodically (cf. Fig. 6). This effectively stabilizes the evolution of perturbations, and the “catastrophic” instability first

discussed in the context of MaVaNs is avoided [19]. The (short-lived) overdensities induce oscillating gravitational potentials, whose relative strength compared to those of cold dark matter remains at the percent level (cf. Fig. 9).

By virtue of the coupling between dark energy and the neutrinos, the nonlinear dynamics of neutrino perturbations exert a backreaction effect on the evolution of dark energy at the background level. Relativistic neutrino velocities reduce the strength of the effect of the coupling and thereby weaken the dark energy stopping mechanism. Although the backreaction is clearly visible quantitatively for the equations of state of individual components, it does not alter the qualitative picture with a usual crossover to the accelerated expansion epoch (cf. Fig. 7). For our parameter set, the backreaction effect becomes negligible for the evolution of the overall energy fraction for the coupled cosmon-neutrino fluid which constitutes dark energy, see Fig. 1. This finding is in contrast to the constant coupling model in which stable neutrino lumps form and effectively decouple from the homogeneous component. There, a much stronger backreaction effect substantially postpones the onset of the accelerated expansion [16] and makes it difficult to find realistic models [43].

We have obtained our numerical results from an  $N$ -body-based simulation technique [16], specifically developed for the growing neutrino quintessence model, together with a Newton-Gauß-Seidel solver for the local dark energy perturbations [38]. Our method (described in Sec. III) has allowed us to show, for the first time, the nonlinear evolution of the model until redshift zero. Earlier attempts had to stop at  $z \approx 1$  and were restricted to the technically simpler constant coupling model [16,36]. Still, the very strong coupling parameters and the violent perturbation evolution have so far prevented a scan of the model's parameter space for the field-dependent coupling model. This, however, would be a decisive step towards a confrontation of the model with observational constraints. Further efforts are required to render the numerical method faster and more robust.

A complementary road consists in a semianalytical approach allowing for a simplified yet reliable description of the cosmological dynamics. In the constant coupling model, this had inspired the physical picture of a cosmon-neutrino lump fluid [17]. We have laid the ground here for such an effective description of the field-dependent coupling model, whose cornerstones we have explained in Sec. V. In periods during which the cosmon evolves rapidly, the neutrino momenta are approximately conserved. This conservation has enabled us to define an effective

self-interaction potential for the scalar field  $V_{\text{eff}}(\varphi)$  (cf. Fig. 10) that fully describes the evolution of the homogeneous dark energy. For the neutrino component, our findings motivate an adapted spherical collapse approach that would allow us to estimate the momentum buildup during the overdensity formation process. Such a semianalytical approach will be shaped along with the continuing work on the numerical simulation method.

Despite the important steps still to be done, the overall picture for the confrontation of growing neutrino quintessence with observations already takes a clear shape. For the varying coupling  $\beta(\varphi)$  and the parameter set chosen for the present paper, the background evolution is essentially indistinguishable from the  $\Lambda$ CDM model. (The small fraction of early dark energy can be further reduced by a larger value of the parameter  $\alpha$ .) Also the gravitational potential induced by the neutrino lumps seems too small for an easy observational detection. Such models appear to be compatible with present observations to the same degree as  $\Lambda$ CDM. On the other side, the models with constant coupling  $\beta$  may allow for parameters such that the present dark energy can be adjusted to the observed value. In this case, we expect much stronger neutrino-induced gravitational potentials observable by the Integrated-Sachs-Wolf effect or other tests. It is obvious that, for part of the parameter space, growing neutrino quintessence deviates substantially from observation and the  $\Lambda$ CDM model. Large parameter regions lie between the two extremes. They will allow for clear signals for future observations without being inconsistent with present observations. The cosmic neutrino background may finally become observable.

## ACKNOWLEDGMENTS

The authors are thankful to Valeria Pettorino and Santiago Casas for numerous inspiring discussions and ideas. They would also like to thank Luca Amendola, Volker Springel, and Maik Weber for valuable suggestions, and David Mota for providing his numerical implementation of linear perturbation theory in GNQ. F. F. acknowledges support from the IMPRS-PTFS and the DFG through the TRR33 project “The Dark Universe.” M. B. is supported by the Marie Curie Intra European Fellowship “SIDUN” within the 7th Framework Programme of the European Commission. E. P. acknowledges support by the DFG through TRR33 and by the ERC grant “The Emergence of Structure during the Epoch of Reionization.”

- [1] S. Perlmutter, G. Aldering, G. Goldhaber, R. Knop, P. Nugent *et al.* (Supernova Cosmology Project), *Astrophys. J.* **517**, 565 (1999).
- [2] A. G. Riess, A. V. Filippenko, P. Challis, A. Clocchiatti, A. Diercks *et al.* (Supernova Search Team), *Astron. J.* **116**, 1009 (1998).
- [3] M. Bartelmann, *Rev. Mod. Phys.* **82**, 331 (2010).
- [4] E. J. Copeland, M. Sami, and S. Tsujikawa, *Int. J. Mod. Phys. D* **15**, 1753 (2006).
- [5] L. Amendola, M. Baldi, and C. Wetterich, *Phys. Rev. D* **78**, 023015 (2008).
- [6] C. Wetterich, *Phys. Lett. B* **655**, 201 (2007).
- [7] S. Weinberg, *Rev. Mod. Phys.* **61**, 1 (1989).
- [8] S. M. Carroll, *Living Rev. Relativity* **4**, 1 (2001).
- [9] D. Mota, V. Pettorino, G. Robbers, and C. Wetterich, *Phys. Lett. B* **663**, 160 (2008).
- [10] C. Wetterich, *Nucl. Phys.* **B302**, 668 (1988).
- [11] B. Ratra and P. Peebles, *Phys. Rev. D* **37**, 3406 (1988).
- [12] C. Wetterich, *Phys. Dark Univ.* **2**, 184 (2013).
- [13] C. Wetterich, *Phys. Rev. D* **90**, 043520 (2014).
- [14] C. Wetterich, *Nucl. Phys. B*, **897**, 111 (2015).
- [15] V. Pettorino, N. Wintergerst, L. Amendola, and C. Wetterich, *Phys. Rev. D* **82**, 123001 (2010).
- [16] Y. Ayaita, M. Weber, and C. Wetterich, *Phys. Rev. D* **85**, 123010 (2012).
- [17] Y. Ayaita, M. Weber, and C. Wetterich, *Phys. Rev. D* **87**, 043519 (2013).
- [18] R. Fardon, A. E. Nelson, and N. Weiner, *J. Cosmol. Astropart. Phys.* **10** (2004) 005.
- [19] N. Afshordi, M. Zaldarriaga, and K. Kohri, *Phys. Rev. D* **72**, 065024 (2005).
- [20] O. E. Bjaelde, A. W. Brookfield, C. van de Bruck, S. Hannestad, D. F. Mota, L. Schrempp, and D. Tocchini-Valentini, *J. Cosmol. Astropart. Phys.* **01** (2008) 026.
- [21] N. Brouzakis, N. Tetradis, and C. Wetterich, *Phys. Lett. B* **665**, 131 (2008).
- [22] C. Wetterich, *Phys. Rev. D* **77**, 103505 (2008).
- [23] M. Doran, G. Robbers, and C. Wetterich, *Phys. Rev. D* **75**, 023003 (2007).
- [24] C. L. Reichardt, R. de Putter, O. Zahn, and Z. Hou, *Astrophys. J.* **749**, L9 (2012).
- [25] V. Pettorino, L. Amendola, and C. Wetterich, *Phys. Rev. D* **87**, 083009 (2013).
- [26] M. Magg and C. Wetterich, *Phys. Lett.* **94B**, 61 (1980).
- [27] G. Lazarides, Q. Shafi, and C. Wetterich, *Nucl. Phys.* **B181**, 287 (1981).
- [28] R. N. Mohapatra and G. Senjanovic, *Phys. Rev. D* **23**, 165 (1981).
- [29] J. Schechter and J. Valle, *Phys. Rev. D* **22**, 2227 (1980).
- [30] C. Wetterich, *Nucl. Phys.* **B897**, 111 (2015).
- [31] C. Wetterich, *Astron. Astrophys.* **301**, 321 (1995).
- [32] L. Amendola, *Phys. Rev. D* **62**, 043511 (2000).
- [33] N. Wintergerst, V. Pettorino, D. Mota, and C. Wetterich, *Phys. Rev. D* **81**, 063525 (2010).
- [34] L. Schrempp and I. Brown, *J. Cosmol. Astropart. Phys.* **05** (2010) 023.
- [35] N. J. Nunes, L. Schrempp, and C. Wetterich, *Phys. Rev. D* **83**, 083523 (2011).
- [36] M. Baldi, V. Pettorino, L. Amendola, and C. Wetterich, *Mon. Not. R. Astron. Soc.* **418**, 214 (2011).
- [37] Y. Ayaita, M. Weber, and C. Wetterich, [arXiv:0908.2903](https://arxiv.org/abs/0908.2903).
- [38] E. Puchwein, M. Baldi, and V. Springel, *Mon. Not. R. Astron. Soc.* **436**, 348 (2013).
- [39] H. Oyaizu, *Phys. Rev. D* **78**, 123523 (2008).
- [40] J. Lesgourgues and S. Pastor, *Phys. Rep.* **429**, 307 (2006).
- [41] Y. Y. Wong, *Annu. Rev. Nucl. Part. Sci.* **61**, 69 (2011).
- [42] N. Wintergerst and V. Pettorino, *Phys. Rev. D* **82**, 103516 (2010).
- [43] F. Führer and C. Wetterich, *Phys. Rev. D* **91**, 123542 (2015).

## Backreaction in Growing Neutrino Quintessence



**Backreaction in growing neutrino quintessence**

Florian Führer\* and Christof Wetterich

*Institut für Theoretische Physik, Universität Heidelberg,  
Philosophenweg 16, D-69120 Heidelberg, Germany  
(Received 13 April 2015; published 30 June 2015)*

We investigate the cosmological effects of neutrino lumps in growing neutrino quintessence. The strongly nonlinear effects are resolved by means of numerical N-body simulations which include relativistic particles, nonlinear scalar field equations, and backreaction effects. For the investigated models with a constant coupling between the scalar field and the neutrinos, the backreaction effects are so strong that a realistic cosmology is hard to realize. This points toward the necessity of a field-dependent coupling in growing neutrino quintessence. In this case realistic models of dynamical dark energy exist which are testable by the observation or nonobservation of large neutrino lumps.

DOI: [10.1103/PhysRevD.91.123542](https://doi.org/10.1103/PhysRevD.91.123542)

PACS numbers: 98.80.-k, 95.36.+x

**I. INTRODUCTION**

The origin of the observed accelerated expansion of the Universe is still unknown [1,2]. It is usually accounted for by a dark energy (DE) component. The simplest possibility consistent with observations is a cosmological constant  $\Lambda$ , but a lot of alternatives have been proposed [3]. Prime candidates are dynamical dark energy models mediated by a scalar field or modified gravity—the latter being often equivalent to the former [4]. For many alternatives the cosmological constant problem [5,6] of explaining the small value of  $\Lambda$  persists, however. Also the explanation of why DE becomes important in the present cosmological epoch is often not more convincing than for a cosmological constant.

Growing neutrino quintessence (GNQ) [7,8] offers some advantages here. As a quintessence model [9,10], the late time acceleration is driven by a scalar field  $\varphi$  (the cosmon), employing a mechanism similar to inflation. It is possible to unify the late and early time acceleration into a single picture [11–13] so that the same field is responsible for DE and inflation. As an overall description within quantum gravity crossover cosmology [14], GNQ also addresses the cosmological constant problem.

GNQ is able to explain the smallness of the DE component, since the dynamical DE density decays during the cosmic history, just as the other energy densities in the Universe. The DE density being small is then just a matter of time—it is small because the Universe is old. In contrast to simpler quintessence models, GNQ solves the why-now problem. No fine-tuning of the self-interaction potential is needed for this purpose. A coupling between the cosmon and the neutrinos provides a mechanism for stopping the evolution of the cosmon field as soon as the neutrinos become nonrelativistic. The phenomenology of a very slowly evolving scalar field resembles a cosmological constant. The transition from relativistic to nonrelativistic

neutrinos acts as a trigger for the DE domination. For neutrino masses allowed by observations, this transition happens in the “recent” past, explaining why DE has become important now.

Despite a background evolution similar to the  $\Lambda$ CDM model for redshift  $z \lesssim 5$ , GNQ has a phenomenology which is distinct from other models. It predicts a time varying neutrino mass and the formation of neutrino lumps, which might be detectable through their gravitational potentials [15]. The formation of lumps is a consequence of the large coupling between neutrinos and the cosmon, which is required for the stopping mechanism. The resulting additional attraction between neutrinos is about  $10^3$  times stronger than the gravitational attraction. It can have a natural explanation in a particle physics framework [8].

While the strong coupling on the one hand offers with the lumps a clear and distinct way of testing the model, on the other hand, it renders the model technically difficult to study. In GNQ perturbations in the neutrino density become nonlinear already at  $z \approx 1$ , this happens on very large scales [15]. This has led to the development of a comprehensive N-body simulation [16,17] to follow the formation of the neutrino lumps. The simulation is different from the usual cold dark matter (CDM) only simulations: To include backreaction effects, induced by the highly nonlinear nature of the lumps [18], the background is solved simultaneously with the perturbations. Additionally, neutrinos becoming relativistic during the formation of lumps are captured by the simulation. A similar framework for relativistic N-body simulation with focus on the metric perturbations was explored recently in Ref. [19]. With our simulation it was possible to draw a consistent picture of neutrino structures within GNQ. For stable lumps the main characteristic features can be understood within an approximation in terms of a nonrelativistic fluid of neutrino lumps [20].

In this work we investigate if GNQ can provide a realistic expansion history. Therefore, we study the equation of state and the energy density of the cosmon for different model

\*fuhrer@thphys.uni-heidelberg.de

parameters. We aim to find model parameters for which the backreaction effect remains compatible with an accelerated expansion with  $\Omega_{\text{DE}} \approx 0.7$ . At the same time, the accelerated expansion of the Universe must start early enough to be consistent with observations.

A time-dependent neutrino mass related to a scalar dark energy field concerns a wider setting than GNQ. Mass varying neutrino scenarios have been studied earlier in Ref. [21] and share common features with GNQ as the instability of neutrino perturbations [22–24].

This work is organized as follows. We start with a brief review of GNQ in Sec. II. In Sec. III we discuss the formation of lumps and their backreaction on the cosmological expansion. In Sec. IV we describe our simulation, which we use to perform a parameter scan. Results are presented in Sec. V. Finally, we conclude in Sec. VI.

## II. GROWING NEUTRINO QUINTESSENCE

### A. Basic concepts

In this section we briefly describe GNQ. The ingredients of GNQ are a scalar field  $\varphi$  (the cosmon) and neutrinos. The neutrino mass depends on the value of  $\varphi$ , thereby coupling the cosmon and the neutrinos. The cosmon itself is described by the standard Lagrangian of a scalar field which takes, using the metric signature  $(-, +, +, +)$  and setting the reduced Planck mass to unity,  $8\pi G = 1$ , the form

$$-\mathcal{L}_\varphi = \frac{1}{2} \partial_\mu \varphi \partial^\mu \varphi + V(\varphi). \quad (1)$$

We choose an exponential potential  $V(\varphi) \propto e^{-\alpha\varphi}$ . As long as the neutrino mass can be neglected, the exponential potential leads to scaling solutions of the cosmon field. The background energy density of the cosmon becomes independent of the initial conditions and mimics matter (radiation) during matter (radiation) domination [9], where the energy density of the cosmon is a constant fraction of the total energy density  $\Omega_\varphi = 3 \frac{1+w}{\alpha^2}$ . Here  $w$  is the equation of state of the dominating species. Constraints on early dark energy (EDE) require  $\alpha \gtrsim 10$  [25–28], where we use a conservative bound in view of possible unexplored parameter degeneracies.

The dependence of the neutrino mass on the cosmon is given by

$$\beta = -\frac{d \ln m_\nu(\varphi)}{d\varphi} < 0. \quad (2)$$

In general the coupling  $\beta$  can be  $\varphi$  dependent. We establish in this paper that the size of the backreaction effect depends crucially on the presence or absence of a variation of  $\beta(\varphi)$ . An investigation of a particle physics motivated variation of  $\beta$  [8] in Ref. [17] has revealed a small backreaction effect and an overall cosmology consistent with present observations. For a constant  $\beta$ , large backreaction effects have been observed [16]. We address here the question if the model remains compatible with observations in this case as well.

A constant coupling implies for the neutrino mass

$$m_\nu(\varphi) = m_i e^{-\beta\varphi}, \quad (3)$$

where an additive constant in  $\varphi$  is fixed such that  $V(\varphi = 0) = 2.915 \times 10^{-7}$  eV. The  $\varphi$ -dependent neutrino mass allows for energy transfer between neutrinos and the cosmon, which is proportional to the trace of neutrino energy-momentum tensor:

$$\begin{aligned} \nabla_\nu T_{(\varphi)}^{\mu\nu} &= +\beta T_{(\nu)} \dot{\varphi} \\ \nabla_\nu T_{(\nu)}^{\mu\nu} &= -\beta T_{(\nu)} \dot{\varphi}. \end{aligned} \quad (4)$$

The trace of the energy-momentum tensor  $T_{(\nu)} = T_{\mu(\nu)}^\mu = -\rho_\nu + 3P_\nu$  vanishes for ultrarelativistic neutrinos. The coupling between neutrinos and the cosmon is therefore ineffective for relativistic neutrinos. The neutrino energy-momentum tensor also sources the Klein–Gordon equation which governs the evolution of the cosmon:

$$\nabla_\mu \nabla^\mu \varphi - V'(\varphi) = \beta T_{(\nu)}. \quad (5)$$

We will describe neutrinos and dark matter by an N-body simulation. The trajectories of classical neutrinos obey a modification of the geodesic equation [16],

$$\frac{du^\mu}{d\tau} + \Gamma_{\nu\lambda}^\mu u^\nu u^\lambda = \beta \partial^\mu \varphi + \beta u^\nu \partial_\nu \varphi u^\mu, \quad (6)$$

where  $u^\mu$  denotes the 4-velocity and  $\tau$  the proper time. The left-hand side is the usual gravitational motion, with the Christoffel symbols  $\Gamma_{\mu\nu}^\lambda$  determined by the metric. Throughout this work we use the Newtonian gauge for the metric:

$$ds^2 = -(1 + 2\Psi)dt^2 + a^2(1 - 2\Phi)d\mathbf{x}^2. \quad (7)$$

We will work to first order in the gravitational potentials  $\Phi$  and  $\Psi$  and neglect their time derivatives.

The right-hand side of Eq. (6) describes an additional force due to the coupling to the cosmon. It consists of two parts. First, a velocity-dependent part  $\beta u^\nu \partial_\nu \varphi u^\mu$  compensates changes in the mass for neutrinos moving in a varying cosmon field so that momentum is conserved. A neutrino moving into a region with smaller (larger) values of  $\varphi$  will lose (gain) mass. To compensate the loss (gain) of momentum, it will be accelerated (decelerated). Second, the term  $\beta \partial^\mu \varphi$  is a velocity-independent fifth force. In the nonrelativistic limit, it acts as an attractive force about  $2\beta^2$  times stronger than gravity [29].

### B. Homogeneous evolution

Let us now turn to the homogeneous limit and discuss how GNQ in its simplest form can lead to an accelerated expansion of the Universe. At early times when the

neutrinos are relativistic, the evolution of the cosmon is determined by the potential. Therefore, the cosmon will evolve toward its scaling solution with the DE density decreasing with  $a^{-3}$  during matter domination. In view of the growing mass, the neutrinos become nonrelativistic rather late. The interaction becomes important once  $\alpha V(\varphi) \approx \beta T_{(\nu)} \approx -\beta\rho_\nu$ . It acts as an effective potential barrier stopping the time evolution of the energy density of the cosmon-neutrino fluid. The constant energy density then mimics a cosmological constant. Since the energy density of the neutrinos is small compared to the cosmon energy density, the coupling must be rather large.

Most of the cosmological parameters as  $\Omega_{\text{DE}} = \Omega_\varphi + \Omega_\nu$  and  $m_\nu$  depend to a good approximation only on the ratio  $-\frac{\beta}{\alpha}$ ; see Fig. 1. Demanding a dark energy density of  $\Omega_{\text{DE}} \approx 0.7$  enforces  $-\frac{\beta}{\alpha} \approx 5$  [7] for a present neutrino mass  $m_\nu = O(1 \text{ eV})$ , where smaller neutrino masses require large  $-\frac{\beta}{\alpha}$ . We note that the usual cosmological bounds on the neutrino mass from CMB and large scale structure observations [30,31] do not apply here, since neutrino masses have been substantially smaller in the past. In the homogeneous limit, the neutrino mass is mainly constrained by Earth-based experiments. Also the scale factor at which the neutrinos stop the cosmon evolution has only a moderate dependence on the individual values of  $\alpha$  and  $\beta$ . The energy density fraction of the cosmon before stopping is given by  $\Omega_\varphi \propto \alpha^{-2}$  and hence becomes smaller for larger  $\alpha$ . The time at which the interaction with neutrinos compensates the self-interaction of the cosmon becomes earlier for larger  $\alpha$ . The onset of dark energy is therefore earlier for larger values of  $\alpha$  and  $\beta$ ; see Fig. 1.

As we will discuss later, strong backreaction effects will alter this simple picture. We will see in Sec. III that backreaction effects always counteract the stopping

mechanism and the cosmon will evolve again, so that it is not guaranteed that values for  $\alpha$  and  $\beta$  which describe a realistic cosmology in the homogeneous limit will also describe a close-to-realistic cosmology including backreaction.

Since backreaction effects can only be important after the neutrinos became nonrelativistic, the homogeneous description remains valid at early times. Large values for  $\alpha$  are preferred by bounds on EDE. For large  $\alpha$  the stopping mechanism acts earlier, and hence also the backreaction becomes important earlier. From these qualitative considerations, we already find some tension between reducing the backreaction effects, which spoil the stopping of the cosmon evolution, and satisfying bounds on EDE.

### III. BACKREACTION AND EFFECTIVE EQUATION OF STATE

#### A. Neutrino lumps

In GNQ it is important to understand structure formation, not only in view of using large scale structure observation as a probe for our cosmological models, especially to test DE models or “measure” the neutrino mass. It is crucial to understand the formation and evolution of neutrino lumps before being able to judge about the viability of GNQ as a DE model. In this section we shortly review the progress toward an understanding of the neutrino lumps, for details we refer to previous work [15,16,18,20,24,29,32–34]. Our main focus lies on the strong backreaction effects from nonlinear perturbations in the neutrino-cosmon fluid.

The large nonlinearities have their origin in the large coupling  $\beta = O(10^2)$ . Therefore, the additional force between neutrinos will be about  $10^3 - 10^4$  times larger than the gravitational interaction between neutrinos and between neutrinos and CDM. In turn the neutrino perturbations grow very quickly as soon as neutrinos become nonrelativistic. This implies that the fluctuations in the neutrino energy density become nonlinear even at large scales. The scale factor  $a_{\text{NL}}$  at which this happens for a neutrino perturbation of a given wavelength  $k^{-1}$  can be estimated by the value of  $a$  at which the linear dimensionless neutrino power spectrum  $\Delta_\nu(k) = k^3 P_\nu(k)/(2\pi^2)$  becomes order unity. Looking at Fig. 2, we see that for the particular choice of parameters  $\alpha = 10$  and  $\beta = -52$  already at  $a \sim 0.4$  scales around  $k_{\text{NL},\nu} \sim 0.01 \text{ hMpc}^{-1}$  become nonlinear, while today scales around  $k_{\text{NL},\nu} \sim 0.002 \text{ hMpc}^{-1}$  are nonlinear. The exact value of the nonlinear scale of neutrino-cosmon perturbations depends on the chosen parameters, but it is a generic finding that  $k_{\text{NL},\nu}$  is smaller than the corresponding wave vector for CDM perturbations,  $k_{\text{NL},\text{C},0} \sim 0.1 \text{ hMpc}^{-1}$ . These can be traced back to instabilities in the neutrino perturbations already present at linear order. These instabilities are stabilized nonperturbatively by the formation of neutrino lumps.

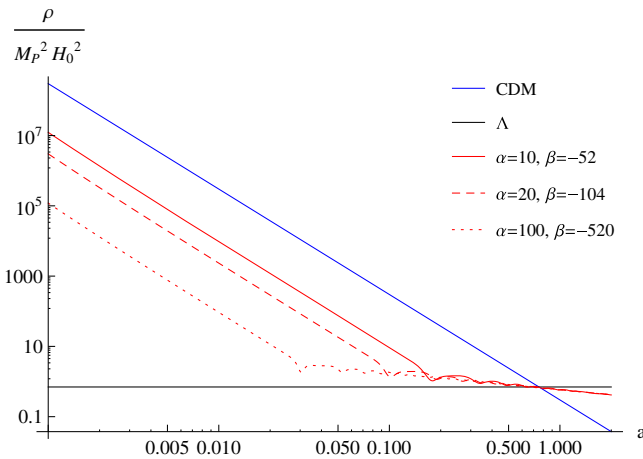


FIG. 1 (color online). Energy density of the cosmon-neutrino fluid, for different parameters  $\alpha$  and  $\beta$ . We compare to the CDM density and the density of a cosmological constant  $\Omega_\Lambda$ . The parameters were chosen to match  $\Omega_\Lambda$  today. The stopping occurs earlier for larger  $\alpha$ , with a smaller amount of EDE.

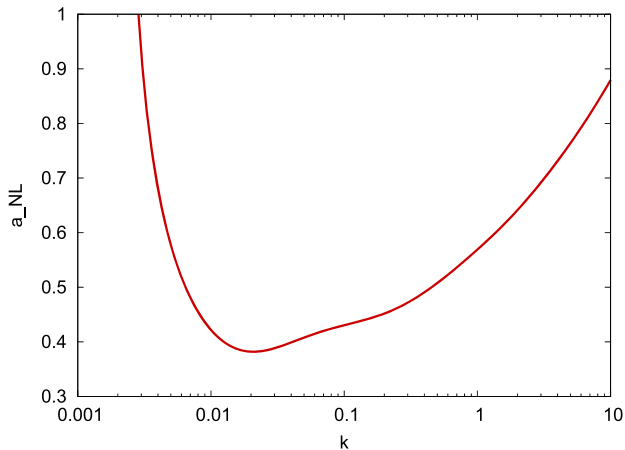


FIG. 2 (color online). The scale factor  $a_{\text{NL}}$  at which the dimensionless linear neutrino power spectrum becomes unity,  $\Delta(k, a_{\text{NL}}) = 1$ , as a function of scale, for the parameters  $\alpha = 10$  and  $\beta = -52$ . Already at  $a \sim 0.40$  scales around  $k \sim 0.02$  are nonlinear, demonstrating the failure of standard perturbative methods compared to the same figure in Ref. [17].

### B. Backreaction

Usually backreaction in cosmology is assumed to be negligible. In the last years, several quantitative estimates [35–37] came to the conclusion that backreaction is indeed small in the  $\Lambda$ CDM model. In contrast, backreaction effects are crucial in GNQ. We demonstrate this in Fig. 3, where we compare the numerical results for the clumping neutrinos with the pure background evolution for which the effects of nonlinear neutrino perturbations are neglected. We choose the parameters  $\alpha = 10$  and  $\beta = -52$  that have often been employed in the literature.

We find two types of backreaction effects. First, the Friedmann equation involves the volume averaged energy density, which we will define below. Second, the average value of the cosmon  $\bar{\varphi}$  cannot be obtained by solving the homogeneous equation of motion. The Klein–Gordon equation needs to be modified to include backreaction effects from the neutrino lumps. The reason is that the typical velocities and masses of the neutrinos do not coincide with their counterparts of the homogeneous calculation. While the first effect mainly affects the expansion history of the Universe, the second effect is also important for an understanding of the lump dynamics.

Let us first discuss the second effect. Due to the strong interaction, most of neutrinos are bound in the lumps. Inside gravitational bound objects, the gravitational potential has a well. Similarly, inside neutrino lumps the local field value is smaller than its average by an amount of  $\delta\varphi$ . The mass of a neutrino inside a lump is therefore smaller than the mass of a free-streaming neutrino  $m(\bar{\varphi} + \delta\varphi) < m(\bar{\varphi})$ . As a consequence most of the neutrinos have a mass substantially smaller than the mass estimated from the homogenous calculation. Due to the

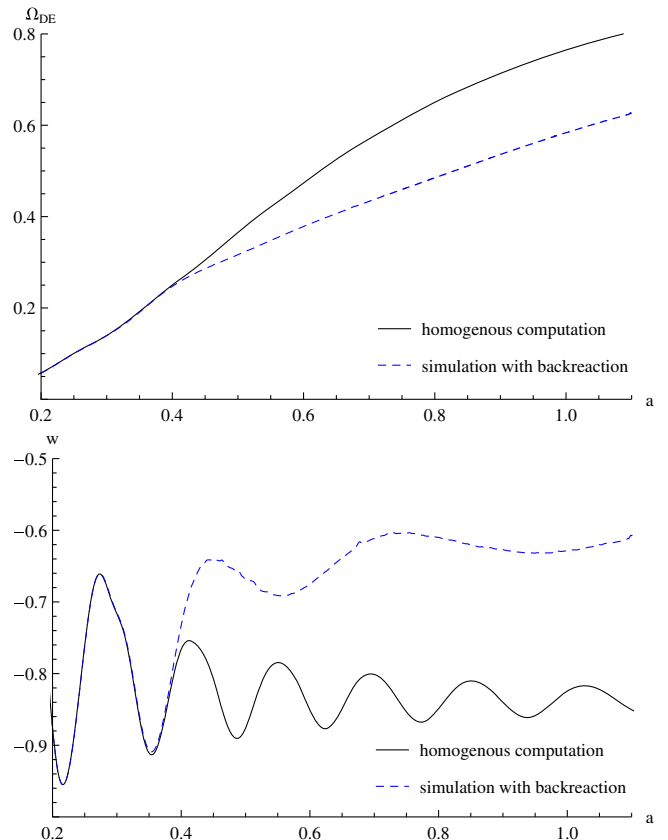


FIG. 3 (color online). Dark energy density fraction  $\Omega_{\text{DE}}$  (top) and equation of state  $w$  (bottom) as a function of the scale factor, for  $\alpha = 10$  and  $\beta = -52$ , with and without backreaction.

velocity-dependent force, the loss of mass during the formation of lumps is accompanied by an acceleration to relativistic velocities. These two effects lead to a mismatch between the energy-momentum tensor of neutrinos from the homogeneous calculation and its average value, as soon as the formation of lumps has started.

We account for the backreaction effects by using the volume averaged energy-momentum tensor. The Klein–Gordon equation for the average field is given approximately by

$$\ddot{\bar{\varphi}} + 3H\dot{\bar{\varphi}} + \alpha V(\bar{\varphi}) = -\beta\bar{T}_{(\nu)}, \quad (8)$$

where the volume average is defined as

$$\bar{T}_{(\nu)} = \frac{1}{V} \int d^3x \sqrt{g^{(3)}} T_{(\nu)} \approx \frac{a^3}{V} \int d^3x (1 - 3\Phi) T_{(\nu)}. \quad (9)$$

The determinant of the spatial 3-metric up to first order in metric perturbations is given by  $\sqrt{g^{(3)}} \approx a^3(1 - 3\Phi)$ . The integration is to be understood over the whole simulation box. The volume is given by  $V \approx a^3 \int d^3x (1 - 3\Phi)$ . Taking backreaction effects consistently into account and evolving the volume averaged field  $\bar{\varphi}$ , additional modifications arise

in the equation. However, we will neglect these terms for the qualitative discussion of backreaction in this section and postpone a more detailed discussion to Sec. IV.

The right-hand side of Eq. (8) can be written as

$$\beta \bar{T}_{(\nu)} = \beta(-\bar{\rho}_\nu + 3\bar{P}_\nu) = -\beta\bar{\rho}_\nu(1 - 3w_\nu) < -\beta\bar{\rho}_\nu, \quad (10)$$

where the energy density and pressure are understood as volume averages. We use them to define the equation of state  $w_\nu$ . The neutrino pressure is positive ( $w_\nu \geq 0$ ) such that pressure effects lower the effective potential barrier which stops the cosmon evolution. As a consequence, the time at which the cosmon evolution stops is postponed toward the future. If the evolution has already stopped, the effective reduction of the barrier can have the effect that the cosmon will evolve again. The weaker interaction between the neutrinos and the cosmon after the formation of lumps can also be interpreted as a lower effective coupling  $\beta_l$ , which gets renormalized by integrating out short wavelength modes [20]. In a qualitative sense,  $\beta_l$  can be interpreted as the effective coupling between a fluid of neutrino lumps and the homogenous cosmon field. The smaller value of  $\beta_l$  as compared to  $\beta$  is the dominant backreaction effect in our model.

We next turn to the backreaction effect for the evolution of the background metric. One needs to replace the background density of neutrinos and the cosmon by their volume average, such that the Friedmann equation becomes

$$H^2 = \bar{\rho}_{\text{CDM}} + \bar{\rho}_\nu + \bar{\rho}_\varphi. \quad (11)$$

In the presence of lumps,  $\rho_\nu$  has contributions from the neutrino velocities, and  $\rho_\varphi$  involves additional gradient contributions. The observable DE component is the combined neutrino-cosmon fluid  $\rho_{\text{DE}}$ . The neutrinos are typically subdominant but still contribute a significant fraction  $\frac{\bar{\rho}_\nu}{\rho_{\text{DE}}} \sim 0.1$ . With an equation of state  $w_\nu \sim 0.1$ , the neutrinos lift the dark energy equation of state away from  $w \approx -1$  to some higher value.

The volume average of the cosmon energy density is given by

$$\bar{\rho}_\varphi = \frac{1}{2}\bar{\dot{\varphi}}^2 + \frac{1}{2a^2} \overline{(1 + 2\Phi)(\partial_i\varphi)(\partial_j\varphi)\delta^{ij}} + \overline{V(\varphi)}, \quad (12)$$

where we only keep metric perturbations up to first order, neglect their time derivatives, and use that the volume average of the gravitational potentials vanishes  $\bar{\Phi} = \bar{\Psi} = 0$ . Also assuming that time derivatives of the cosmon perturbation  $\delta\varphi$  are small allows us to approximate  $\bar{\dot{\varphi}}^2 \approx \bar{\dot{\varphi}}^2$ . Using the quasistatic approximation is justified although the individual neutrino velocities are large. For the quasistatic approximation to hold, it is sufficient that the energy-momentum tensor for all neutrinos does not evolve quickly, so that there are no quickly varying sources for the cosmon.

A nonzero  $\delta\dot{\varphi}$  results in a positive contribution to the pressure, making it even harder to achieve an almost constant energy density for the cosmon-neutrino fluid.

Without the gradient term, one has the usual competition between potential and kinetic energy. The potential energy should be dominant in order to have an accelerated expansion. The averaged potential energy  $\overline{V(\varphi)}$  differs from the potential energy  $V(\bar{\varphi})$  of the averaged field  $\bar{\varphi}$  only by a few percent, such that no major backreaction effect arises from this source. In contrast, the gradient term can be almost as large as the potential energy. From the expression for the pressure

$$\bar{P}_\varphi \approx \frac{1}{2}\bar{\dot{\varphi}}^2 - \frac{1}{6a^2} \overline{(1 + 2\Phi)(\partial_i\varphi)(\partial_j\varphi)\delta^{ij}} - \overline{V(\varphi)}, \quad (13)$$

we see that a gradient term dominated equation of state would be  $w_\nu = -\frac{1}{3}$ . We emphasize that all backreaction effects individually lead to an evolving energy density of neutrino-cosmon fluid and typically push  $w$  away from  $-1$ .

For models with constant  $\beta$ , the lumps have the tendency to stabilize and to remain present once formed. The neutrino-cosmon fluid can be understood as an effective fluid of nearly virialized neutrino lumps with parameters differing from the microscopic ones [20]. The observable DE is then the sum of a neutrino lump fluid and a homogenous background field. For virialized lumps the pressure between relativistic neutrinos and cosmon gradients is expected to cancel [20]. Therefore, the equation of state of the lump fluid is close to zero, similar to the fluid of nonrelativistic neutrinos. The backreaction effect that remains even in this limit is the reduced effective coupling  $\beta_l$  between neutrino lumps and the cosmon background field. Due to the not completely virialized lumps, the pressure contribution from the neutrinos and the cosmon gradients do not cancel exactly, adding a small but relevant additional backreaction effect. This is different to gravitationally bound objects, for which a nonrenormalization theorem states that small virialized objects decouple completely from the background evolution and there is no backreaction effect from small virialized objects at all [36].

#### IV. N-BODY SIMULATION

The highly nonlinear nature of the neutrino lumps makes their description nonamenable to standard perturbative techniques. Instead we use a N-body simulation specially designed for GNQ. The N-body simulation solves the background and the inhomogeneities simultaneously and therefore allows us to study the backreaction effect of lumps on the homogeneous background evolution. The concept and many details of the simulation were already described in Refs. [16,17], and we focus here on the equation of motion for the average cosmon field  $\bar{\varphi}$  and its perturbation  $\delta\varphi$ .

In our simulation we follow the usual motion of non-relativistic CDM particles and their clustering due to gravity. In contrast to the standard picture of structure formation, the two gravitational potentials differ,  $\Phi \neq \Psi$ , because of the anisotropic stress from the neutrinos. This is accounted for by solving the Poisson equation for  $\Phi - \Psi$ , which yields  $\Phi$  once the Newtonian potential  $\Psi$  is known. The Poisson equation for  $\Psi$  is sourced by the energy density of CDM, neutrinos, and to a small part by the one of the cosmon perturbations.

The neutrinos are evolved using Eq. (6). The cosmon evolution is governed by the Klein–Gordon equation (5). We split the cosmon into the volume average  $\bar{\varphi} = \frac{1}{V} \int d^3x \sqrt{g^{(3)}} \varphi$  and a perturbation  $\delta\varphi = \varphi - \bar{\varphi}$ . Neglecting time derivatives of the gravitational potentials, time derivatives commute with the process of averaging  $\dot{\bar{\varphi}} \approx \bar{\dot{\varphi}}$ . The averaged equation (5) is

$$\begin{aligned} \ddot{\bar{\varphi}} + 3H\dot{\bar{\varphi}} + \overline{\alpha(1+2\Psi)V(\varphi)} \\ = -\overline{\beta(1+2\Psi)T_{(\nu)}} + a^{-2}\overline{\delta^{ij}(\partial_j\Psi)(\partial_i\delta\varphi)}, \end{aligned} \quad (14)$$

where we expanded up to first order in metric perturbations. Equation (14) is the full version of Eq. (8). As already discussed in Sec. III, the most important difference as compared to a naive homogeneous calculation is the use of the actual average of the neutrino momentum tensor. Including the gravitational potential in the average gives only a minor correction. Also the averaged potential term agrees up to a few percent with the homogeneous estimate. The gradient terms are roughly 1 order of magnitude smaller than the potential term and therefore only subdominant. Nevertheless, our numerical code includes all these effects.

By subtracting Eq. (14) from the Klein–Gordon equation (5), we find the equation for the perturbation:

$$\begin{aligned} \delta\ddot{\varphi} + 3H\delta\dot{\varphi} - a^{-2}\delta^{ij}\partial_i\partial_j\delta\varphi(1+2\Phi) \\ - a^{-2}\delta^{ij}(\partial_j(\Psi-\Phi))(\partial_i\varphi) + a^{-2}\overline{\delta^{ij}(\partial_j\Psi)(\partial_i\varphi)} \\ + \alpha((1+2\Psi)V(\varphi) - \overline{(1+2\Psi)V(\varphi)}) \\ = -\beta((1+2\Psi)T_{(\nu)} - \overline{(1+2\Psi)T_{(\nu)}}). \end{aligned} \quad (15)$$

This equation is a nonlinear wave equation, which is, due to the averaging, nonlocal in position space. To be able to solve this equation, we need to make some approximations. We employ a quasistatic approximation for the cosmon perturbation for which we neglect the second-order time derivative  $\delta\ddot{\varphi}$ . Simply neglecting all time derivatives is not a consistent approximation. Doing so the resulting equation does not ensure that the perturbation has a vanishing mean  $\bar{\delta\varphi} = 0$ . This can be seen by averaging Eq. (15). Taking into account the  $\Phi$  dependence in the volume element and only keeping terms to first order in the metric perturbations, all terms except the time derivatives cancel:

$$\ddot{\bar{\delta\varphi}} + 3H\dot{\bar{\delta\varphi}} = 0. \quad (16)$$

This relation ensures that if the average vanishes initially it will vanish at all times. This is still true if we neglect the second time derivative while keeping the first one. This approximation is consistent with the approximation for the kinetic term of the average energy density and pressure

$$\overline{\dot{\varphi}^2} = \dot{\bar{\varphi}}^2 + \overline{\delta\dot{\varphi}^2}, \quad (17)$$

where we neglected the  $\overline{\delta\dot{\varphi}^2}$  term, which is also second order in time derivatives of the cosmon perturbation.

If one instead neglects the second derivative with respect to conformal time, the Hubble damping changes  $3H \rightarrow 2H$ ; we compared both possibilities and found only a small difference. We interpret this as a sign that the quasistatic approximation is justified. To solve the equation for  $\delta\varphi$ , we use a Newton–Gauss–Seidel (NGS) multigrid relaxation method, already applied to the varying coupling model [17] and originally developed for modified gravity [38]. The quasistatic approximation is crucial for applying the NGS method, which is not applicable to wavelike equations but can be applied to diffusionlike equations [39]. The idea of the NGS solver is to rewrite the equation to be solved into a functional form,

$$\mathcal{L}[\delta\varphi] = D\delta\varphi - F[\delta\varphi] = 0, \quad (18)$$

with some differential operator  $D$  and a nonlinear functional  $F$ . The root of  $\mathcal{L}[\delta\varphi] = 0$  can be obtained by a Newton-like iterative procedure,

$$\delta\varphi^{(n+1)} = \delta\varphi^{(n)} - \mathcal{L}[\delta\varphi^{(n)}] \left( \frac{\partial \mathcal{L}[\delta\varphi^{(n)}]}{\partial \delta\varphi^{(n)}} \right)^{-1}; \quad (19)$$

the derivative is taken at each point individually, and the coupling between different points, induced by the derivatives, is taken into account solely by the iterative procedure. The derivative of the differential operator  $\frac{\partial D\delta\varphi}{\partial \delta\varphi}$  is defined by the discretization rule used in the simulation. We define the gradient and the Laplacian by relating a grid point to its neighbors in the  $j$  direction by a Taylor expansion,  $\delta\varphi(x_i \pm \Delta x \delta_{ij}) = \delta\varphi(x_i) \pm \partial_j \delta\varphi(x_i) \Delta x + \frac{1}{2} \partial_j^2 \delta\varphi(x_i) \Delta x^2 + \dots$ , with  $\Delta x$  the spacing between two grid points. The Laplacian is then approximated by a seven-point stencil, and the derivative is  $-6/\Delta x^2$ . The derivative of the gradient vanishes.

In principle this method can be applied even in the presence of the nonlocal terms present in Eq. (15). In practice this is not possible because calculating the nonlocal terms involves an integration over the full simulation box in each iteration step. We account for these terms iteratively. The difference between the values of the average terms of

two time steps is small. So we use at a given time step the average terms of the proceeding time step as a first approximation and apply the NGS solver a few times to correct for the difference.

## V. RESULTS AND DISCUSSION

Using the N-body simulation described in Sec. IV, we perform a parameter scan and search for parameters describing a realistic universe with accelerated expansion. For the details on the formation of lumps and their characteristics, we refer to previous work [16,20]. We use a simulation box with a comoving volume of  $V = (600 h^{-1} \text{Mpc})^3$ , which we divide into  $N_c = 128$  cells. The numbers of effective CDM particles  $N_C$  and neutrino particles  $N_\nu$  are chosen to be equal to the number of cells  $N_c = N_C = N_\nu$ . The initial power spectrum has a spectral index of  $n_s = 0.96$  and an amplitude of  $A_s = 2.3 \times 10^{-9}$  at the pivot scale  $k_{\text{pivot}} = 0.05 \text{Mpc}^{-1}$ . We start our simulation with the CDM particles only at  $a_{\text{ini,C}} = 0.02$  and add the neutrinos at a later time, after they became nonrelativistic.

In view of the strong backreaction effects, it is no longer clear that the stopping power of neutrinos for the time evolution of the cosmon is sufficient in order to account for a large present fraction of dark energy and an acceleration of the expansion similar to a cosmological constant. If so, the parameter range where this happens may be rather different from the one where the background evolution neglects the effect of neutrino structures.

Our model has three parameters relevant for this investigation, namely  $\alpha$  related to the amount of EDE, the cosmon neutrino coupling  $\beta$  and the parameter  $m_i$  which is related to the size of the neutrino mass. We have performed a parameter scan in order to search for a parameter range consistent with observations. For this purpose we vary the parameters  $\alpha$  and  $\beta$  individually while fixing the mass parameter

to  $m_i = 1 \text{eV}$ . Figure 4 shows that changing the mass parameter by a factor of 10 affects the effective equation of state and the energy density by no more than 10%.

A realistic DE model must certainly assume the benchmark values for the present DE density  $\Omega_{\text{DE},0} \approx 0.7$  and the present equation of state  $w_0 \approx -1$ . In Fig. 5 we show the values of  $\Omega_{\text{DE},0}$  and  $w_0$  for a grid in the parameter space for  $\alpha$  and  $\beta$ . Sufficient acceleration typically requires rather small values  $\alpha \lesssim 5$ . A band with an acceptable fraction of present DE is typically found in the range  $5 \lesssim \alpha \lesssim 10$ , showing some tension already at this stage.

The parameter range yielding an accelerated expansion ( $\alpha \lesssim 5$ ) is problematic also in view of the bounds on EDE, which require  $\alpha \gtrsim 10$ . In the parameter range where one finds  $w_0 < -0.9$ , some tension persists if one tries to get both the equation of state and the energy density compatible with observations. For  $\alpha = 3$  and  $\alpha = 4$ , we indeed find  $w_0 \lesssim -0.9$ , but the energy density exceeds with

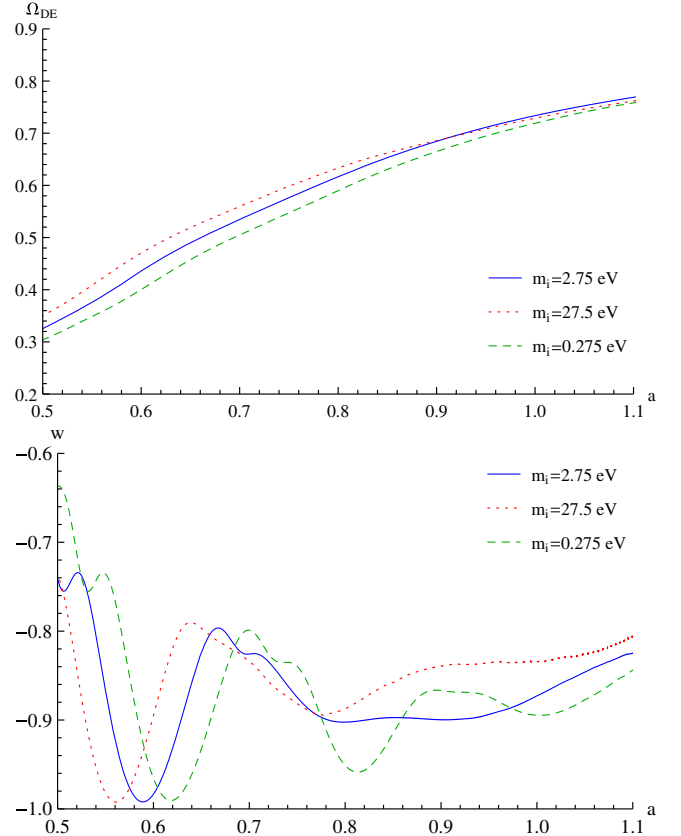


FIG. 4 (color online). Energy density fraction of the cosmon-neutrino fluid  $\Omega_{\text{DE}}$  and effective equation of state  $w$ , for different mass parameters  $m_i$ , with  $\alpha = 5$  and  $\beta = -78$ . Even for mass parameters different by a factor of 100, the equation of state varies at a maximum of about 10%, indicating that the value of  $m_i$  plays only a minor role.

$\Omega_{\text{DE}} \approx 0.75$  the benchmark value of  $\Omega_{\text{DE},0} \approx 0.7$ . On the other hand, for  $\alpha = 5$  one has  $\Omega_{\text{DE}} \approx 0.7$ , but the equation of state is  $w_0 \approx -0.7$ . Although we could not find parameters for which  $w_0$  and  $\Omega_{\text{DE},0}$  match the benchmark values precisely, our results are not too far from those values, either. It might be that varying also the mass parameter  $m_i$  could bring them into agreement with observations.

The equation of state is not constant in time, and it can even possess oscillating features; see Fig. 4. It may happen that the present time coincides with a minimum (maximum) of  $w$  during an oscillation. In this case the cosmic evolution is actually better described by an average value somewhat larger (smaller) than  $w_0$ . The time evolution of the equation of state is shown in Fig. 6 for a range of parameters  $\alpha$  and  $\beta$  in the region not too far from the benchmark values. One typically observes a first stop of the scalar field ( $w \approx -1$ ). Due to backreaction this is followed by a slow decrease of the dark energy, typically with  $-0.9 \lesssim w \lesssim -0.8$ .

Only looking at the energy density and the equation of state today is not sufficient. In the parameter range acceptable for the benchmark, the neutrinos become

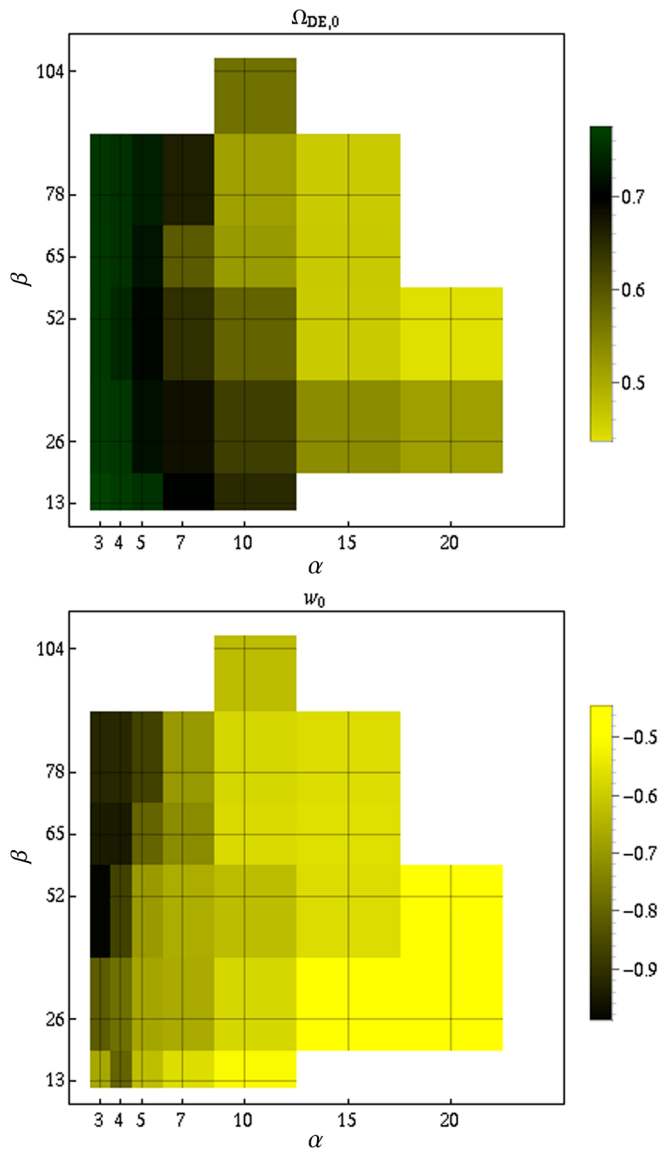


FIG. 5 (color online). Present energy density  $\Omega_{\text{DE},0}$  and equation of state  $w_0$  of the cosmon-neutrino fluid. Realistic values ( $w_0 \approx -1$ ,  $\Omega_{\text{DE},0} \approx 0.7$ ) are found for small values of  $\alpha$ . It is hard to get both values “correct” simultaneously, for sufficiently large  $\alpha$ .

nonrelativistic late. Consequently the cosmon evolution stops late. This is visible in Fig. 6, where the first pronounced minimum in  $w$  precisely corresponds to the time when the increase of  $\varphi$  is first stopped and the oscillations set in. Supernova observations probe the expansion history up to redshifts higher than  $z \approx 1$  and prefer an almost constant dark energy [40]. We find that for close-to-realistic models the equation of state reaches values around  $-1$  only for scale factors  $a \gtrsim 0.6$ , which is difficult to get into agreement with  $w \approx -1$  from  $a \lesssim 0.5$  until today.

Figure 6 shows the generic evolution of the equation of state: It drops down after the neutrinos become

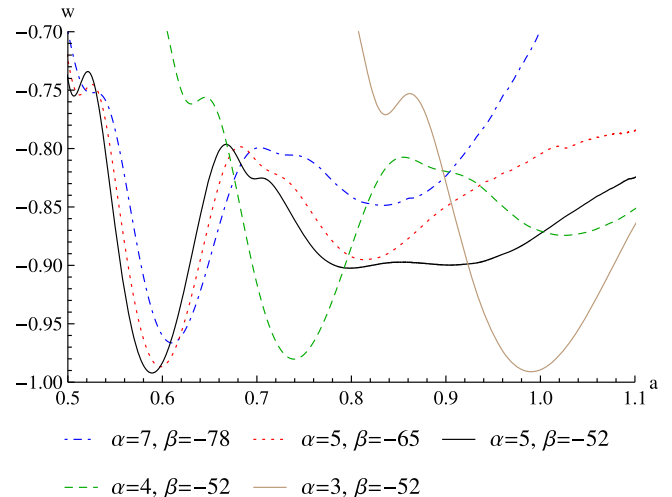


FIG. 6 (color online). Equation of state as a function of the scale factor. The model parameters are chosen such that  $w$  and  $\Omega_{\text{DE},0}$  are near the benchmark values. Values  $w_0 \lesssim -0.9$  are only reached before backreaction effects become important. Thus,  $w \approx -0.99$  for  $\alpha = 5$  and  $\beta = -52$  is not accompanied by large negative  $w$  at redshifts relevant for supernova observations.

nonrelativistic followed by a few damped oscillations. In the homogeneous evolution, these oscillations are damped away quickly, and the equation of state assumes an almost constant value rather close to  $w = -1$ . In fact the equation of state grows again due to the backreaction and typically reaches values  $w \approx -0.8$ . An equation of state of  $w_0 \lesssim -0.9$  is only reached before or shortly after backreaction becomes important. This simply means that lumps do not have enough time to grow large enough for being able to induce significant backreaction effects.

From these results we conclude that GNQ with a constant coupling  $\beta$  is probably not a viable DE model. Realistic values for  $w_0$  and  $\Omega_{\text{DE},0}$  seem only possible if the cosmon evolution is stopped late, so that backreaction effects have no time to become important. Stopping the cosmon evolution late is in some tension with supernova data and involves a large amount of EDE, probably not consistent with observations.

## VI. CONCLUSION

We have performed a numerical analysis of GNQ with a constant cosmon-neutrino coupling  $\beta$ . Due to strong backreaction effects from the formation of large neutrino lumps, these models have difficulties being compatible with the observed properties of dark energy.

A specific choice for the model parameters  $\alpha$ ,  $\beta$ , and  $m_i$ , which appears to be compatible with observations at the homogenous level, is typically no longer viable if backreaction is included. Our parameter scan reveals regions for which the backreaction effects are small enough to allow a slowly evolving cosmon and consequently an almost

constant DE density. However, this is only possible if the neutrino lumps form late so that backreaction effects are still small today. In this case an accelerated expansion is only possible for scale factors  $a \gtrsim 0.6$ , in tension with an almost constant equation of state for scale factors  $a \lesssim 0.5$ , as preferred by supernova data. Furthermore, the parameter region for which the equation of state is close to  $-1$  and the DE density is not too far from  $0.7$  requires  $\alpha \lesssim 5$ . This contradicts constraints on EDE for which  $\alpha \gtrsim 10$  is necessary. We conclude that GNQ with a constant coupling  $\beta$  is probably not a viable DE model.

These results for a constant coupling should be contrasted with models where  $\beta$  increases with  $\varphi$ . For this second class of models, the backreaction effect is found to be small since the neutrino lumps form and disrupt periodically [17]. At the present stage this second class of models seems compatible with observations. In certain parameter ranges, it may even be hard to detect a difference from the  $\Lambda$ CDM model and its variants.

These two classes of models may be seen as particular points in a larger class of models where  $\beta$  is allowed to vary with  $\varphi$ . Having established points that are viable with only rather small deviations from  $\Lambda$ CDM, as well as other points where the deviations are so strong that the model is no longer acceptable, we can conclude by continuity that in between there will be models which are still compatible with observations today but also offer highly interesting prospects of finding deviations from  $\Lambda$ CDM. Finding large neutrino lumps, thereby observing the cosmic neutrinos directly, would be a direct hint for GNQ. Even for models with small neutrino perturbations, we expect observable deviations from the  $\Lambda$ CDM model, due to the different evolution of the neutrino sector. First, the transition of relativistic to nonrelativistic standard massive neutrinos is imprinted in the CMB fluctuations as well as in the matter distribution, with a specific scale dependence [30,31]. The signal differs for constant or time-varying neutrino masses. Second, free-streaming standard massive neutrinos

attenuate the growth of matter perturbations on small scales and therefore add an additional scale-dependent effect to the matter distribution. Observing these scale-dependent effects as predicted for standard neutrinos with a constant mass would be a strong argument for the  $\Lambda$ CDM model and against GNQ.

The result for models with constant  $\beta$  presented in this note as well the results on the varying  $\beta$  model presented in Ref. [17] suggest that only those models are viable in which the small scale nonlinear neutrino perturbations have only a moderate effect on the large scale dynamics. Nevertheless, the neutrino lumps can have a observable effects on larger scales. One possibility to account for these effects is to construct an effective fluid for the long wavelength perturbations by averaging over small scale nonlinearities as proposed in Ref. [36]. A similar route has already been taken in Ref. [20] to describe the large scale dynamics of virialized neutrino lumps in the constant  $\beta$  model by means of an effective lump fluid. These ideas were already successfully applied to the mildly nonlinear regime of structure formation in the form of the effective field theory of large scale structure [41–46]; see also Ref. [47]. Adopting these ideas to GNQ, we hope that it will become possible to study the dynamics of perturbations in GNQ on large scales qualitatively. It might even become possible to study some effects of lumps on the CMB, without running time-consuming simulations.

## ACKNOWLEDGMENTS

The authors are thankful to Youness Ayaita, Valeria Pettorino, and Santiago Casas for numerous inspiring discussions and ideas. They would also like to thank Ewald Puchwein for providing his NGS code and David Mota for providing his numerical implementation of linear perturbation theory in GNQ. F.F. acknowledges support from the IMPRS-PTFS and the DFG through the TRR33 project “The Dark Universe.”

- 
- [1] S. Perlmutter *et al.* (Supernova Cosmology Project), *Astrophys. J.* **517**, 565 (1999).
  - [2] A. G. Riess *et al.* (Supernova Search Team), *Astron. J.* **116**, 1009 (1998).
  - [3] E. J. Copeland, M. Sami, and S. Tsujikawa, *Int. J. Mod. Phys. D* **15**, 1753 (2006).
  - [4] C. Wetterich, arXiv:1402.5031v1.
  - [5] S. Weinberg, *Rev. Mod. Phys.* **61**, 1 (1989).
  - [6] S. M. Carroll, *Living Rev. Relativity* **4**, 1 (2001).
  - [7] L. Amendola, M. Baldi, and C. Wetterich, *Phys. Rev. D* **78**, 023015 (2008).
  - [8] C. Wetterich, *Phys. Lett. B* **655**, 201 (2007).
  - [9] C. Wetterich, *Nucl. Phys.* **B302**, 668 (1988).
  - [10] B. Ratra and P. Peebles, *Phys. Rev. D* **37**, 3406 (1988).
  - [11] C. Wetterich, *Phys. Dark Univ.* **2**, 184 (2013).
  - [12] C. Wetterich, *Phys. Rev. D* **89**, 024005 (2014).
  - [13] C. Wetterich, *Phys. Rev. D* **90**, 043520 (2014).
  - [14] C. Wetterich, *Nucl. Phys.* **B897**, 111 (2015).
  - [15] D. Mota, V. Pettorino, G. Robbers, and C. Wetterich, *Phys. Lett. B* **663**, 160 (2008).
  - [16] Y. Ayaita, M. Weber, and C. Wetterich, *Phys. Rev. D* **85**, 123010 (2012).
  - [17] Y. Ayaita, M. Baldi, F. Führer, E. Puchwein, and C. Wetterich, arXiv:1407.8414v1.

- [18] V. Pettorino, N. Wintergerst, L. Amendola, and C. Wetterich, *Phys. Rev. D* **82**, 123001 (2010).
- [19] J. Adamek, D. Daverio, R. Durrer, and M. Kunz, *Phys. Rev. D* **88**, 103527 (2013).
- [20] Y. Ayaita, M. Weber, and C. Wetterich, *Phys. Rev. D* **87**, 043519 (2013).
- [21] R. Fardon, A. E. Nelson, and N. Weiner, *J. Cosmol. Astropart. Phys.* **10** (2004) 005.
- [22] N. Afshordi, M. Zaldarriaga, and K. Kohri, *Phys. Rev. D* **72**, 065024 (2005).
- [23] O. E. Bjaelde, A. W. Brookfield, Carsten van de Bruck, S. Hannestad, D. F. Mota, L. Schrempp, and D. Tocchini-Valentini, *J. Cosmol. Astropart. Phys.* **01** (2008) 026.
- [24] N. Brouzakis, N. Tetradis, and C. Wetterich, *Phys. Lett. B* **665**, 131 (2008).
- [25] M. Doran, G. Robbers, and C. Wetterich, *Phys. Rev. D* **75**, 023003 (2007).
- [26] C. L. Reichardt, R. de Putter, O. Zahn, and Z. Hou, *Astrophys. J.* **749**, L9 (2012).
- [27] V. Pettorino, L. Amendola, and C. Wetterich, *Phys. Rev. D* **87**, 083009 (2013).
- [28] P. Collaboration *et al.*, arXiv:1502.01590v1.
- [29] N. Wintergerst, V. Pettorino, D. Mota, and C. Wetterich, *Phys. Rev. D* **81**, 063525 (2010).
- [30] J. Lesgourgues and S. Pastor, *Phys. Rep.* **429**, 307 (2006).
- [31] Y. Y. Y. Wong, *Annu. Rev. Nucl. Part. Sci.* **61**, 69 (2011).
- [32] L. Schrempp and I. Brown, *J. Cosmol. Astropart. Phys.* **05** (2010) 023.
- [33] N. J. Nunes, L. Schrempp, and C. Wetterich, *Phys. Rev. D* **83**, 083523 (2011).
- [34] M. Baldi, V. Pettorino, L. Amendola, and C. Wetterich, *Mon. Not. R. Astron. Soc.* **418**, 214 (2011).
- [35] C. Wetterich, *Phys. Rev. D* **67**, 043513 (2003).
- [36] D. Baumann, A. Nicolis, L. Senatore, and M. Zaldarriaga, *J. Cosmol. Astropart. Phys.* **07** (2012) 051.
- [37] J. Adamek, C. Clarkson, R. Durrer, and M. Kunz, *Phys. Rev. Lett.* **114**, 051302 (2015).
- [38] E. Puchwein, M. Baldi, and V. Springel, *Mon. Not. R. Astron. Soc.* **436**, 348 (2013).
- [39] J. Van Lent, Ph.D. Thesis, Katholieke Universiteit Leuven, 2006.
- [40] M. Betoule *et al.*, *Astron. Astrophys.* **568**, A22 (2014).
- [41] J. J. M. Carrasco, M. P. Hertzberg, and L. Senatore, *J. High Energy Phys.* **09** (2012) 82.
- [42] M. P. Hertzberg, *Phys. Rev. D* **89**, 043521 (2014).
- [43] E. Pajer and M. Zaldarriaga, *J. Cosmol. Astropart. Phys.* **08** (2013) 037.
- [44] L. Mercolli and E. Pajer, *J. Cosmol. Astropart. Phys.* **03** (2014) 006.
- [45] J. J. M. Carrasco, S. Foreman, D. Green, and L. Senatore, *J. Cosmol. Astropart. Phys.* **07** (2014) 057.
- [46] S. M. Carroll, S. Leichenauer, and J. Pollack, *Phys. Rev. D* **90**, 023518 (2014).
- [47] G. Rigopoulos, *J. Cosmol. Astropart. Phys.* **01** (2015) 014.

# Renormalizing a viscous fluid model for large-scale structure formation



# Renormalizing a viscous fluid model for large scale structure formation

Florian Führer<sup>a</sup> and Gerasimos Rigopoulos<sup>b</sup>

<sup>a</sup>Institut für Theoretische Physik, Universität Heidelberg,  
Philosophenweg 16, Heidelberg, 69120 Germany

<sup>b</sup>School of Mathematics & Statistics, Newcastle University,  
Herschel Building, Newcastle upon Tyne, NE1 7RU U.K.

E-mail: [fuhrer@thphys.uni-heidelberg.de](mailto:fuhrer@thphys.uni-heidelberg.de), [gerasimos.rigopoulos@ncl.ac.uk](mailto:gerasimos.rigopoulos@ncl.ac.uk)

Received September 21, 2015

Revised January 3, 2016

Accepted January 20, 2016

Published February 12, 2016

**Abstract.** Using the Stochastic Adhesion Model (SAM) as a simple toy model for cosmic structure formation, we study renormalization and the removal of the cutoff dependence from loop integrals in perturbative calculations. SAM shares the same symmetry with the full system of continuity+Euler equations and includes a viscosity term and a stochastic noise term, similar to the effective theories recently put forward to model CDM clustering. We show in this context that if the viscosity and noise terms are treated as perturbative corrections to the standard eulerian perturbation theory, they are necessarily non-local in time. To ensure Galilean Invariance higher order vertices related to the viscosity and the noise must then be added and we explicitly show at one-loop that these terms act as counter terms for vertex diagrams. The Ward Identities ensure that the non-local-in-time theory can be renormalized consistently. Another possibility is to include the viscosity in the linear propagator, resulting in exponential damping at high wavenumber. The resulting local-in-time theory is then renormalizable to one loop, requiring less free parameters for its renormalization.

**Keywords:** power spectrum, cosmological perturbation theory, cosmic flows, cosmic web

**ArXiv ePrint:** [1509.03073](https://arxiv.org/abs/1509.03073)

---

## Contents

<b>1</b>	<b>Introduction</b>	<b>1</b>
<b>2</b>	<b>The stochastic adhesion model</b>	<b>3</b>
<b>3</b>	<b>Galilean Invariance</b>	<b>6</b>
<b>4</b>	<b>Renormalization</b>	<b>8</b>
4.1	Non local in time	9
4.2	Local in time	11
4.3	Ward Identities	14
4.4	The bispectrum in the local and non-local theories	15
<b>5</b>	<b>Conclusion</b>	<b>16</b>

---

## 1 Introduction

Understanding the evolution of density fluctuations under the influence of gravity is a central, but still open issue in cosmology. While fluctuations on large scales are small and can be well described using linear perturbation theory, on small scales the fluctuations grow large and the Standard Perturbation Theory (SPT) fails, see [1] for a classic review. Two possible sources of the failure of SPT have been identified. The first relates to the influence of very long-wavelength modes, still within the perturbative regime, on very small scales. After [2, 3] first presented their resummation scheme, a lot of progress has been made towards a better understanding of how long-wavelength modes effect smaller scales [4–10], but also different resummation schemes have been explored [11, 12]. The effect of long-wavelength modes on very short modes is absent for equal time correlators due to Galilean Invariance (GI) [13–16]. Nevertheless, it is still possible that long-wavelength modes can strongly affect intermediate modes and one can hope that the effect of the former on the latter can be inferred from the effect on short modes by adopting a Galilean invariant resummation scheme (see the appendix of [9] for one possible approach).

The second source of failure, that large density fluctuations on small scales can in principle have a sizable effect on the small fluctuations on large scales, must be investigated independently of the importance of long-wavelength modes. On small scales not only is the density contrast large but also, and crucially, the single-stream approximation fails and hence the fluid approximation fails. Calculating the effect of small on large scales is therefore not possible within the framework of SPT or Lagrangian Perturbation Theory (LPT). To address the issue, it has been proposed to average over small scales such that one is left with equations for the large scale density contrast  $\delta$  and velocity  $\frac{dx}{dD} = \mathbf{w}$  plus an additional effective stress tensor  $\sigma$  which encodes the small scale dynamics [17–19]. The Euler equation then takes the form

$$\partial_D \mathbf{w} + \frac{3}{2} \frac{\gamma}{D} (\mathbf{w} + \nabla \Phi) + \mathbf{w} \cdot \nabla \mathbf{w} = \frac{\nabla \cdot ((1 + \delta) \boldsymbol{\sigma})}{1 + \delta}, \quad (1.1)$$

where  $D$  is the linear growth factor, the background cosmology is encoded in  $\gamma = \frac{\Omega_m}{\left(\frac{d \ln(D)}{d \ln(a)}\right)^2}$  and  $\Phi$  is the rescaled gravitational potential, determined by the Poisson equation  $\nabla^2 \Phi = \frac{\delta}{D}$ . For a  $\Lambda$ CDM cosmology we have  $\gamma \approx 1$ . The effective stress  $\boldsymbol{\sigma}$  is unknown. One possible strategy of treating this term is to measure it directly from N-body simulations, in which case  $\boldsymbol{\sigma}$  acts as a source for the perturbations on large scales [19, 20]. Another possible strategy is to attempt its parametrization in terms of the velocity and the density contrast as follows

$$\frac{\nabla \cdot ((1 + \delta)\boldsymbol{\sigma})}{1 + \delta} = \mathbf{J} - \frac{\nu_1}{D} \nabla \delta + \nu_2 \nabla^2 \mathbf{w} + \nu_3 \nabla \times \nabla \times \mathbf{w} + \dots, \quad (1.2)$$

where the  $\nu_i$  are effective viscosity parameters and  $\mathbf{J}$  is a stochastic noise. The ellipses denote terms which are higher order in fields or derivatives which are expected to be suppressed compared to the leading terms. This second strategy goes under the name of Effective Field Theory of Large Scale Structure (EFToLSS) and has, in its eulerian formulation, drawn a lot of attention in recent years [21–28], including the possibility to resum long-wavelength modes [29]. A Lagrangian version has also been formulated in [30, 31]. The unknown parameters  $\nu_i$  are to be fitted to observations or simulations.

The added effective terms not only encode the small scale dynamics, they also ensure that physical quantities, for example correlation functions, are independent of the arbitrary smoothing scale. These terms could be treated perturbatively, employing a power counting where the linear propagator does not involve any damping due to the viscosity terms — see for example (4.1) for this kind of propagator in the model considered here. The EFToLSS approach effectively corresponds to such a power counting applied to the full set of fluid equations. As we argue below, to ensure cutoff independence of correlation functions with such a power counting the r.h.s. of (1.2) must be non-local in time. Galilean Invariance of this non-local-in-time theory also dictates the inclusion of higher order non-local-in-time terms of a certain form on the r.h.s. of (1.2). As we will see, these terms ensure cutoff independence and renormalization is possible and consistent with GI. In the EFToLSS literature, the physical meaning of this non-locality in time is traced to the lack of a fast timescale for short wavelengths. It should be noted however that fitting the Power Spectrum obtained by an EFToLSS calculation to a fully non-linear Power Spectrum is possible with a similar accuracy using both local and non-local counter terms [32].

Another possibility is to include the effective viscosity terms in the linear propagator, see (4.13). This power-counting scheme was employed in [33]. The authors of [34] have used a closely related approach by including a local viscosity and sound speed in the linear fluid perturbation equations, and find that better agreement with N-body simulations can be achieved compared with the usual SPT calculation. We show that in this case the theory is Galilean invariant, local in time and one-loop renormalizable. A theory local in time is expected if the effective terms are dominated by sufficiently small scales, where, according to the gravitational free-fall time  $\Delta D \sim \delta^{-1/2}$ , the typical time scale is much smaller than the time scale on large scales. This is in particular the case if the cutoff of the theory is given by the scale where multi-streaming becomes relevant. For example the viscosity is then given by the microscopic viscosity plus a contribution from scales beyond the cutoff.

Let us emphasize that the effective terms aim to encapsulate the influence on large scales of the highly non-linear evolution of short wavelength perturbations, accounting for short wavelength deviations from a single stream fluid. They are not meant to include the effect of a possible non-trivial background phase space distribution or an initial deviation from a

single stream fluid, as is the case for free-streaming particles like neutrinos. Nevertheless, the fluid description of such free-streaming particles on scales larger than the free-streaming scale  $k_{\text{FS}}$  can also be interpreted as an Effective Field Theory with  $k_{\text{FS}}$  as the cutoff. Let us briefly sketch this idea. For  $n > 1$  moments of the velocity distribution are of the order  $\overline{w^n} \sim k_{\text{FS}}^{-n}$  and thus can be treated as perturbative corrections to  $\delta$  and  $\mathbf{w}$ . The first corrections are then given by the stress tensor, which obeys, neglecting the third moment,

$$\partial_D \boldsymbol{\sigma} + 3 \frac{\gamma}{D} \boldsymbol{\sigma} + \mathbf{w} \nabla \cdot \boldsymbol{\sigma} + \boldsymbol{\sigma} \cdot \nabla \mathbf{w} + (\nabla \mathbf{w})^T \cdot \boldsymbol{\sigma} = 0. \quad (1.3)$$

Splitting the stress into a background and a perturbation  $\boldsymbol{\sigma} = \bar{\boldsymbol{\sigma}} \mathbf{1} + \delta \boldsymbol{\sigma}$  one can write the stress, for  $\gamma = 1$ , as

$$\boldsymbol{\sigma} = \mathbf{1} \bar{\sigma}_i \left( \frac{D_i}{D} \right)^3 + \delta \boldsymbol{\sigma}_i \left( \frac{D_i}{D} \right)^3 + \mathbf{1} \bar{\sigma}_i \left( \frac{D_i}{D} \right)^3 \int_{D_i}^D d\eta (\nabla \mathbf{w} + (\nabla \mathbf{w})^T)(\eta) + \dots, \quad (1.4)$$

with  $\bar{\sigma}_i$  and  $\delta \boldsymbol{\sigma}_i$  being the background value and the perturbation of the stress at some initial time  $D_i$ . Plugging this into the right hand side of the Euler equation (1.1) we have

$$\frac{\nabla \cdot ((1+\delta)\boldsymbol{\sigma})}{1+\delta} = \nabla \cdot \delta \boldsymbol{\sigma}_i \left( \frac{D_i}{D} \right)^3 + \bar{\sigma}_i \left( \frac{D_i}{D} \right)^3 \nabla \delta + \mathbf{1} \bar{\sigma}_i \left( \frac{D_i}{D} \right)^3 \int_{D_i}^D d\eta (\nabla^2 \mathbf{w} + \nabla \nabla \cdot \mathbf{w})(\eta) + \dots \quad (1.5)$$

To this order the initial stress perturbation plays the role of a stochastic noise and the background stress induces a local sound speed and a non-local-in-time viscosity. Higher order contributions can be obtained straightforwardly in the double expansion in  $\frac{\nabla}{k_{\text{FS}}}$  and the fields  $\delta$  and  $\mathbf{w}$ . Note that the time dependence of the effective terms is fixed and does not coincide with the SPT loop time dependence so the theory cannot be renormalized. Since the velocity moments of the background and the initial distribution are in principle known, they can be resummed such that one obtains a theory which is non-local and valid at all scales as long as the density contrast is small [35]. We see that the effective long wavelength theory for CDM may be thought off as analogous to this approach to free-streaming particles. The analogy is imperfect though, given that different time dependences of the effective terms are required for CDM.

The outline of our paper is as follows. In section 2 we introduce our simplified toy model, the Stochastic Adhesion Model. Then in section 3 we discuss GI and how it constrains the allowed terms that can be used to parameterize the effective stress tensor. In section 4 we discuss renormalization of the local-in-time and non-local-in-time versions of the effective theory. We conclude in section 5.

## 2 The stochastic adhesion model

Instead of discussing the full set of equations consisting of the continuity and the Euler equation, we study the technically simpler Stochastic Adhesion Model (SAM) as a toy model. The SAM, as already discussed in [33], can be obtained from the fluid equations by a Zeldovich approximation, see also [36–39] for earlier work on the Adhesion Model and the Burgers Equation. The Zel'dovich approximation reads  $\mathbf{w} = -\nabla \Phi$  and as a result  $d\mathbf{w}/dD = \partial_D \mathbf{w} + \mathbf{w} \cdot \nabla \mathbf{w} = 0$ . This approximation decouples the Euler equation from the continuity equation. In principle one can obtain  $\delta$  from the continuity equation once  $h$  is known, for details see [33]. In the following we will not consider the continuity equation,

since the scope of this paper is to discuss the interplay between renormalization and GI, which can be done by considering the Euler equation alone. The SAM is obtained by writing  $d\mathbf{w}/dD = \partial_D \mathbf{w} + \mathbf{w} \cdot \nabla \mathbf{w} = \frac{\nabla \cdot ((1+\delta)\boldsymbol{\sigma})}{1+\delta}$  and expressing the effective stress tensor as discussed above. It thus approximates deviations of fluid elements from their long wavelength Zel'dovich trajectories. One ends up with a time dependent Kadar-Parisi-Zhang (KPZ) equation [40] for the velocity potential  $h$ , defined by  $\mathbf{w} = -\nabla h$ .

SAM is a stochastic field theory and is most conveniently formulated by defining the MSRJD action<sup>1</sup>

$$\begin{aligned}
 S &= \frac{1}{2} \int dD dD' \frac{d^3 k}{(2\pi)^3} \left[ (h_{\mathbf{k}}, \chi_{\mathbf{k}})_D \begin{pmatrix} 0 & (-\partial_D + \nu k^2) \delta(D-D') \\ (\partial_D + \nu k^2) \delta(D-D') & i\mathcal{N}(k, D, D') \end{pmatrix} \begin{pmatrix} h_{-\mathbf{k}} \\ \chi_{-\mathbf{k}} \end{pmatrix}_{D'} + \mathcal{L}_{\text{int}} \right] \\
 &= \frac{1}{2} \int_{DD'} \frac{d^3 k}{(2\pi)^3} \left[ (h_{\mathbf{k}}, \chi_{\mathbf{k}}) \hat{G}_0^{-1} \begin{pmatrix} h_{-\mathbf{k}} \\ \chi_{-\mathbf{k}} \end{pmatrix} + \mathcal{L}_{\text{int}} \right],
 \end{aligned} \tag{2.1}$$

where

$$\hat{G}_0^{-1} = \begin{pmatrix} 0 & [G_0^A]^{-1} \\ [G_0^R]^{-1} & i\mathcal{N}(k) \end{pmatrix}. \tag{2.2}$$

and

$$\mathcal{L}_{\text{int}} = \int \frac{d^3 q_1}{(2\pi)^3} \frac{d^3 q_2}{(2\pi)^3} (\mathbf{q}_1 \cdot \mathbf{q}_2) \chi_{\mathbf{k}} h_{\mathbf{q}_1} h_{\mathbf{q}_2} \delta(\mathbf{k} + \mathbf{q}_1 + \mathbf{q}_2) \tag{2.3}$$

is the interaction vertex. In the second line of (2.1) we condensed the notation for time integrations. The field  $\chi$  is an auxiliary field and the  $\chi^2$  term in the action encodes stochasticity. It can be used to encode both stochastic initial conditions as well as the continuously acting stochastic part of the stress tensor, modeling the action of small scale fluctuations. Accordingly,  $\mathcal{N}$  contains the initial Power Spectrum  $P_{\Phi_{\text{in}}}$  as well as the Power Spectrum  $\Delta = \langle JJ \rangle$  of the (gaussian) noise  $J$ . For the Fourier transform of  $\mathcal{N}$  we assume

$$\mathcal{N}(D, D'; \mathbf{k}, \mathbf{k}') = P_{\Phi_{\text{in}}}(k) (2\pi)^3 \delta_D(\mathbf{k} + \mathbf{k}') \delta_D(D - D_{\text{in}}) \delta_D(D' - D_{\text{in}}) + \Delta(D, D') (2\pi)^3 \delta_D(\mathbf{k} + \mathbf{k}'), \tag{2.4}$$

with the scale independence of  $\Delta$  ensuring that the small scale fluctuations induce the well known  $k^2$  peculiar velocity Power Spectrum at large scales and, correspondingly the  $k^4$  tail in the density. The term  $\nu \nabla^2 h$  is the effective viscosity term.  $G_0^{R(A)}$  is the *free* Retarded (Advanced) Green function and the notation  $[G_0^{R(A)}]^{-1}$  is used to denote the operators appearing in (2.1) with Retarded (Advanced) boundary conditions. All correlators of interest can then be obtained from the generating functional

$$\mathcal{Z} = \int Dh D\chi e^{iS}, \tag{2.5}$$

with the MSRJD propagator  $\hat{G}$  defined as the functional and matrix inverse of the matrix in the quadratic part of the MSRJD action:

$$\hat{G}_0 = \begin{pmatrix} F_0(D, D'; k) & -iG_0^R(D, D'; k) \\ -iG_0^A(D, D'; k) & 0 \end{pmatrix} = \begin{pmatrix} \langle h_{\mathbf{k}}(D) h_{\mathbf{k}}^*(D') \rangle & \langle h_{\mathbf{k}}(D) \chi_{\mathbf{k}}^*(D') \rangle \\ \langle \chi_{\mathbf{k}}(D) h_{\mathbf{k}}^*(D') \rangle & \langle \chi_{\mathbf{k}}(D) \chi_{\mathbf{k}}^*(D') \rangle \end{pmatrix}. \tag{2.6}$$

<sup>1</sup>Named after Martin, Siggia, Rose, Jansen and De Dominicis [41].

$$G_0^R(D_1, D_2; k) = D_1 \text{ --- } \underset{k}{\text{---}} \text{ --- } D_2 \quad F_0(D_1, D_2; k) = D_1 \text{ --- } \underset{k}{\text{---}} \text{ --- } D_2 \quad \frac{\mathbf{k}_1 \cdot \mathbf{k}_2}{2} = \mathbf{k} \text{ --- } \left\langle \begin{array}{l} \mathbf{k}_1 \\ \mathbf{k}_2 \end{array} \right.$$

**Figure 1.** The Feynman rules for the action (2.1) — for more details see [33]. As usual, wave-vector conservation applies and the vertex has to be integrated over internal momenta and time.

The advanced and retarded Green functions are not independent since  $G_0^R(D, D') = G_0^{A*}(D', D)$ . Furthermore, knowledge of  $G_0^R$  allows the computation of  $F_0$  as

$$F_0(D, D'; k) = \int_0^D dudv G_0^R(D, u; k) \mathcal{N}(u, v; k) G_0^A(v, D'; k). \quad (2.7)$$

As we already discussed, the theory is expected to be non-local in time and this can be implemented by the replacement  $\nu(D) \nabla^2 h(D) \rightarrow \int_{D_{\text{in}}}^D dD' \nu(D, D') \nabla^2 h(D')$ . From the action (2.1) one can read off the Feynman rules depicted in figure 1. Note, that the form of the propagators  $G_0^R(D, D'; \mathbf{k})$  and  $F_0(D, D'; \mathbf{k})$  is different if the viscosity and the noise are treated perturbatively (à la EFToLSS) or non-perturbatively. Note also that  $F_0$  is simply the linear Power Spectrum  $P_L$  of  $h$ .

The MSRJD action and propagator imply that the “self-energy” (the sum of all 1PI diagrams<sup>2</sup>) also has the structure

$$\hat{\Sigma} = \begin{pmatrix} 0 & \Sigma^A(D, D'; k) \\ \Sigma^R(D, D'; k) & i\Phi(D, D'; k) \end{pmatrix}. \quad (2.8)$$

If  $G$  is the full *dressed* Green function it satisfies the Schwinger-Dyson equation

$$\left( \hat{G}_0^{-1} - \hat{\Sigma} \right) \circ \hat{G} = \hat{1} \quad (2.9)$$

where the circle product denotes integrations over time and matrix multiplications. Writing it explicitly we obtain

$$(\partial_D + \nu k^2) G^R(D, D') - \int du \Sigma^R(D, u) G^R(u, D') = \delta(D - D'), \quad (2.10)$$

$$(-\partial_D + \nu k^2) G^A(D, D') - \int du \Sigma^A(D, u) G^A(u, D') = \delta(D - D'), \quad (2.11)$$

$$(\partial_D + \nu k^2) F(D, D') - \int du \Sigma^R(D, u) F(u, D') + \int du (\mathcal{N}(D, u) - \Phi(D, u)) G^A(u, D') = 0. \quad (2.12)$$

To close this section, we emphasize that SAM is not intended as a tool for precision cosmology calculations as it contains uncontrolled approximations. Nonetheless, it can reproduce qualitatively the morphological structure of the cosmic web obtained from N-Body simulations — see [42–44] for some early works on the adhesion model. The addition of a stochastic

<sup>2</sup>1PI-diagrams are those diagrams which cannot be cut into two by cutting a single line.

component could be used to parametrize short scale, highly non-linear processes and could improve the results of those early works by generating more realistic short scale power. Furthermore, it seems that an irreducible stochastic component is necessary for describing the effects of short scales and becomes dominant over further additions to the stress energy tensor [45]. With these remarks we postpone a detailed evaluation of SAM for future work. What is important for us here is simply that the SAM is invariant under Extended Galilean Transformations (GT), like the complete fluid equations, and we are therefore able to discuss the interplay between Galilean Invariance (GI), non-locality in time and renormalization with the SAM as a conceptually useful toy model.

### 3 Galilean Invariance

Symmetries constrain the allowed terms to be added to the fluid equations for CDM. In the previous section we already stressed that the fluid equations as well as the SAM are invariant under GT. The GI of the fluid equations in the context of LSS and the corresponding consistency relations were already discussed in [14, 15, 46, 47]. GI of the fluid equations is the symmetry of the relativistic equations with a non-trivial Newtonian limit [48] and are therefore related to diffeomorphism invariance of the full relativistic theory. A GT is a time dependent boost with a velocity  $\boldsymbol{\beta}(D)$ . The coordinates then transform according to

$$\begin{aligned} D &\rightarrow D' = D \\ \mathbf{x} &\rightarrow \mathbf{x}' = \mathbf{x} + \int_{D_i}^D d\eta \boldsymbol{\beta}(\eta) \equiv \mathbf{x} + \mathbf{T}(D), \end{aligned} \quad (3.1)$$

and the velocity potential transforms accordingly as

$$h(D, \mathbf{x}) \rightarrow h(D', \mathbf{x}') = h(D, \mathbf{x} + \mathbf{T}(D)) - \mathbf{x} \cdot \boldsymbol{\beta}(D). \quad (3.2)$$

The action (2.1) then transform as follows

$$S[h, \chi] \rightarrow S[h, \chi] + \delta S_{\mathcal{N}}[h, \chi] + \int dD d^3x \chi \left( -\mathbf{x} \cdot \partial_D \boldsymbol{\beta} + \frac{1}{2} \boldsymbol{\beta}^2 \right), \quad (3.3)$$

where we used that time derivatives are not GI, but the convective derivative  $\partial_D + \frac{1}{2} \nabla h \cdot \nabla$  is GI. Compared to the action in equation (2.1), equation (3.3) contains two extra terms. The term  $\delta S_{\mathcal{N}}[h, \chi]$  will vanish for a GI stochastic noise. The term  $\int dD d^3x \chi \left( -\mathbf{x} \cdot \partial_D \boldsymbol{\beta} + \frac{1}{2} \boldsymbol{\beta}^2 \right)$  contains two unobservable contributions. The  $\boldsymbol{\beta}^2$  terms simply adds a constant contribution to the velocity potential, while the  $\mathbf{x} \cdot \partial_D \boldsymbol{\beta}$  term is a frame fixing term and ensures that the homogeneous mode of the velocity is given by  $\boldsymbol{\beta}$  [15].

As discussed above, higher order terms are allowed but GI only allows terms built of second or higher derivatives of  $h$ . For example we can add a second order viscosity

$$\nu^{(2)} \nabla^4 h \quad (3.4)$$

or new vertices as

$$\lambda (\nabla^2 h)^2 + g (\partial_i \partial_j h) (\partial^i \partial^j h). \quad (3.5)$$

Let us now have look at the noise and how it is constrained by GI. The Power Spectrum of a statistically homogeneous and isotropic noise  $J$  is of the form  $\langle J(D_1, \mathbf{x}_1) J(D_1, \mathbf{x}_2) \rangle =$

$\Delta(D_1, D_2, |\mathbf{x}_1 - \mathbf{x}_2|)$ . The noise term in the action is only GI if the noise Power Spectrum is invariant

$$\Delta(D_1, D_2, |\mathbf{x}_1 - \mathbf{x}_2|) = \Delta(D_1, D_2, |\mathbf{x}_1 + \mathbf{T}(D_1) - \mathbf{x}_2 - \mathbf{T}(D_2)|), \quad (3.6)$$

which is only the case if the noise is temporally white

$$\Delta(D_1, D_2, |\mathbf{x}_1 - \mathbf{x}_2|) = \Delta(D_1, |\mathbf{x}_1 - \mathbf{x}_2|) \delta_D(D_1 - D_2). \quad (3.7)$$

Similar arguments hold for higher order correlators or a multiplicative noise.

A noise with a finite correlation time is not apparently GI. However, consider the noise term evaluated along the path of a fluid element [23]

$$J(D; \mathbf{x}_{\text{fl}}(D, D_i)), \quad (3.8)$$

where the position of the fluid element can be obtained by solving

$$\mathbf{x}_{\text{fl}}(D, D') = \mathbf{x} + \int_{D'}^D d\eta \nabla h(\eta, \mathbf{x}_{\text{fl}}(D, \eta)). \quad (3.9)$$

Since  $\mathbf{x}_{\text{fl}}$  does not change under GTs, neither does the argument of  $J$  and its correlators are invariant. It is interesting to note that a noise of the form given in equation (3.8) is nothing but a solution of an equation of the form:

$$\left. \frac{dJ}{dD} \right|_{\mathbf{x}_{\text{fl}}} = \partial_D J + \mathbf{w} \cdot \nabla J = \dots, \quad (3.10)$$

i.e. of a derivative taken along the fluid flow lines. The ellipses denote possible further terms consistent with Galilean symmetry. So a non-local noise can be seen as new degree of freedom, governed by (3.10), which can be added to the set of equations. As we will discuss in section 4 the time dependence of the noise is fixed by the time dependence of the loops. This means that it is sufficient to provide initial conditions to specify the noise, suggesting that a non-local noise arises from coarse graining over the initial conditions.<sup>3</sup>

If we treat the dependence on the fluid path perturbatively we find for the noise

$$J(D; \mathbf{x}_{\text{fl}}(D, D_i)) = J(D; \mathbf{x}) + \int_{D_i}^D d\eta \nabla h(\eta; \mathbf{x}) \cdot \nabla J(D; \mathbf{x}) + \dots \quad (3.11)$$

For the corresponding Power Spectrum we find a temporal non-white noise plus corrections in form of a multiplicative noise

$$\begin{aligned} \Delta(D_1, D_2; |\mathbf{x}_{\text{fl}}(D_1, D_i) - \mathbf{x}_{\text{fl}}(D_2, D_i)|) &= \Delta(D_1, D_2; |\mathbf{x}_1 - \mathbf{x}_2|) \\ &+ \int_{D_i}^{D_1} d\eta (\nabla h)(\eta; \mathbf{x}_1) \cdot \nabla_1 \Delta(D_1, D_2; |\mathbf{x}_1 - \mathbf{x}_2|) \\ &+ \int_{D_i}^{D_2} d\eta (\nabla h)(\eta; \mathbf{x}_2) \cdot \nabla_2 \Delta(D_1, D_2; |\mathbf{x}_1 - \mathbf{x}_2|) + \dots \end{aligned} \quad (3.12)$$

---

<sup>3</sup>Our discussion of free-streaming particles in the introduction provides another example where the initial stress tensor has been integrated out.

So a non-local noise is allowed as long as it is the first term in a series of terms all with the *same* coefficient function.

Evaluating the fields along the fluid path  $\mathbf{x}_\Pi$  we can likewise generalize local terms containing  $h$  to non-local terms. For example a non-local viscosity reads

$$\int_{D_{\text{in}}}^D dD' \nu(D, D') \nabla^2 h(D'; \mathbf{x}_\Pi(D', D_i)) = \int_{D_{\text{in}}}^D dD' \nu(D, D') \nabla^2 h(D'; \mathbf{x}) + \int_{D_{\text{in}}}^D dD' \int_{D_{\text{in}}}^{D'} d\eta \nu(D, D') \nabla^2 ((\nabla h(\eta; \mathbf{x})) \cdot \nabla h(D'; \mathbf{x})) \dots \quad (3.13)$$

Similarly to the noise, a non-local viscosity is allowed as the first term in a series of terms, all with the *same* coefficient.

Observe that these extra terms can and must contain the velocity itself, so terms with only one derivative acting on  $h$  appear in the action. The non-local-in-time terms in (3.12) and (3.13), a consequence of GI, lead at one loop to the new vertices

$$\begin{aligned} \begin{array}{c} D_1, \mathbf{k}_1 \\ \diagup \\ D, \mathbf{k} \text{ ---} \bullet \\ \diagdown \\ D_2, \mathbf{k}_2 \end{array} &= -\frac{k^2 \mathbf{k}_1 \cdot \mathbf{k}_2}{2} (\nu(D, D_1) \theta(D_1 - D_2) + \nu(D, D_2) \theta(D_2 - D_1)) \\ \begin{array}{c} D_1, \mathbf{k}_1 \\ \diagup \\ D, \mathbf{k} \text{ ---} \bullet \\ \diagdown \\ D_2, \mathbf{k}_2 \end{array} &= (\mathbf{k} \cdot \mathbf{k}_2 \Delta(D_1, D_2; k_2) + \mathbf{k} \cdot \mathbf{k}_1 \Delta(D_1, D_2; k_1)) (\theta(D_1 - D) + \theta(D_2 - D)), \end{aligned} \quad (3.14)$$

$$(3.15)$$

where as usual “momentum” conservation is implied. In contrast to the usual vertex one has to integrate over all three times  $D, D_1$  and  $D_2$ . In the EFToLSS approach these terms will only appear at second order, so are relevant for the one-loop bispectrum and the two-loop Power Spectrum.

## 4 Renormalization

We now discuss the implications of GI for the renormalization of UV-divergences. By a UV-divergence we refer to the leading contribution from hard loop momenta, irrespectively of whether the loop integrals are finite or infinite. In both cases these are unphysical contributions and must be removed from physical quantities by counter terms corresponding to the effective terms. Since in SPT loop integrals are finite for realistic initial conditions, actual divergences are not present at low orders, but will arise at higher orders from loops containing the effective terms.

When renormalizing the loop integrals one has to pay attention to the fact that they have a non-trivial time dependence, so the counter terms must match the time dependence of the UV-divergences, either local or non-local in time. Since the time dependence of the



They can be renormalized by constant contributions to the viscosity and noise

$$\begin{aligned}\nu(D_1, D_2) &= c_v^2 \\ \Delta(D_1, D_2) &= \Delta.\end{aligned}\tag{4.7}$$

It has been noticed [26, 27] that at lowest order a non-local viscosity can be mimicked by a local one. In principle this is still possible at higher order but then new terms are necessary correcting for the error made by using a local viscosity instead of a non-local one. For the noise a similar procedure is not possible.

As discussed in section 3 the same constants  $c_v^2$  and  $\Delta$  appear as coefficients of vertices, so the same divergences as in the vertices must be present in the vertex corrections, which are given by the sum of the three upper diagrams shown in figure 2

$$\begin{aligned}\Pi(D, D_1, D_2; \mathbf{k}_1, \mathbf{k}_2) &= -\theta(D-D_1)\theta(D_1-D_2)\frac{k^2\mathbf{k}_1\cdot\mathbf{k}_2}{12}I_2 + \theta(D-D_1)\theta(D-D_2)\frac{(\mathbf{k}_1\cdot\mathbf{k}_2)^2}{12}I_2 \\ &+ (D_1 \leftrightarrow D_2).\end{aligned}\tag{4.8}$$

Note that contributions to  $\Pi$  which would renormalize the vertex  $\frac{\mathbf{k}_1\cdot\mathbf{k}_2}{2}$  cancel among the three different diagrams. The first term in equation (4.8) has exactly the form required by GI, the second term can be renormalized by a non-local version of the  $g$ -term in equation (3.5) while the non appearance of a term corresponding to  $\lambda$  in (3.5) is a consequence of the simple form of the vertex.

The second class of diagrams we have to consider are those generating a multiplicative noise (the two diagrams in the second line of figure 2). Their sum is

$$\begin{aligned}\Psi(D, D_1, D_2; \mathbf{k}_1, \mathbf{k}_2) &= \theta(D_1-D)\left(-\frac{\mathbf{k}_1\cdot\mathbf{k}}{16}Y_4(k_1) - \frac{\mathbf{k}_2\cdot\mathbf{k}}{16}Y_4(k_2) + \frac{1}{8}\mathbf{k}\cdot(\mathbf{Y}_4(k_1) + \mathbf{Y}_4(k_2))\cdot\mathbf{k}\right. \\ &+ \frac{k_1^2\mathbf{k}_1\cdot\mathbf{k} - (\mathbf{k}_1\cdot\mathbf{k})^2}{32}Y_2(k_1) + \frac{k_2^2\mathbf{k}_2\cdot\mathbf{k} - (\mathbf{k}_2\cdot\mathbf{k})^2}{32}Y_2(k_2) \\ &- \frac{1}{32}\mathbf{k}\cdot(k_1^2\mathbf{Y}_2(k_1) + k_2^2\mathbf{Y}_2(k_2))\cdot\mathbf{k} \\ &\left. - \frac{k_1^4\mathbf{k}\cdot\mathbf{k}_1 - k_1^2(\mathbf{k}\cdot\mathbf{k}_1)^2}{128}Y_0(k_1) - \frac{k_2^4\mathbf{k}\cdot\mathbf{k}_2 - k_2^2(\mathbf{k}\cdot\mathbf{k}_2)^2}{128}Y_0(k_2)\right) + (D_1 \leftrightarrow D_2),\end{aligned}\tag{4.9}$$

where we used that  $\int d^3q \mathbf{q}q^n P_{\Phi_{\text{in}}}(|\mathbf{q} - \frac{\mathbf{k}}{2}|) P_{\Phi_{\text{in}}}(|\mathbf{q} + \frac{\mathbf{k}}{2}|) = 0$  and defined

$$\mathbf{Y}_{n+2}(k) = \int \frac{d^3q}{(2\pi)^3} \mathbf{q}q^n P_{\Phi_{\text{in}}}\left(\left|\mathbf{q} - \frac{\mathbf{k}}{2}\right|\right) P_{\Phi_{\text{in}}}\left(\left|\mathbf{q} + \frac{\mathbf{k}}{2}\right|\right).\tag{4.10}$$

The leading divergences are again those of  $Y_4$  and  $\mathbf{Y}_4$ , where due to rotational invariance  $\mathbf{Y}$  must be of the form

$$\mathbf{Y}_{n+2}(\mathbf{k}) = F(k)\mathbf{1} + G(k)\mathbf{k}\mathbf{k}.\tag{4.11}$$

Since in the limit  $q \gg k$ ,  $\mathbf{Y}_{n+2}(\mathbf{k})$  depends only on the absolute value  $k$ , we conclude that the leading divergence stems from  $F(k)$ , which is the same as that of  $Y_4$ . So we can simply

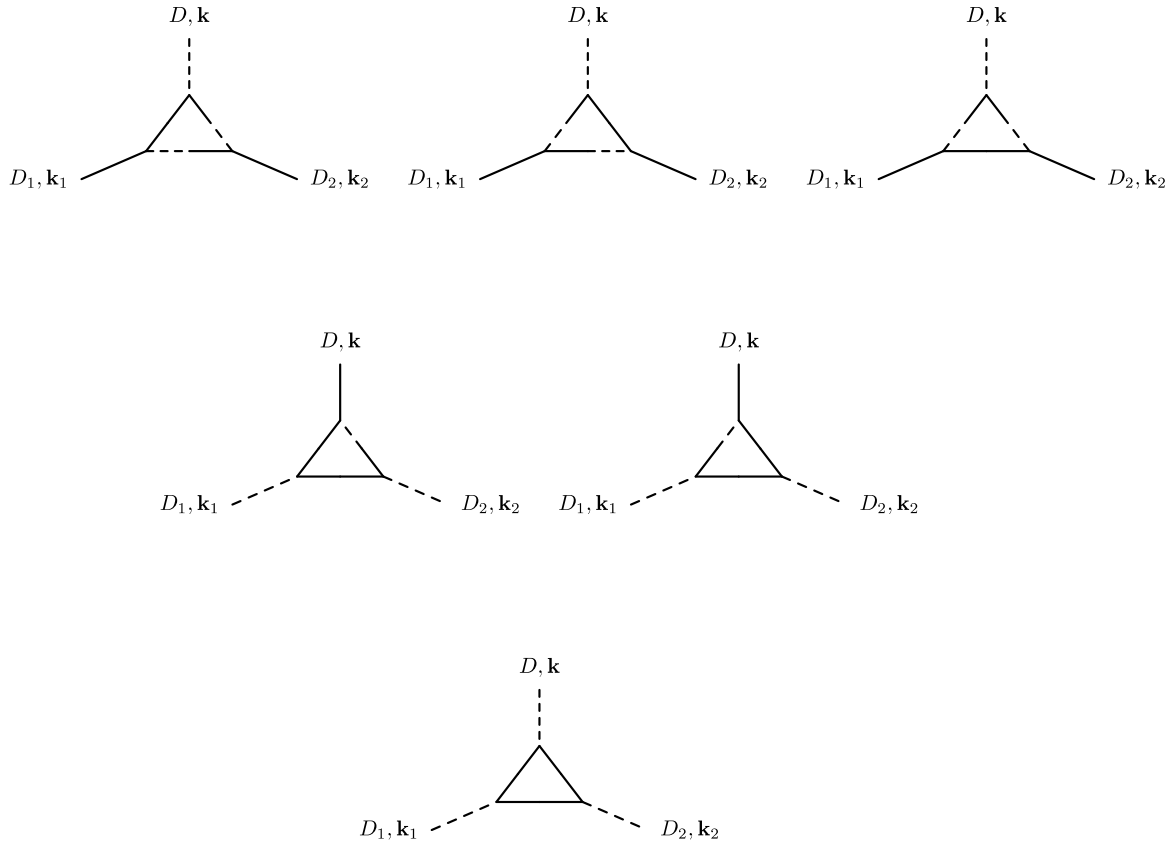


**Figure 2.** The 6 one-loop contribution to the bispectrum. The upper three renormalize the vertex. The two diagrams in the second line generate a multiplicative noise. The diagram in the last line generates a bispectrum for the noise.

replace  $F$  by  $\frac{Y_{n+2}}{3}$ . In that limit  $\Psi$  reads

$$\Psi(D, D_1, D_2; \mathbf{k}_1, \mathbf{k}_2) \sim \theta(D_1 - D) \left( -\frac{\mathbf{k}_1 \cdot \mathbf{k}}{16} Y_4(k_1) - \frac{\mathbf{k}_2 \cdot \mathbf{k}}{16} Y_4(k_2) + \frac{k^2}{24} (Y_4(k_1) + Y_4(k_2)) \right) + (D_1 \leftrightarrow D_2). \quad (4.12)$$

We are left with two divergences. First, the one in  $k^2 Y_4(k_i)$  which can be renormalized by a multiplicative noise of the form  $\tilde{J} \nabla^2 h$  and the one in  $\mathbf{k}_i \cdot \mathbf{k} Y_4(k_i)$  which as required by GI is the same as in the Power Spectrum.

## 4.2 Local in time

The power counting of the effective viscosity and noise terms discussed above, corresponding to that employed in the EFToLSS literature, implies that loops are renormalizable if the effective terms are non-local in time. We will now demonstrate that by including the effective viscosity and the noise in the propagators, loops can also be renormalized in a theory local in time. In that case the theory is similar to an ordinary viscous fluid with stochastic noise.

Let us in the following write the viscosity as  $\nu(D) = c_v^2 \tilde{\nu}(D)$ , with  $\tilde{\nu}(D) = O(1)$ . We chose the time dependence of the noise to be  $\Delta(D, D') = \Delta \tilde{\nu}^3(D) \delta_D(D - D')$ . The linear

propagator and the linear power spectrum are then given by

$$G_0^R(D, D'; k) = e^{-c_v^2 k^2 \int_{D'}^D d\eta \tilde{\nu}(\eta)} \theta(D - D') \quad (4.13)$$

$$F_0(D, D'; k) = e^{-c_v^2 k^2 \left( \int_0^D d\eta \tilde{\nu}(\eta) + \int_0^{D'} d\eta \tilde{\nu}(\eta) \right)} P_{\Phi_{\text{in}}}(k) \\ + e^{-c_v^2 k^2 \left( \int_0^D d\eta \tilde{\nu}(\eta) + \int_0^{D'} d\eta \tilde{\nu}(\eta) \right)} \Delta \int_0^{\min(D, D')} d\eta e^{2c_v^2 k^2 \int_0^\eta d\eta' \tilde{\nu}(\eta')} \tilde{\nu}^3(\eta).$$

As already argued in [33] on large scales we recover the usual linear Power Spectrum, while on small scales the Power Spectrum is dominated by the noise.

$$F_0(D, D'; k) = e^{-c_v^2 k^2 \left( \int_0^D d\eta \tilde{\nu}(\eta) + \int_0^{D'} d\eta \tilde{\nu}(\eta) \right)} \Delta \int_0^{\min(D, D')} d\eta \tilde{\nu}(\eta) e^{2c_v^2 k^2 \int_0^\eta d\eta' \tilde{\nu}(\eta')} \tilde{\nu}^2(\eta) \\ = e^{-c_v^2 k^2 \left( \int_0^D d\eta \tilde{\nu}(\eta) + \int_0^{D'} d\eta \tilde{\nu}(\eta) \right)} \frac{\Delta}{2c_v^2 k^2} \int_0^{\min(D, D')} d\eta \tilde{\nu}^2(\eta) \frac{d}{d\eta} e^{2c_v^2 k^2 \int_0^\eta d\eta' \tilde{\nu}(\eta')} \quad (4.14)$$

$$= \frac{\tilde{\nu}^2(D') \Delta}{2c_v^2 k^2} e^{-c_v^2 k^2 \int_{D'}^D d\eta \tilde{\nu}(\eta)} \theta(D - D') + (D \leftrightarrow D') + O((c_v k)^{-4}). \quad (4.15)$$

To obtain the last line we performed a partial integration and neglected terms which are exponentially suppressed. Repeated partial integration would allow to calculate the  $O((c_v k)^{-4})$  terms and higher. Note that on small scales the Power Spectrum is exponentially suppressed unless  $D \approx D'$ .<sup>4</sup>

The leading UV-divergences of the self energies are then

$$\Sigma(D, D'; k) \sim \frac{\Delta}{2c^2} \int \frac{d^3 q}{(2\pi)^3} \frac{(q^2 + \mathbf{q} \cdot \mathbf{k}) \mathbf{q} \cdot \mathbf{k}}{q^2} \tilde{\nu}^2(D') \theta(D - D') G_0^R(D, D'; q) G_0^R(D, D'; |\mathbf{q} + \mathbf{k}|) \\ \Phi(D, D'; k) \sim \frac{\Delta^2}{4c^4} \int \frac{d^3 q}{(2\pi)^3} \frac{\left( q^2 - \frac{k^2}{4} \right)^2}{\left( \mathbf{q} + \frac{\mathbf{k}}{2} \right)^2 \left( \mathbf{q} - \frac{\mathbf{k}}{2} \right)^2} \tilde{\nu}^4(D') \theta(D - D') G_0^R \left( D, D'; \left| \mathbf{q} - \frac{\mathbf{k}}{2} \right| \right) \\ \cdot G_0^R \left( D, D'; \left| \mathbf{q} + \frac{\mathbf{k}}{2} \right| \right) + (D \leftrightarrow D'). \quad (4.16)$$

The above expressions are non-vanishing only for  $D_1 \approx D_2$  and they can therefore be approximated as local in time. Integrating over time we obtain to leading order

$$\Sigma(D, D'; k) \sim \tilde{\nu}(D_2) \frac{\Delta}{2c^4} \delta_D(D - D') \int \frac{d^3 q}{(2\pi)^3} \frac{(q^2 + \mathbf{q} \cdot \mathbf{k}) \mathbf{q} \cdot \mathbf{k}}{q^2 (q^2 + (\mathbf{q} + \mathbf{k})^2)} \\ \Phi(D, D'; k) \sim \tilde{\nu}^3(D_2) \frac{\Delta^2}{8c^6} \delta_D(D - D') \int \frac{d^3 q}{(2\pi)^3} \frac{\left( q^2 - \frac{k^2}{4} \right)^2}{\left( \mathbf{q} + \frac{\mathbf{k}}{2} \right)^2 \left( \mathbf{q} - \frac{\mathbf{k}}{2} \right)^2 \left( q^2 + \frac{k^2}{4} \right)}. \quad (4.17)$$

We immediately see that the time dependence matches the one of the viscosity and the noise.<sup>5</sup> The  $q$ -integrals are actually UV-divergent and must be regularized by an appropriate

<sup>4</sup>More precisely it is suppressed unless  $c_v^2 k^2 \int_{D'}^D d\eta \tilde{\nu}(\eta) \ll 1$ , which translates for monotonic (growing)  $\tilde{\nu}(D)$  into  $(D - D') \ll \frac{1}{c_v^2 k^2 \tilde{\nu}(D')} \sim \frac{1}{c_v^2 k^2}$ .

<sup>5</sup>Reference [33] treated the special case of  $\tilde{\nu}(D) = D$ .

prescription. From inspecting the integrals we see that  $\Sigma$  has a quadratic and a linear divergence. The quadratic vanishes due to rotational invariance and the linear divergence has the correct  $k$  dependence to be absorbed into the viscosity. There is also a logarithmic divergence stemming from the sub leading terms  $O(\frac{1}{q^4})$ , we dropped this term since the divergence vanishes. The linear divergence in  $\Phi$  can be absorbed into the noise.

Observe that the divergences are the same as in the time independent theory with  $\tilde{\nu} = 1$ , as are the leading divergences at higher orders. There will also be additional divergences with new time dependencies at higher orders which will require new counter terms, including terms with additional time derivatives. This is not a problem since the theory is non-renormalizable and new counter terms must be added any way. It is interesting to note that if instead of a scale independent noise we chose one with  $\Delta \sim k^{-1}$  in the UV, the theory becomes renormalizable by power counting.

If we follow the same procedure as for the self-energies for the triangle diagrams we find

$$\begin{aligned}
 \Pi(D, D_1, D_2; \mathbf{k}_1, \mathbf{k}_2) &\sim -\frac{\Delta}{16c^6} \delta_D(D-D_1) \delta_D(D-D_2) \left( \int \frac{d^3q}{(2\pi)^3} \frac{\mathbf{k}_1 \cdot \mathbf{q} \mathbf{k}_2 \cdot (\mathbf{k}_1 + \mathbf{q}) \mathbf{q} \cdot (\mathbf{k} + \mathbf{q})}{q^2 (q^2 + (\mathbf{k}_1 + \mathbf{q})^2) (q^2 + (\mathbf{k} - \mathbf{q})^2)} \right. \\
 &\quad \left. + \int \frac{d^3q}{(2\pi)^3} \frac{\mathbf{k}_1 \cdot \mathbf{q} \mathbf{k}_2 \cdot \mathbf{q} (\mathbf{k}_1 + \mathbf{q}) (\mathbf{k}_2 - \mathbf{q})}{q^2 (q^2 + (\mathbf{k}_1 + \mathbf{q})^2) (q^2 + (\mathbf{k}_2 - \mathbf{q})^2)} \right) + (D_1 \leftrightarrow D_2) \\
 \Psi(D, D_1, D_2; \mathbf{k}_1, \mathbf{k}_2) &\sim \frac{\Delta^2 \tilde{\nu}^2(D)}{16c^6} \delta_D(D-D_1) \delta_D(D-D_2) \\
 &\quad \cdot \left( \int \frac{d^3q}{(2\pi)^3} \frac{(k_1^2 - 4q^2) \mathbf{k} \cdot (\mathbf{k}_1 + 2\mathbf{q}) (\mathbf{k}_1 - 2\mathbf{q}) \cdot (\mathbf{k}_1 + 2\mathbf{k} - 2\mathbf{q})}{(\mathbf{k}_1 + 2\mathbf{q})^2 (\mathbf{k}_1 - 2\mathbf{q})^2} \right. \\
 &\quad \cdot \left( \frac{1}{(k^2 + 4q^2)(k^2 + 4q^2 + \mathbf{q} \cdot (\mathbf{k}_1 - 2\mathbf{q}))} \right. \\
 &\quad \left. + \frac{1}{(2k^2 + (\mathbf{k} - 2\mathbf{q})^2 + \mathbf{k} \cdot (\mathbf{k}_1 - 2\mathbf{q}))((k^2 + 4q^2) + \mathbf{q} \cdot (\mathbf{k}_1 - 2\mathbf{q}))} \right. \\
 &\quad \left. \left. + \frac{1}{(k^2 + 4q^2)(2k^2 + (\mathbf{k} - 2\mathbf{q})^2 + \mathbf{k} \cdot (\mathbf{k}_1 - 2\mathbf{q}))} \right) \right) + (D_1 \leftrightarrow D_2). \quad (4.18)
 \end{aligned}$$

The individual diagrams contributing to  $\Pi$  are linearly divergent, but the divergences cancel among the integrals, ensuring that the vertex is not renormalized, as required by GI.  $\Psi$  is by power counting logarithmically divergent, but this divergence vanishes due to rotational invariance.

The third triangle diagram with three external dashed lines is finite and no non-gaussian noise is required to obtain finite results. Similarly, higher order correlators are finite at one-loop, so the SAM and most likely also the fluid equations are one-loop renormalizable. Of course, the loop integrals still contain unphysical contributions from modes beyond a UV-cutoff  $\Lambda \gg k_i$  and must in principle be renormalized, but the error made by not renormalizing the triangle diagrams is suppressed by  $k_i/\Lambda$  and therefore of the same order as the residual cutoff dependence of renormalized self-energies, and hence only subleading. So the minimal set of counter terms required to make the local-in-time theory cutoff independent at leading order, and hence the number of free parameters, is smaller than in the non-local-in-time version. Note that finite contribution from the  $g$ - and  $\lambda$ -type vertices or new noise terms as

discussed in section 3 can still be important but a detailed analysis is beyond the scope of our paper and we leave it for future work.

### 4.3 Ward Identities

The Ward Identities (WI) encode the statement that the effective action  $\Gamma$  transforms under infinitesimal GT in the same way as the bare action  $S$ . This implies a set of relations that counterterms necessarily satisfy. The effective action  $\Gamma$  is related to the generating functional of connected correlation functions and any physical information about a system can be obtained from it. We will now briefly discuss how the WI ensure that in a non-local theory the same divergences arise in different n-point functions.

The WI for the fluid equations were already derived in [15, 46], see also [49]. The corresponding WI for the SAM are

$$\int dD d^3k \left( \mathbf{k} \cdot \mathbf{T}(D) \left( \frac{\delta\Gamma}{\delta h_{\mathbf{k}}(D)} h_{\mathbf{k}}(D) + \frac{\delta\Gamma}{\delta \chi_{\mathbf{k}}(D)} \chi_{\mathbf{k}}(D) \right) + \delta_D(\mathbf{k}) \left( \beta(D) \cdot \partial_{\mathbf{k}} \frac{\delta\Gamma}{\delta h_{\mathbf{k}}(D)} - \partial_D \beta(D) \cdot \partial_{\mathbf{k}} \chi_{\mathbf{k}}(D) + \frac{i}{2} \chi_{\mathbf{k}}(D) \beta^2(D) \right) \right) = 0. \quad (4.19)$$

The  $\partial_{\mathbf{k}}\chi$ -term relates the mean velocity to the Galilean boost  $\beta$  and the  $\chi$ -term is related to an unobservable shift in the potential. These terms correspond to the change of the bare action under GT, see equation (3.3). The 1-particle-irreducible vertices (1PI-vertices) defined as

$$\Gamma^{(n,m)} \equiv \frac{\delta^{n+m}\Gamma}{\delta \chi_{\mathbf{p}_1}(\eta_1) \dots \delta \chi_{\mathbf{p}_n}(\eta_n) \delta h_{\mathbf{q}_1}(\lambda_1) \dots \delta h_{\mathbf{q}_m}(\lambda_m)} \Big|_{h=\chi=0}, \quad (4.20)$$

are given by the sum over all 1PI-diagrams with  $n$  dashed and  $m$  solid lines. Taking  $n$  derivatives with respect to  $\chi$  and  $m$  derivatives with respect to  $\varphi$  of equation (4.19), we arrive after a partial integration, for  $n \neq 1$  and  $m \neq 0$ , at a relation between a vertex with  $n + m$  legs and one with  $n + m + 1$  legs of the form

$$\sum_{i=1}^n \mathbf{p}_i \delta_D(D - \eta_i) \Gamma^{(n,m)} + \sum_{i=1}^m \mathbf{q}_i \delta_D(D - \lambda_i) \Gamma^{(n,m)} - \int d^3k \delta_D(\mathbf{k}) \partial_D \partial_{\mathbf{k}} \Gamma^{(n,m+1)} = 0. \quad (4.21)$$

Note that  $\Gamma^{(0,m)} = 0$  for any  $m$ . The WI in this form relate a 1PI-vertex to another 1PI-vertex with one more leg. The extra leg thereby corresponds to a velocity i.e. a solid line. The delta-function picks out the limit  $k \rightarrow 0$ . Terms with more than one factor of  $k$  are therefore unconstrained by the WI, as expected from our discussion in section 3. Since each velocity leg must contain at least one factor of  $k$  the WI relate 1PI-vertices with velocity legs with *one* factor of  $k$  to a 1PI-vertices with one velocity leg less. This is exactly what is required by GI as discussed in section 3.

Let us illustrate that this ensures that loops can be renormalized with GI counter terms at any order in perturbation theory with the example of 2-vertices and 3-vertices. For  $n = 1$  and  $m = 1$  the WI read

$$\mathbf{k}_1 G^{-1}(D_1, D_2; k_1) (\theta(\eta - D_1) - \theta(\eta - D_2)) = \lim_{\mathbf{p} \rightarrow 0} \partial_{\mathbf{k}} \Gamma^{(1,2)}(D_1, D_2, \eta; \mathbf{k}_1, \mathbf{p}) \quad (4.22)$$

where the full inverse propagator is given by

$$G^{-1}(D_1, D_2; k_1) = (G_0^{-1}(D_1, D_2; k_1) - \Sigma(D_1, D_2, k_1)) \quad (4.23)$$

and similarly the full vertex is composed of the tree level vertex  $\tilde{\gamma}$ , containing both the usual vertex and a possible contribution from the non-local viscosity, and the loop corrections

$$\Gamma^{(1,2)}(D_1, D_2, \eta; \mathbf{k}_1, \mathbf{k}_2, \mathbf{p}) = -2\tilde{\gamma}(D_1, D_2, \eta; \mathbf{k}_1, \mathbf{k}_2, \mathbf{p}) - \Pi(D_1, D_2, \eta; \mathbf{k}_1, \mathbf{k}_2, \mathbf{p}). \quad (4.24)$$

Using that in the local theory the tree level propagator is  $G_0^{-1}(D_1, D_2; k_1) = \partial_{D_1} \delta_D(D_1 - D_2) + k_1^2 \nu(D_1) \delta_D(D_1 - D_2)$  and the vertex is  $\tilde{\gamma} = \delta(\eta - D_1) \delta(\eta - D_2) \frac{\mathbf{k}_1 \cdot \mathbf{p}}{2}$  in equation (4.22) we find that convective derivative is GI. If the viscosity is non-local, its contribution does not cancel and the vertex gets an extra contribution, as discussed in section 3.

For  $n = 2$  and  $m = 0$  a similar relation holds. At loop level we have

$$\begin{aligned} \Sigma(D_1, D_2; k_1) \mathbf{k}_1 (\theta(\eta - D_1) - \theta(\eta - D_2)) &= \lim_{\mathbf{p} \rightarrow 0} \partial_{\mathbf{p}} \Pi(D_1, D_2, \eta; \mathbf{k}_1, \mathbf{p}) \\ \Phi(D_1, D_2; k_1) \mathbf{k}_1 (\theta(\eta - D_1) - \theta(\eta - D_2)) &= \lim_{\mathbf{p} \rightarrow 0} \partial_{\mathbf{p}} \Psi(D_1, D_2, \eta; \mathbf{k}_1, \mathbf{p}). \end{aligned} \quad (4.25)$$

As an example the relations at one loop are depicted in figure 3. If we now use that in the limit  $p \rightarrow 0$  the vertices are  $\Pi(\mathbf{k}_1, \mathbf{p}) \propto \mathbf{p} \cdot \mathbf{k}_1 \Pi(k_1)$  and  $\Psi(\mathbf{k}_1, \mathbf{p}) \propto \mathbf{p} \cdot \mathbf{k}_1 \Psi(k_1)$ , we explicitly find the same relation as as we found in section 3:

$$\begin{aligned} \Pi(D_1, D_2, \eta; \mathbf{k}_1, \mathbf{p}) &= \mathbf{p} \cdot \mathbf{k}_1 \Sigma(D_1, D_2; k_1) (\theta(\eta - D_1) - \theta(\eta - D_2)) + O(p^2) \\ \Psi(D_1, D_2, \eta; \mathbf{k}_1, \mathbf{p}) &= \mathbf{p} \cdot \mathbf{k}_1 \Phi(D_1, D_2; k_1) (\theta(\eta - D_1) - \theta(\eta - D_2)) + O(p^2). \end{aligned} \quad (4.26)$$

These relations guarantee that the same divergence appearing in loop corrections to the power spectrum also appears in loop corrections to the bispectrum. In particular since the leading UV-divergences scale as  $\Sigma \propto k^2$  and  $\Phi \propto k^0$ , the WI guarantee that the same divergence also appear in  $\Pi$  and  $\Psi$ , if the theory is non-local in time, while if the divergence is local in time the WI guarantee that there is *no* vertex correction of this type, unless the self energies contain time derivatives. Then as at tree level the WI guarantee that the time derivatives are always part of a convective derivative.<sup>6</sup>

From the form of the WI in equation (4.21) it is immediately clear that the same procedure also applies to higher order vertices. The general relation between vertices with  $n + m$  legs and  $n + m + i$  legs can be obtained by applying equation (4.21) recursively.

#### 4.4 The bispectrum in the local and non-local theories

The scale and time dependence of correlation functions obtained from the local-in-time theory is much more complex than that obtained from the non-local-in-time one. But on sufficiently large scales  $c_v^2 k^2 \ll 1$ , and if the noises are neglected, the one-loop Power Spectra of both theories are expected to agree. Nevertheless, the two theories give different results for the one-loop bispectrum. In the non-local-in-time power counting, the one-loop bispectrum consists of the SPT tree-level and one loop bispectrum plus EFT corrections in form of the new

<sup>6</sup>These terms are redundant i.e. for practical calculations they can be simplified using the equation of motion.

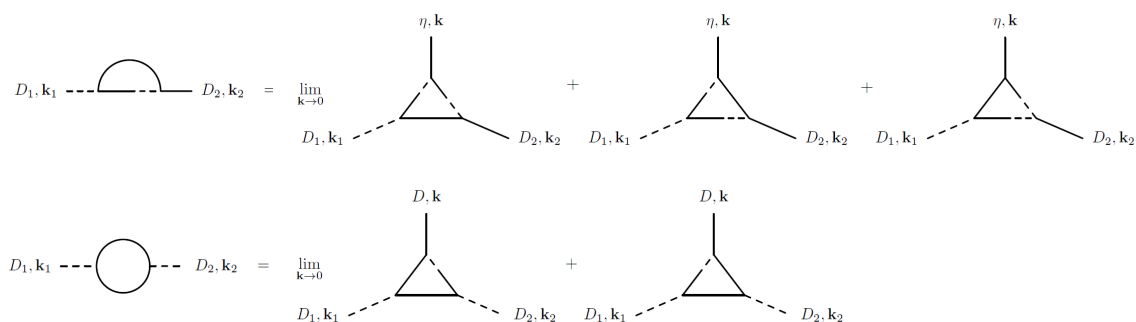


**Figure 3.** The WI in equation (4.25) at one loop.

vertex, with the coupling  $g$ , and the counter terms for  $\Sigma$ :

$$\begin{aligned}
 B_{\text{NLT}}(D_1, D_2, D_3; k_1, k_2, k_3) &= B_{\text{tree}}(k_1, k_2, k_3) + B_{1\text{-loop}}(D_1, D_2, D_3; k_1, k_2, k_3) + g D_3^3 \frac{(\mathbf{k}_1 \cdot \mathbf{k}_2)^2}{6} P_L(k_1) P_L(k_2) \\
 &\quad - c_v^2 \frac{\mathbf{k}_1 \cdot \mathbf{k}_2}{2} P_L(k_1) P_L(k_2) \left( \frac{k_1^2}{6} (D_3^3 + 3D_1^2 D_3) + \frac{k_2^2}{6} (D_3^3 + 3D_2^2 D_3) + \frac{k_3^2}{2} D_3^3 \right) \\
 &\quad + \text{permutations.} \tag{4.27}
 \end{aligned}$$

For the bispectrum in the local theory we find

$$\begin{aligned}
 B_{\text{LT}}(D_1, D_2, D_3; k_1, k_2, k_3) &= B_{\text{NLT}}(D_1, D_2, D_3; k_1, k_2, k_3) - g D_3^3 \frac{(\mathbf{k}_1 \cdot \mathbf{k}_2)^2}{6} P_L(k_1) P_L(k_2) \\
 &\quad + c_v^2 D_3^3 \frac{k_3^2 \mathbf{k}_1 \cdot \mathbf{k}_2}{12} P_L(k_1) P_L(k_2) + \text{permutations.} \tag{4.28}
 \end{aligned}$$

That  $g$  appears in  $B_{\text{NLT}}$  but not in  $B_{\text{LT}}$  is an illustration that less free parameters are required for consistency in the local theory compared to the non local one. Of course, a  $g$ -type vertex can still be added to action but is not needed for renormalization. Similiar a  $\lambda$ -type vertex can be added to both the local and non-local theory, but is not required for renormalization. The second term which is different comes from the extra vertex enforced by GI and by integrals in the local theory of the form  $\int_0^D d\eta \eta f(\eta)$  which must be replaced by integrals of the form  $\int_0^D d\eta \int_0^{\eta'} d\eta' f(\eta')$  in the non-local theory. These integrals are the same only if  $f = 1$ , while for a power law  $f \propto D^n$  both integrals become  $\propto D^{n+2}$  but with a different prefactor. Since for the full system the time dependence of the propagator is more complicated one should expect that the difference between  $B_{\text{LT}}$  and  $B_{\text{NLT}}$ , the bispectra in the local and non-local theories, becomes larger within the full theory.

## 5 Conclusion

In this paper we discussed renormalization of the stochastic adhesion model (SAM). This is a toy model of structure formation, based on a simple parameterization of deviations from the Zel'dovich trajectories, which shares the same symmetries as the full set of Euler and continuity equations along with extra effective ‘‘viscosity’’ terms and a stochastic noise term.

Because of these features we expect that the general conclusions arrived at here should also be applicable to the complete theory.

Treating the viscosity terms as counter terms, one is led through a one-loop calculation to a theory necessarily non-local in time. To ensure Galilean Invariance, non-local counter-terms must be evaluated along the fluid element path, introducing vertices at higher orders which are related to the lowest order counter terms by having the same coefficients. These terms are individually not GI, so their dependence on the wave-vector differs from that of local counter terms. As we have shown, these terms are required to ensure cutoff independence. This implies that the EFToLSS type approach with non-local-in-time counter terms is consistent with respect to renormalization, while the EFToLSS with local counter terms is not.

Alternatively, if the effective viscosity is included in the computation of the linear propagator [33, 34], leading to exponential damping on short scales, one obtains a consistent theory, renormalizable to one loop. For a numerically small viscosity one naturally recovers the known results with perturbative local counter terms for the one-loop Power Spectrum. In contrast to the EFToLSS type of approach though, no new counter terms are required to renormalize the one-loop bispectrum in this case.

We briefly discussed the possibility to decide whether a theory local or non-local in time would be appropriate as an effective description of CDM by considering the bispectrum. As we pointed out, the precise size of corrections stemming from virialized scales are crucial in that respect. The local-in-time approach requires a minimal set of counter terms for renormalization and as a consequence the one-loop bispectrum is fully predicted by the one-loop Power Spectrum, although extra parameters are allowed. The non-local-in-time approach requires one more parameter for the renormalized bispectrum. We expect that similar conclusions would hold in the full system of continuity + Euler equations. Renormalized bispectra have only been computed in the EFToLSS approach which uses the non-local-in-time power counting. It would therefore be interesting to contrast the predictions of the local and non-local in time approaches in the full theory against the bispectrum from N-Body simulations.

## Acknowledgments

F.F. acknowledges support by the IMPRS-PTFS.

## References

- [1] F. Bernardeau, S. Colombi, E. Gaztanaga and R. Scoccimarro, *Large scale structure of the universe and cosmological perturbation theory*, *Phys. Rept.* **367** (2002) 1 [[astro-ph/0112551](#)] [[INSPIRE](#)].
- [2] M. Crocce and R. Scoccimarro, *Renormalized cosmological perturbation theory*, *Phys. Rev. D* **73** (2006) 063519 [[astro-ph/0509418](#)] [[INSPIRE](#)].
- [3] M. Crocce and R. Scoccimarro, *Memory of initial conditions in gravitational clustering*, *Phys. Rev. D* **73** (2006) 063520 [[astro-ph/0509419](#)] [[INSPIRE](#)].
- [4] S. Matarrese and M. Pietroni, *Resumming Cosmic Perturbations*, *JCAP* **06** (2007) 026 [[astro-ph/0703563](#)] [[INSPIRE](#)].
- [5] P. Valageas, *Large-N expansions applied to gravitational clustering*, *Astron. Astrophys.* **465** (2007) 725 [[astro-ph/0611849](#)] [[INSPIRE](#)].

- [6] T. Matsubara, *Resumming Cosmological Perturbations via the Lagrangian Picture: One-loop Results in Real Space and in Redshift Space*, *Phys. Rev. D* **77** (2008) 063530 [[arXiv:0711.2521](#)] [[INSPIRE](#)].
- [7] F. Bernardeau, N. Van de Rijdt and F. Vernizzi, *Resummed propagators in multi-component cosmic fluids with the eikonal approximation*, *Phys. Rev. D* **85** (2012) 063509 [[arXiv:1109.3400](#)] [[INSPIRE](#)].
- [8] S. Anselmi, S. Matarrese and M. Pietroni, *Next-to-leading resummations in cosmological perturbation theory*, *JCAP* **06** (2011) 015 [[arXiv:1011.4477](#)] [[INSPIRE](#)].
- [9] S. Anselmi and M. Pietroni, *Nonlinear Power Spectrum from Resummed Perturbation Theory: a Leap Beyond the BAO Scale*, *JCAP* **12** (2012) 013 [[arXiv:1205.2235](#)] [[INSPIRE](#)].
- [10] M. Crocce, R. Scoccimarro and F. Bernardeau, *MPTbreeze: A fast renormalized perturbative scheme*, *Mon. Not. Roy. Astron. Soc.* **427** (2012) 2537 [[arXiv:1207.1465](#)] [[INSPIRE](#)].
- [11] M. Pietroni, *Flowing with Time: a New Approach to Nonlinear Cosmological Perturbations*, *JCAP* **10** (2008) 036 [[arXiv:0806.0971](#)] [[INSPIRE](#)].
- [12] D. Blas, M. Garny and T. Konstandin, *Cosmological perturbation theory at three-loop order*, *JCAP* **01** (2014) 010 [[arXiv:1309.3308](#)] [[INSPIRE](#)].
- [13] R. Scoccimarro and J. Frieman, *Loop corrections in nonlinear cosmological perturbation theory*, *Astrophys. J. Suppl.* **105** (1996) 37 [[astro-ph/9509047](#)] [[INSPIRE](#)].
- [14] A. Kehagias and A. Riotto, *Symmetries and Consistency Relations in the Large Scale Structure of the Universe*, *Nucl. Phys. B* **873** (2013) 514 [[arXiv:1302.0130](#)] [[INSPIRE](#)].
- [15] M. Peloso and M. Pietroni, *Galilean invariance and the consistency relation for the nonlinear squeezed bispectrum of large scale structure*, *JCAP* **05** (2013) 031 [[arXiv:1302.0223](#)] [[INSPIRE](#)].
- [16] D. Blas, M. Garny and T. Konstandin, *On the non-linear scale of cosmological perturbation theory*, *JCAP* **09** (2013) 024 [[arXiv:1304.1546](#)] [[INSPIRE](#)].
- [17] T. Buchert and A. Dominguez, *Modeling multistream flow in collisionless matter: approximations for large scale structure beyond shell crossing*, *Astron. Astrophys.* **335** (1998) 395 [[astro-ph/9702139](#)] [[INSPIRE](#)].
- [18] D. Baumann, A. Nicolis, L. Senatore and M. Zaldarriaga, *Cosmological Non-Linearities as an Effective Fluid*, *JCAP* **07** (2012) 051 [[arXiv:1004.2488](#)] [[INSPIRE](#)].
- [19] M. Pietroni, G. Mangano, N. Saviano and M. Viel, *Coarse-Grained Cosmological Perturbation Theory*, *JCAP* **01** (2012) 019 [[arXiv:1108.5203](#)] [[INSPIRE](#)].
- [20] A. Manzotti, M. Peloso, M. Pietroni, M. Viel and F. Villaescusa-Navarro, *A coarse grained perturbation theory for the Large Scale Structure, with cosmology and time independence in the UV*, *JCAP* **09** (2014) 047 [[arXiv:1407.1342](#)] [[INSPIRE](#)].
- [21] J.J.M. Carrasco, M.P. Hertzberg and L. Senatore, *The Effective Field Theory of Cosmological Large Scale Structures*, *JHEP* **09** (2012) 082 [[arXiv:1206.2926](#)] [[INSPIRE](#)].
- [22] L. Mercolli and E. Pajer, *On the velocity in the Effective Field Theory of Large Scale Structures*, *JCAP* **03** (2014) 006 [[arXiv:1307.3220](#)] [[INSPIRE](#)].
- [23] J.J.M. Carrasco, S. Foreman, D. Green and L. Senatore, *The Effective Field Theory of Large Scale Structures at Two Loops*, *JCAP* **07** (2014) 057 [[arXiv:1310.0464](#)] [[INSPIRE](#)].
- [24] E. Pajer and M. Zaldarriaga, *On the Renormalization of the Effective Field Theory of Large Scale Structures*, *JCAP* **08** (2013) 037 [[arXiv:1301.7182](#)] [[INSPIRE](#)].
- [25] M.P. Hertzberg, *Effective field theory of dark matter and structure formation: Semianalytical results*, *Phys. Rev. D* **89** (2014) 043521 [[arXiv:1208.0839](#)] [[INSPIRE](#)].

- [26] S.M. Carroll, S. Leichenauer and J. Pollack, *Consistent effective theory of long-wavelength cosmological perturbations*, *Phys. Rev. D* **90** (2014) 023518 [[arXiv:1310.2920](#)] [[INSPIRE](#)].
- [27] T. Baldauf, L. Mercolli, M. Mirbabayi and E. Pajer, *The Bispectrum in the Effective Field Theory of Large Scale Structure*, *JCAP* **05** (2015) 007 [[arXiv:1406.4135](#)] [[INSPIRE](#)].
- [28] R.E. Angulo, S. Foreman, M. Schmittfull and L. Senatore, *The One-Loop Matter Bispectrum in the Effective Field Theory of Large Scale Structures*, *JCAP* **10** (2015) 039 [[arXiv:1406.4143](#)] [[INSPIRE](#)].
- [29] L. Senatore and M. Zaldarriaga, *The IR-resummed Effective Field Theory of Large Scale Structures*, *JCAP* **02** (2015) 013 [[arXiv:1404.5954](#)] [[INSPIRE](#)].
- [30] R.A. Porto, L. Senatore and M. Zaldarriaga, *The Lagrangian-space Effective Field Theory of Large Scale Structures*, *JCAP* **05** (2014) 022 [[arXiv:1311.2168](#)] [[INSPIRE](#)].
- [31] Z. Vlah, M. White and A. Aviles, *A Lagrangian effective field theory*, *JCAP* **09** (2015) 014 [[arXiv:1506.05264](#)] [[INSPIRE](#)].
- [32] S. Foreman and L. Senatore, *The EFT of Large Scale Structures at All Redshifts: Analytical Predictions for Lensing*, [arXiv:1503.01775](#) [[INSPIRE](#)].
- [33] G. Rigopoulos, *The adhesion model as a field theory for cosmological clustering*, *JCAP* **01** (2015) 014 [[arXiv:1404.7283](#)] [[INSPIRE](#)].
- [34] D. Blas, S. Floerchinger, M. Garny, N. Tetradis and U.A. Wiedemann, *Large scale structure from viscous dark matter*, *JCAP* **11** (2015) 049 [[arXiv:1507.06665](#)] [[INSPIRE](#)].
- [35] F. Fühner and Y.Y.Y. Wong, *Higher-order massive neutrino perturbations in large-scale structure*, *JCAP* **03** (2015) 046 [[arXiv:1412.2764](#)] [[INSPIRE](#)].
- [36] S.N. Gurbatov, A.I. Saichev and S.F. Shandarin, *The large-scale structure of the universe in the frame of the model equation of non-linear diffusion*, *Mon. Not. Roy. Astron. Soc.* **236** (1989) 385 [[INSPIRE](#)].
- [37] T. Buchert, A. Dominguez and J. Perez-Mercader, *Extending the scope of models for large scale structure formation in the universe*, *Astron. Astrophys.* **349** (1999) 343 [[astro-ph/9709218](#)] [[INSPIRE](#)].
- [38] S. Matarrese and R. Mohayaee, *The Growth of structure in the intergalactic medium*, *Mon. Not. Roy. Astron. Soc.* **329** (2002) 37 [[astro-ph/0102220](#)] [[INSPIRE](#)].
- [39] J. Gaite, *Turbulence model of the cosmic structure*, [arXiv:1202.3011](#) [[INSPIRE](#)].
- [40] M. Kardar, G. Parisi and Y.-C. Zhang, *Dynamic Scaling of Growing Interfaces*, *Phys. Rev. Lett.* **56** (1986) 889 [[INSPIRE](#)].
- [41] A. Altland and B. Simons, *Condensed matter field theory*, Cambridge University Press, Cambridge U.K. (2010).
- [42] D.H. Weinberg and J.E. Gunn, *Large Scale Structure And The Adhesion Approximation*, *Mon. Not. Roy. Astron. Soc.* **247** (1990) 260 [[INSPIRE](#)].
- [43] L. Kofman, D. Pogosian, A. Melott and S.F. Shandarin, *Coherent structures in the universe and the adhesion model*, *Astrophys. J.* **393** (1992) 437 [[INSPIRE](#)].
- [44] A. Nusser and A. Dekel, *Filamentary structure from Gaussian fluctuations using the adhesion approximation*, *Astrophys. J.* **362** (1990) 14.
- [45] T. Baldauf, E. Schaan and M. Zaldarriaga, *On the reach of perturbative descriptions for dark matter displacement fields*, [arXiv:1505.07098](#) [[INSPIRE](#)].

- [46] M. Peloso and M. Pietroni, *Ward identities and consistency relations for the large scale structure with multiple species*, *JCAP* **04** (2014) 011 [[arXiv:1310.7915](#)] [[INSPIRE](#)].
- [47] I. Ben-Dayan, T. Konstandin, R.A. Porto and L. Sagunski, *On Soft Limits of Large-Scale Structure Correlation Functions*, *JCAP* **02** (2015) 026 [[arXiv:1411.3225](#)] [[INSPIRE](#)].
- [48] B. Horn, L. Hui and X. Xiao, *Soft-Pion Theorems for Large Scale Structure*, *JCAP* **09** (2014) 044 [[arXiv:1406.0842](#)] [[INSPIRE](#)].
- [49] E. Frey and U.C. Täuber, *Two-loop renormalization-group analysis of the Burgers-Kardar-Parisi-Zhang equation*, *Phys. Rev.* **E 50** (1994) 1024 [[INSPIRE](#)].



## Summary, discussion and outlook

### 5.1 Growing Neutrino Quintessence

GNQ is a theoretically well motivated DE model. In GNQ the accelerated expansion of the universe starts when the cosmic neutrinos become non-relativistic, therefore in contrast to other Quintessence models no fine tuning of the self-interaction potentials is required. But studying the cosmological dynamics is challenging. In the two publications 1 and 2 we explored the possibility of two different variants of GNQ as a DE model. The large non-linearities, induced by the strong interaction between neutrinos and the cosmon, did not allow for a perturbative treatment, instead N-body simulations with relativistic particles and non-linear scalar field equations are required. In both scenarios backreaction effects alter the expansion history, but the phenomenology is different. In the constant coupling model stable neutrino lumps form, inducing strong backreaction effects, while in varying coupling model an oscillation pattern of forming and dissolving lumps is observed, the backreaction effects remain small.

In publication 2, we explored the parameter space aiming at finding parameters for which the constant coupling model is a viable DE model. Indeed we found regions in the parameter space for which the cosmon evolves slow enough to allow for an accelerated expansion of the universe. However, in order to have an accelerated expansion today, the lumps must have formed late, such that backreaction effects are still small. Since, lumps form quickly after the cosmon evolution stopped, the accelerated expansion also starts late,  $a \gtrsim 0.6$ . This is difficult to bring into agreement with an approximately constant energy density for  $a \gtrsim 0.5$ . Furthermore, we could observe the tendency that for a smaller  $w$  the energy density is larger. Hence, we had difficulties to get  $w_{\text{DE},0} \approx -1$  and  $\Omega_{\text{DE},0} \approx 0.7$  simultaneously, but  $w_{\text{DE},0} \lesssim -0.9$  and  $\Omega_{\text{DE},0} \sim 0.75$  is possible. Which is not too far from the target values. Although we could only scan a limited range of parameters, we believe that late forming lumps and a large amount of DE are related. The reason can be understood from the homogeneous evolution. The cosmon evolution stops after the neutrinos became non-relativistic once  $\beta\rho_\nu = -\alpha V \propto \alpha^{-1}a^{-3}$  is reached. For a smaller  $\alpha$  the right hand side is larger, to full fill the equation  $\rho_\nu$  must have grown larger, i.e. longer. For a smaller  $\alpha$  the cosmon evolution is stopped later, with a larger energy density, see also publication 2, figure 1. Furthermore, a small  $\alpha$  implies EDE. We found that the equation of state can be close to  $-1$  for  $\alpha \lesssim 5$ , violating

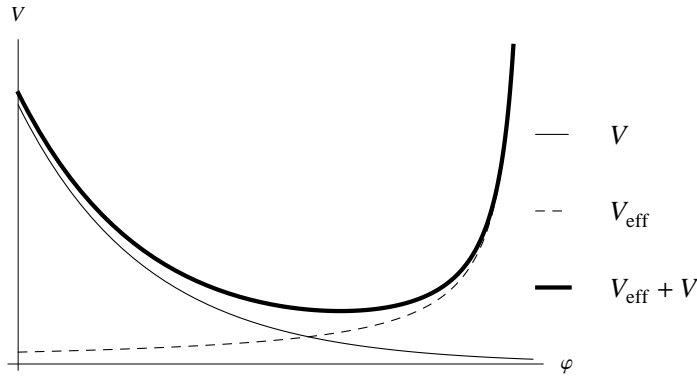


**Fig. 5.1:** A sketch of the effective potential felt by the cosmon during the process of lump formation and dissolving. The cosmon performs damped oscillations, eventually it settles near the minimum. Note that the amplitude of neutrino induced effective potential  $V_{\text{eff}}$  is space and time dependent. For non-relativistic neutrinos  $V_{\text{eff}} = m_\nu n_\nu$  with the neutrino number density  $n_\nu$ , while for relativistic neutrinos  $V_{\text{eff}}$  vanishes.

bounds on EDE  $\alpha \lesssim 10$ . Given the fact that an approximately constant DE density is only possible, at the prize of a late stopping cosmon, which seems to imply a large amount EDE and a large DE density today, we find it unlikely that a region in parameter space with a realistic cosmology exists.

The publication 1 explores non-linear structure formation in the varying constant model. Here, in contrast to the constant coupling model no stable lumps form. Instead mild neutrino over densities form and dissolve. The reason is the form of the coupling and mass  $m_\nu \propto \beta \propto 1/(\varphi - \varphi_{\text{crit}})$ , which grows large near the critical value  $\varphi_{\text{crit}}$ . For the cosmon the coupling constitutes an effective potential barrier, see figure 5.1, which can not be crossed, so that  $\varphi_{\text{crit}}$  is never reached. The cosmon performs damped oscillation around the minimum of the effective potential. As in the constant coupling model neutrinos start to cluster, when they are non-relativistic. During the oscillation the sign of the cosmon acceleration changes. Instead of being decelerated the neutrinos are accelerated to relativistic velocities and the lumps dissolve. Here, similar to the constant coupling model the neutrinos being relativistic, weakens the stopping power. The phases at the beginning of lump formation, during which the neutrinos are non-relativistic, ensures that that the cosmon is stopped and finally reaches  $w \approx -1$ . It is interesting to note, that at the microscopic level the dynamics is very complicated and at the first sight one does not expect the overall cosmology to be close to the rather simple homogeneous limit. The reason is that instabilities in the varying coupling model are stabilized and the neutrino density contrast never grows large. This can serve as a proof (of principle) that an unhealthy cosmological model, can be cured by taking into account all relevant effects.

The average dynamics of the varying coupling model is close to the pure homogeneous dynamics. The most important difference is that the neutrinos are “heated”

during the lump formation. In the publication 1 we proposed to account for the effect of the faster neutrinos on the background cosmon, by introducing a new parameter  $\gamma$ , characterizing the typical momentum scale. The parameter  $\gamma$  is closely related to the effective temperature of [75]. The heating and cooling of the cosmic neutrinos can be emulated by adding the term  $-\Gamma\beta\dot{\varphi}p\partial_p\bar{f}$  to the neutrino Vlasov equation. The effect of this term can be translated to a temperature varying in time as  $T = T_i e^{\int d\tau \Gamma\beta\dot{\varphi}}$ . For  $\Gamma > 0$  the temperature decreases when the cosmon moves towards  $\varphi_{\text{crit}}$ , as observed in the simulations. In the future, fixing  $\Gamma$  by the temperature measured in [75] some effects on the CMB can be studied using corrected Boltzmann codes.

Thanks to the differences in the neutrino sector, compared to  $\Lambda$ CDM, can GNQ be tested with cosmology. A “measurement” of the neutrino mass by observing the specific scale dependent effect of constant mass neutrinos in the CMB and the LSS, would be clear signal against GNQ. Furthermore, the gravitational potential of neutrino lumps allows for direct tests of GNQ. The neutrino induced potentials in varying coupling model are at the order of a few percent of the matter induced potential. This is probably small enough to be consistent with the CMB and structure formation, but might be still large enough to be detectable. This should be contrasted to the lump potential in the constant coupling model, which can be larger than the matter potential. Here, we like to note that if the mass amplitude  $m_i$  is increased the lumps in the varying coupling model become more stable [75]. In that case models exist with a viable background cosmology, but neutrino lumps might contribute to the gravitational potential by more than a few percent.

Let us first have a look at the oscillating lump potential in the varying coupling model, which might be detectable in the CMB via the Integrated-Sachs-Wolf (ISW) effect, see [4, 76]. Let us consider a photon which is deflected by the gravitational potentials. We are interested in deviations  $\delta n^\mu$  from the four velocity in an unperturbed FRW-metric  $\bar{n}^\mu$ . To first order in the perturbations the geodesic equation becomes

$$\frac{d\delta n^\mu}{d\lambda} = -\delta\Gamma_{\nu\rho}^\mu \bar{n}^\nu \bar{n}^\rho, \quad (5.1)$$

where we used the conformal invariance of like light-geodesics to rescale the affine parameter  $\lambda$ , in such away that we get rid of the cosmological redshift. We are interested in the energy change of photons, emitted at some initial time  $t_{\text{in}}$  and observed at some final time  $t_{\text{f}}$ , which reads

$$\frac{T_{\text{f}}}{T_{\text{in}}} = \frac{a_{\text{in}}}{a_{\text{f}}} \frac{(n^\mu u_\mu)|_{\text{f}}}{(n^\mu u_\mu)|_{\text{in}}}, \quad (5.2)$$

where  $\mathbf{u} = (-a(1 + \Psi), av_i)$  is the 4-velocity of the emitter relative to the observer. The change in the temperature fluctuations is

$$\frac{\Delta T_f}{T_f} = \frac{\Delta T_{\text{in}}}{T_{\text{in}}} + \left. \frac{\delta n^\mu \bar{u}_\mu + \bar{n}^\mu \delta u_\mu}{\bar{n}^\mu \bar{u}_\mu} \right|_f - \left. \frac{\delta n^\mu \bar{u}_\mu + \bar{n}^\mu \delta u_\mu}{\bar{n}^\mu \bar{u}_\mu} \right|_{\text{in}}. \quad (5.3)$$

Integrating the geodesic equation 5.1 one obtains

$$\delta n_f^0 - \delta n_{\text{in}}^0 = -2\Psi|_{\text{in}}^f - \int_{\text{in}}^f d\lambda \partial_\tau (\Psi + \Phi)(\mathbf{x}(\lambda), \lambda), \quad (5.4)$$

where  $\mathbf{x} = \mathbf{x}_f - \bar{\mathbf{n}}(\lambda_f - \lambda)$  is the unperturbed photon path. Plugging this into equation 5.3 we arrive at an equation for the temperature difference

$$\frac{\Delta T_f}{T_f} = \frac{\Delta T_{\text{in}}}{T_{\text{in}}} + \bar{n}^i v_i - \Psi|_{\text{in}}^f + \int_{\text{in}}^f d\tau \partial_\tau (\Psi + \Phi)(\mathbf{x}(\tau), \tau). \quad (5.5)$$

$\Delta T_{\text{in}}/T_{\text{in}} = \delta_{\text{rad,in}}/4$  is the intrinsic temperature fluctuation of the CMB,  $\bar{n}^i v_i$  is a Doppler term and  $\Psi|_{\text{in}}^f$  gives rise to the ordinary Sachs-Wolf-effect. Here, we are only interested in the integral, giving rise to the ISW. The ISW effect can not be larger than the maximal potential difference. For neutrino induced potentials they are of the order  $\Psi_\nu \sim O(1\%) \Psi_{\text{Matter}} \sim 10^{-7}$ , hence, the change in the temperature can not be larger than  $\frac{\Delta T}{T} \sim 10^{-7}$ . Each cycle of lump formation consists of a phase with positive and negative time derivatives, such that the ISW effect is smaller than  $10^{-7}$ , we found for a single lump  $\frac{\Delta T}{T} \sim 10^{-8}$ , the precise number depends on the details of the lump. This is too small to be detected for a single lump. In principle the effect can be enhanced for photons travelling through several lumps. Given that lumps are large,  $\sim 100 h\text{Mpc}^{-1}$ , and form late, it is unlikely that a photon travelled through several lumps. We conclude that for the simulated parameters the ISW effect is probably too small to be observed. However, in a model with more stable lumps the effect can be larger.

Even though small, the lump neutrino induced gravitational potential could leave its trace in the LSS. The performed simulations are restricted with respect to box size and resolution, this hinders a detailed analysis. Nevertheless, on general grounds we can discuss expected effects, worth studying once the numerics has been refined, see below. Until neutrino lumps form, structure formation is only affected by the different background cosmology. Only at low redshift,  $z \lesssim 4$ , lumps can leave a trace in the LSS. Here, it is interesting to differentiate between direct measurements of the matter distribution, e.g. by gravitational lensing, and indirect measurements, e.g. by galaxy surveys. Galaxy surveys infer the matter distribution from the observed distribution of galaxies. Galaxies are biased with respect to the underlying matter distribution, i.e. they are not perfect tracers of the matter distribution. Since, for lump formation gravity is irrelevant, lumps can form independent of ordinary structures. We expect a bias between galaxies and neutrino lumps, probably the correlation

between them is small. So galaxy surveys are not sensitive to the lump potential. This is different for gravitational lensing, which is caused by the deflection of light by the gravitational potentials, hence it is sensitive to the total gravitational potential. The neutrino induced potentials should give for  $a \gtrsim 0.2$  rise to an effect of the order of a few percent, while in the galaxy distribution even for  $a \gtrsim 0.2$  a smaller effect is expected.

Testing GNQ outside cosmology is difficult for two reasons. First, earth based experiments can only measure the neutrino mass locally and today. Given that the cosmon varies only on cosmological time scale observing a time variation on earth seems to be impossible. Second, due to the small mass neutrinos are typically relativistic. Hence, typically the neutrino mass and the neutrino-cosmon interaction can be neglected. However, super nova neutrino oscillations might provide a way of testing GNQ directly, for a review of neutrino oscillations in Super Novae see e.g. [77]. Crucial is the squared mass difference  $\Delta m_{\alpha\gamma}^2 = m_\alpha^2 - m_\gamma^2$  between the different neutrino flavors, labelled by  $\alpha$  and  $\gamma$ . As the individual neutrino masses vary the mass difference varies

$$\begin{aligned}\Delta m_{\alpha\gamma}^2 &= (m_{\alpha,i}^2 - m_{\gamma,i}^2) e^{-\beta\varphi}, & \text{constant coupling,} \\ \Delta m_{\alpha\gamma}^2 &= (m_{\alpha,i}^2 - m_{\gamma,i}^2) \frac{1}{(\varphi_{\text{crit}} - \varphi)^2}, & \text{varying coupling.}\end{aligned}$$

Neutrino oscillations have a significant impact on super nova physics e.g. on the neutrino energy spectrum. This in principle allows to measure or constrain the mass difference. Constrains obtained from different galactic super novae could be converted into constrains on the variation of the mass difference, hence on the variation of the mass. Unfortunately, only a few neutrinos,  $\sim 10$ , from a single galactic super nova, the SN1987A [78], have been observed so far, therefore it is unlikely that the next *two* observed super novae allow to put stringent constrains on a varying neutrino mass.

The search for viable models as well as a detailed study of effects on the matter distribution requires a refined numerics. Furthermore, the study of substructures in neutrino lumps is so far hindered by the restricted resolution of a few Mpc of our simulation. Recently, gevolution [79] a highly parallelized relativistic N-body simulation in the weak field limit became available. Gevolution shares many features with our N-body simulation, but is superior with respect to speed and accuracy. It is desirable to implement GNQ in gevolution. Relativistic neutrinos and backreaction effects are already implemented in gevolution, only minor changes are necessary. The calculation of the gravitational potential goes beyond our code, by taking into account the most important non-linear effects and is not restricted to the quasi-static approximation. The only missing piece is the solver for the cosmon field. The use of the quasi-static approximation in GNQ has never been tested. Therefore,

it is preferable to solve the non-linear wave equation for the cosmon, this is for example possible with an appropriate leapfrog scheme. Although solving the cosmon equation in the quasi-static approximation by implementing the NGS-solver used in our simulation is possible.

## 5.2 Effective fluids in large-scale structure formation

Effective fluid models provide a systematic treatment of mode-coupling between the non-perturbative dynamics on small scales and the perturbative dynamics on large scales. Measuring the effective fluid parameters in simulations allows to extend the applicability of perturbative calculations.

In the publication 3 we investigated renormalization of effective fluid model for LSS, using the Stochastic Adhesion Model (SAM) as a toy model. We contrasted the power counting scheme of the EFToLSS with a different power counting scheme, closer to ordinary fluids. In such a scheme the lowest order effective viscosity and noise are included at linear order. This results in a damping of the propagator on small scales. The theory is renormalizable at one loop, i.e. the local viscosity and noise are sufficient to renormalize *all* one loop diagrams. In contrast, in the power counting scheme of the EFToLSS the lowest order effective terms are counted as one loop terms, i.e. they are counter terms for the loop diagrams. As explicitly shown the counter terms must be non-local in time. Galilean Invariance of the fluid equations, enforces the non-local effective parameters to depend on the whole history of a fluid element. This introduces at every order new vertices, with the lowest order counter terms as coefficients. We have explicitly demonstrated that they are required to renormalize the one loop three point function. Ward-Identities guarantee that this is the case at every loop order. This implies that the EFToLSS can be consistently renormalized with non-local counter terms, but not with local counter terms. Our conclusion is primary a consequence of the Galilean Invariance of the SAM, which is shared by the fluid equations. We therefore expect that our conclusion remains valid, when the fluid equations, including the vorticity, instead of the SAM are considered.

In the last years the EFToLSS and related approaches attracted a lot of attention. Since perturbation theory must be supplemented by parameters measured in simulations, effective fluid models are not a reliable and predictive tool, yet. Certainly, the effective fluid models can provide systematic ways of parameterizing results of simulation and using it to predict other observable e.g. CMB lensing, as proposed in [80]. Note, that the same strategy can be used to calculate the effect of neutrino lumps in GNQ on the CMB, once an interesting and viable set of parameters is found. Furthermore, effective fluid models provide analytical models, which can

be used to study bias [81, 82] and redshift space distortions [83]. But they can be more than a way to parametrize simulation data. Since effective fluid parameters parametrize the effective stress tensor in terms of the long-wavelength field, they measure the response of the effective stress tensor to the long wave-length field. Short-wavelength modes feel the presence of long-wavelength modes effectively as a different background cosmology. Therefore the response of the effective stress tensor to short-wavelength modes can be measured in separate universe simulations [84, 85], in which the long-wavelength mode is absorbed into a change of the background. Therefore the effective parameters can be measured in small simulation and hence fast simulations. This is similar to the measurements of bias parameters in separate universe simulations [86]. Combining small and fast simulations with perturbative calculations on large scale has the potential to become a fast and predictive tool for LSS calculations. It will be interesting to study the dependence of the fluid parameters on the cosmological parameters. If it is possible to map the fluid parameters measured in one cosmology to a different cosmology, without the need of running a new simulation, the predictivity can be further increased. See [87] for an implementation of this idea in the coarse-grained perturbation theory. Finally, it would be interesting to investigate the relation between effective fluid approaches and the halo model [88], by considering the long-wavelength limit of a fluid of virialized structures, this is closely related to the lump fluid in GNQ.

There is a huge body of work applying effective fluids to LSS, but the justification of effective fluid models has been investigated very little. Here most of the works investigate the (self-)consistency of the theory, publication 3 being one of them, other examples are [89, 90]. To our knowledge only the series of works [91, 92, 93] challenges the applicability, by applying the EFToLSS to individual realizations instead of applying it to Power Spectra. Ultimately, the justification and performance of the effective fluids models, as well as all other (semi-)analytical tools, depends on the coupling between different modes. While the focus of most simulation studies of cosmological structure formation lies on the impact of cosmological (background) parameters, [94] studied the response of long-wavelength modes to short-wavelength modes. The authors found, compared to SPT, a reduced sensitivity to short wave-length modes, an indication that their effect can be accounted for in an effective model with a only few free parameters. Studying mode coupling via a change of initial conditions in simulation, see also [95], is a promising way of testing effective models, as well as other perturbative approaches.

By studying mode coupling only via simulations, it is difficult to differentiate between non-perturbative effects within a perfect pressure less fluid and effects arising from shell-crossing. In effective fluid models this is reflected by the fact that by measuring the size of the effective parameters we can only learn something on the importance of short-wavelength modes on the evolution of long-wavelength modes. But the

effective parameters account for both; mode coupling effects and effects beyond the perfect pressureless fluid approximation. We can not get information on the relative importance of the effects and can not decide whether the decoupling of small scales can be understood within the perfect pressureless fluid approximation or not. It would be interesting to quantify the impact of first shell-crossing by analytical calculations. A possible analytical model would be the Schrödinger equation, also describing axion DM, see section 1.3, an alternative would be the statistical field theory of [96]. The Schrödinger equation can be written as the fluid equations 1.64 and 1.65, with an additional quantum pressure term  $\propto \hbar^2 (\nabla^2 \sqrt{\rho}) / \sqrt{\rho}$ . The quantum pressure regulates shell crossing singularities, even in the classical limit. It is therefore possible to calculate the velocity dispersion and vorticity generated by first shell crossing using the Schrödinger equation and estimate their impact on long-wavelength modes, without ad-hoc assumptions as in [97].

Finally, renormalization group techniques provide a systematic way of studying mode coupling and calculating the effective fluid parameters. Recently, a functional renormalization group approach has been employed [98]. Assuming a viscous fluid an infrared fixed point was found, further supporting the use of effective fluid models. It would be interesting to see how the fixed point is related to our findings regarding the form of the effective parameters and the renormalizability of loops. In particular, if they become local in time at the fixed point, when allowing for non-local in time parameters.

# Bibliography

- [1]D. J. Fixsen, E. S. Cheng, J. M. Gales, et al. „The Cosmic Microwave Background Spectrum from the Full COBE/FIRAS Data Set“. In: *Astrophys.J.* 473 (1996), p. 576. arXiv: astro-ph/9605054 [astro-ph].
- [2]John Joseph M. Carrasco, Mark P. Hertzberg, and Leonardo Senatore. „The Effective Field Theory of Cosmological Large Scale Structures“. In: *JHEP, Volume 2012*, (2012), Number9,82. arXiv: 1206.2926 [astro-ph.CO].
- [3]Scott Dodelson. *Modern Cosmology*. Academic Press, Elsevier Science, 2003.
- [4]Ruth Durrer. *The Cosmic Microwave Background*. Cambridge University Press, 2008.
- [5]Steven Weinberg. *Cosmology*. Oxford University Press, 2008.
- [6]C. W. Misner, K. S. Thorne, and J. A. Wheeler. *Gravitation*. 1973.
- [7]Steven Weinberg. *Gravitation and Cosmology: Principles and Applications of the General Theory of Relativity*. New York: Wiley, 1972, XXVIII, 657 S.
- [8]P.P. Coles and F. Lucchin. *Cosmology: The Origin and Evolution of Cosmic Structure*. Wiley, 2002.
- [9]G. Hinshaw, D. Larson, E. Komatsu, et al. „Nine-year Wilkinson Microwave Anisotropy Probe (WMAP) Observations: Cosmological Parameter Results“. In: *The Astrophysical Journal Supplement Series* 208.2 (2013), p. 19.
- [10]Planck Collaboration. „Planck 2015 results. I. Overview of products and scientific results“. In: (2015). arXiv: 1502.01582 [astro-ph].
- [11]Julien Lesgourgues and Sergio Pastor. „Massive neutrinos and cosmology“. In: *Phys.Rept.* 429 (2006), pp. 307–379. arXiv: astro-ph/0603494v2 [astro-ph].
- [12]Edmund J. Copeland, M. Sami, and Shinji Tsujikawa. „Dynamics of dark energy“. In: *Int.J.Mod.Phys.D* 15 (2006), pp. 1753–1936. arXiv: hep-th/0603057 [hep-th].
- [13]S. Perlmutter, G. Aldering, S. Deustua, et al. „Cosmology from Type Ia Supernovae“. In: *Bull.Am.Astron.Soc.* 29:1351 (Bull.Am.Astron.Soc). arXiv: astro-ph/9812473 [astro-ph].
- [14]Adam G. Riess, Alexei V. Filippenko, Peter Challis, et al. „Observational Evidence from Supernovae for an Accelerating Universe and a Cosmological Constant“. In: *Astron.J.* 116 (May 1998), pp. 1009–1038. arXiv: astro-ph/9805201v1 [astro-ph].

- [15]M. Betoule, R. Kessler, J. Guy, et al. „Improved cosmological constraints from a joint analysis of the SDSS-II and SNLS supernova samples“. In: *A&A* 568 (2014), A22. arXiv: 1401.4064 [astro-ph].
- [16]Planck. Collaboration. „Planck 2015 results. XIV. Dark energy and modified gravity“. In: (2015). arXiv: 1502.01590 [astro-ph].
- [17]Chung-Pei Ma and Edmund Bertschinger. „Cosmological Perturbation Theory in the Synchronous and Conformal Newtonian Gauges“. In: *Astrophys.J.* 455 (1995), pp. 7–25. arXiv: astro-ph/9506072 [astro-ph.CO].
- [18]Stephen R. Green and Robert M. Wald. „A new framework for analyzing the effects of small scale inhomogeneities in cosmology“. In: *Phys.Rev.D83:084020* (2011). arXiv: 1011.4920v2 [gr-qc].
- [19]Johannes Noller, Francesca von Braun-Bates, and Pedro G. Ferreira. „Relativistic scalar fields and the quasi-static approximation in theories of modified gravity“. In: *Phys. Rev. D* 89, 023521 (Oct. 2014). arXiv: 1310.3266v1 [astro-ph.CO].
- [20]Sownak Bose, Wojciech A. Hellwing, and Baojiu Li. „Testing the quasi-static approximation in  $f(R)$  gravity simulations“. In: *JCAP* 02 (Nov. 2014). arXiv: 1411.6128v1 [astro-ph.CO].
- [21]Thomas Buchert. „On average properties of inhomogeneous fluids in general relativity I: dust cosmologies“. In: *Gen.Rel.Grav.* 32 (2000), pp. 105–125. arXiv: gr-qc/9906015v2 [gr-qc].
- [22]Daniel Baumann, Alberto Nicolis, Leonardo Senatore, and Matias Zaldarriaga. „Cosmological non-linearities as an effective fluid“. In: *Journal of Cosmology and Astroparticle Physics* 2012.07 (2012), p. 051. arXiv: 1411.0806 [astro-ph].
- [23]Stephen R. Green and Robert M. Wald. „Newtonian and Relativistic Cosmologies“. In: *Phys.Rev.D85:063512* (2012). arXiv: 1111.2997v2 [gr-qc].
- [24]Syksy Rasanen. „Dark energy from backreaction“. In: *JCAP* 0402:003 (2004). arXiv: astro-ph/0311257v3 [astro-ph].
- [25]C. Wetterich. „Can Structure Formation Influence the Cosmological Evolution?“ In: *Phys.Rev. D* 67 (2003), p. 043513. arXiv: astro-ph/0111166 [astro-ph.CO].
- [26]Julian Adamek, Chris Clarkson, Ruth Durrer, and Martin Kunz. „Does small scale structure significantly affect cosmological dynamics?“ In: *Phys. Rev. Lett.* 114, (2014), p. 051302. arXiv: 1408.2741 [astro-ph.CO].
- [27]Jose Beltran Jimenez, Alvaro de la Cruz-Dombriz, Peter K. S. Dunsby, and Diego Saez-Gomez. „Backreaction mechanism in multifluid and extended cosmologies“. In: 2014.05 (2014), p. 031. arXiv: 1312.5680v2 [astro-ph.CO].
- [28]Anthony W. H. Preston and Tim R. Morris. „Cosmological back-reaction in modified gravity and its implications for dark energy“. In: *JCAP* 09 (2014), p. 017. arXiv: 1406.5398v2 [gr-qc].
- [29]Stefan Floerchinger, Nikolaos Tetradis, and Urs Achim Wiedemann. „Accelerating Cosmological Expansion from Shear and Bulk Viscosity“. In: *Phys. Rev. Lett.* 114.9 (2015), p. 091301. arXiv: 1411.3280 [gr-qc].

- [30]Stefan Floerchinger, Nikolaos Tetradis, and Urs Achim Wiedemann. „Backreaction effects on the matter side of Einstein’s field equations“. In: (2015). arXiv: 1506.00407v1 [gr-qc].
- [31]Luca Amendola, Stephen Appleby, Anastasios Avgoustidis, et al. „Cosmology and Fundamental Physics with the Euclid Satellite“. In: (2016). arXiv: 1606.00180v1 [astro-ph.CO].
- [32]Roy Maartens, Filipe B. Abdalla, Matt Jarvis, Mario G. Santos, and for the SKA Cosmology SWG. „Cosmology with the SKA – overview“. In: (2015). arXiv: 1501.04076v1 [astro-ph.CO].
- [33]J. Anthony Tyson and the LSST Collaboration. „Large Synoptic Survey Telescope: Overview“. In: *Proc.SPIE Int.Soc.Opt.Eng.* 4836 (2003), pp. 10–20. arXiv: astro-ph/0302102v1 [astro-ph].
- [34]The Dark Energy Survey Collaboration. „The Dark Energy Survey“. In: (2005). arXiv: astro-ph/0510346v1 [astro-ph].
- [35]Julien Lesgourgues and Sergio Pastor. „Neutrino cosmology and Planck“. In: *New Journal of Physics* 16.6 (2014), p. 065002.
- [36]K. N. Abazajian et al. „Cosmological and Astrophysical Neutrino Mass Measurements“. In: *Astropart. Phys.* 35 (2011), pp. 177–184. arXiv: 1103.5083 [astro-ph.CO].
- [37]David J. E. Marsh. „Axion Cosmology“. In: *Physics Reports* 643 (2016), pp. 1–79. arXiv: 1510.07633v2 [astro-ph.CO].
- [38]L.M. Widrow and N. Kaiser. „Using the Schroedinger Equation to Simulate Collisionless Matter“. In: *apjl* 416 (1993), p. L71.
- [39]Cora Uhlemann, Michael Kopp, and Thomas Haugg. „Schrödinger method as  $N$ -body double and UV completion of dust“. In: *Phys. Rev. D* 90 (2 2014), p. 023517. arXiv: 1403.5567 [astro-ph.CO].
- [40]F. Bernardeau, S. Colombi, E. Gaztanaga, and R. Scoccimarro. „Large-Scale Structure of the Universe and Cosmological Perturbation Theory“. In: *Phys.Rept* 367 (2002), pp. 1–248. arXiv: astro-ph/0112551v1 [astro-ph].
- [41]Sebastián Pueblas and Román Scoccimarro. „Generation of vorticity and velocity dispersion by orbit crossing“. In: *Phys. Rev. D* 80 (4 2009), p. 043504. arXiv: 0809.4606 [astro-ph].
- [42]Masatoshi Shoji and Eiichiro Komatsu. „Third-Order Perturbation Theory with Nonlinear Pressure“. In: *The Astrophysical Journal* 700.1 (2009), p. 705. arXiv: 0903.2669 [astro-ph].
- [43]Diego Blas, Mathias Garny, Thomas Konstandin, and Julien Lesgourgues. „Structure formation with massive neutrinos: going beyond linear theory“. In: *Journal of Cosmology and Astroparticle Physics* 2014.11 (2014), p. 039. arXiv: 1408.2995 [astro-ph].
- [44]Florian Führer and Yvonne Y. Wong. „Higher-order massive neutrino perturbations in large-scale structure“. In: *Journal of Cosmology and Astroparticle Physics* 2015.03 (2015), p. 046. arXiv: 1412.2764v2 [astro-ph.CO].
- [45]A. Altland and B. Simons. *Condensed matter field theory*. Cambridge, UK: Univ. Pr. 786 p, 2010.

- [46]P. Valageas. „A new approach to gravitational clustering: a path-integral formalism and large-N expansions“. In: *Astron.Astrophys.* 421:23-40 (2004). arXiv: astro-ph/0307008 [astro-ph.CO].
- [47]Sabino Matarrese and Massimo Pietroni. „Resumming Cosmic Perturbations“. In: *JCAP* 0706:026 (2007). arXiv: astro-ph/0703563 [astro-ph.CO].
- [48]Gerasimos Rigopoulos. „The adhesion model as a field theory for cosmological clustering“. In: 2015.01 (2015), p. 014. arXiv: 1404.7283 [astro-ph.CO].
- [49]John Joseph M. Carrasco, Simon Foreman, Daniel Green, and Leonardo Senatore. „The 2-loop matter power spectrum and the IR-safe integrand“. In: *Journal of Cosmology and Astroparticle Physics* 2014.07 (2014), p. 056. arXiv: 1304.4946 [astro-ph].
- [50]Diego Blas, Mathias Garny, and Thomas Konstandin. „Cosmological perturbation theory at three-loop order“. In: *JCAP* 01 (2013), p. 010. arXiv: 1309.3308 [astro-ph].
- [51]Francis Bernardeau, Nicolas Van de Rijdt, and Filippo Vernizzi. „Resummed propagators in multi-component cosmic fluids with the eikonal approximation“. In: *Phys. Rev. D* 85 (2012), p. 063509. arXiv: 1109.3400 [astro-ph.CO].
- [52]Diego Blas, Mathias Garny, and Thomas Konstandin. „On the non-linear scale of cosmological perturbation theory“. In: *JCAP* 09 (2013), p. 024. arXiv: 1304.1546 [astro-ph].
- [53]Tobias Baldauf, Mehrdad Mirbabayi, Marko Simonovic, and Matias Zaldarriaga. „Equivalence Principle and the Baryon Acoustic Peak“. In: *Phys. Rev. D* 92, (2015), p. 043514. arXiv: 1504.04366 [astro-ph].
- [54]Jordan Carlson, Martin White, and Nikhil Padmanabhan. „A critical look at cosmological perturbation theory techniques“. In: *Phys.Rev.D* 80:043531 (2009). arXiv: 0905.0479 [astro-ph].
- [55]Massimo Pietroni, Gianpiero Mangano, Ninetta Saviano, and Matteo Viel. „Coarse-Grained Cosmological Perturbation Theory“. In: 2012.01 (2012), p. 019. arXiv: 1108.5203 [astro-ph.CO].
- [56]Edmund Bertschinger. „Simulations of structure formation in the universe“. In: *Ann. Rev. Astron. Astrophys.* 36 (1998), pp. 599–654.
- [57]Anatoly Klypin. „Numerical Simulations in Cosmology I: Methods“. In: (2007). arXiv: astro-ph/0005502 [astro-ph.CO].
- [58]M. Trenti and P. Hut. „Gravitational N-body Simulations“. In: (2008). arXiv: 0806.3950 [astro-ph].
- [59]Alexander Knebe. „How to simulate the Universe in a Computer“. In: *PASA - Publications of the Astronomical Society of Australia* 22 (2005), pp. 184–189. arXiv: astro-ph/0412565 [astro-ph.CO].
- [60]Roman Scoccimarro. „Transients from Initial Conditions: A Perturbative Analysis“. In: *Mon.Not.Roy.Astron.Soc.* 299 (1998), p. 1097. arXiv: astro-ph/9711187 [astro-ph.CO].
- [61]M. Crocce, S. Pueblas, and R. Scoccimarro. „Transients from Initial Conditions in Cosmological Simulations“. In: *Mon.Not.Roy.Astron.Soc.* 373 (2006), pp. 369–381. arXiv: astro-ph/0606505 [astro-ph].

- [62]Volker Springel. „The cosmological simulation code GADGET-2“. In: *Monthly Notices of the Royal Astronomical Society* 364.4 (2005), pp. 1105–1134. arXiv: astro-ph/0505010 [astro-ph].
- [63]P. P. Ewald. „Die Berechnung optischer und elektrostatischer Gitterpotentiale“. In: *Annalen der Physik* 369.3 (1921), pp. 253–287.
- [64]Jerome Martin. „Everything You Always Wanted To Know About The Cosmological Constant Problem (But Were Afraid To Ask)“. In: *Comptes Rendus Physique* 13.6 (2012), pp. 566–665. arXiv: 1205.3365 [astro-ph.CO].
- [65]David Lovelock. „The Four-Dimensionality of Space and the Einstein Tensor“. In: *Journal of Mathematical Physics* 13.6 (1972), p. 874.
- [66]C. Wetterich. „Cosmology and the Fate of Dilatation Symmetry“. In: *Nucl. Phys.* B302 (1988), pp. 668–696.
- [67]Bharat Ratra and P. J. E. Peebles. „Cosmological Consequences of a Rolling Homogeneous Scalar Field“. In: *Phys. Rev.* D37 (1988), p. 3406.
- [68]Paul J. Steinhardt, Limin Wang, and Ivaylo Zlatev. „Cosmological Tracking Solutions“. In: *Phys.Rev.D* 59:123504 (1999). arXiv: astro-ph/9812313 [astro-ph.CO].
- [69]C. Wetterich. „Growing neutrinos and cosmological selection“. In: *Phys.Lett.B* 655 (Aug. 2007), pp. 201–208. arXiv: 0706.4427v2 [hep-ph].
- [70]Luca Amendola, Marco Baldi, and Christof Wetterich. „Growing Matter“. In: *Phys. Rev. D* 78 (2008), p. 023015. arXiv: 0706.3064v1 [astro-ph].
- [71]D. F. Mota, V. Pettorino, G. Robbers, and C. Wetterich. „Neutrino clustering in growing neutrino quintessence“. In: *Phys.Lett.B* 663 (2008), pp. 160–164. eprint: 0802.1515.
- [72]Nico Wintergerst, Valeria Pettorino, David F. Mota, and Christof Wetterich. „Very large scale structures in growing neutrino quintessence“. In: *Phys.Rev.D* 81 (2010), p. 063525. arXiv: 0910.4985 [astro-ph.CO].
- [73]Youness Ayaita, Maik Weber, and Christof Wetterich. „Structure Formation and Back-reaction in Growing Neutrino Quintessence“. In: *Phys.Rev.D* 85 (2011), p. 123010. arXiv: 1112.4762 [astro-ph.CO].
- [74]Youness Ayaita, Maik Weber, and Christof Wetterich. „Neutrino Lump Fluid in Growing Neutrino Quintessence“. In: *Phys. Rev. D* 87 (4 2013), p. 043519. arXiv: 1211.6589 [astro-ph.CO].
- [75]Santiago Casas, Valeria Pettorino, and Christof Wetterich. „Dynamics of neutrino lumps in growing neutrino quintessence“. In: (2016). arXiv: 1608.02358 [astro-ph].
- [76]L. Amendola and S. Tsujikawa. *Dark Energy: Theory and Observations*. Dark Energy: Theory and Observations. Cambridge University Press, 2010.
- [77]Georg G Raffelt. „Supernova Neutrino Oscillations“. In: *Physica Scripta* 2005.T121 (2005), p. 102. arXiv: hep-ph/0501049 [hep-ph].
- [78]K. Hirata, T. Kajita, M. Koshiba, et al. „Observation of a neutrino burst from the supernova SN1987A“. In: *Phys. Rev. Lett.* 58 (14 1987), pp. 1490–1493.
- [79]Julian Adamek, David Daverio, Ruth Durrer, and Martin Kunz. „gevolution: a cosmological N-body code based on General Relativity“. In: *JCAP* 1607 (2016), no.07,053. arXiv: 1604.06065 [astro-ph.CO].

- [80] Simon Foreman and Leonardo Senatore. „The EFT of Large Scale Structures at All Redshifts: Analytical Predictions for Lensing“. In: *Journal of Cosmology and Astroparticle Physics* 2016.04 (2016), p. 033. arXiv: 1503.01775 [astro-ph.CO].
- [81] Leonardo Senatore. „Bias in the Effective Field Theory of Large Scale Structures“. In: *Journal of Cosmology and Astroparticle Physics* 2015.11 (2015), p. 007. arXiv: 1406.7843 [astro-ph.CO].
- [82] Raul Angulo, Matteo Fasiello, Leonardo Senatore, and Zvonimir Vlah. „On the Statistics of Biased Tracers in the Effective Field Theory of Large Scale Structures“. In: *Journal of Cosmology and Astroparticle Physics* 2015.09 (2015), p. 029. arXiv: 1503.08826 [astro-ph].
- [83] Leonardo Senatore and Matias Zaldarriaga. „Redshift Space Distortions in the Effective Field Theory of Large Scale Structures“. In: (2014). arXiv: 1409.1225 [astro-ph.CO].
- [84] Christian Wagner, Fabian Schmidt, Chi-Ting Chiang, and Eiichiro Komatsu. „Separate Universe Simulations“. In: *Monthly Notices of the Royal Astronomical Society: Letters* 448.1 (2015), pp. L11–L15. arXiv: 1409.6294 [astro-ph.CO].
- [85] Mathias Garny, Thomas Konstandin, Rafael A. Porto, and Laura Sagunski. „On the Soft Limit of the Large Scale Structure Power Spectrum: UV Dependence“. In: *Journal of Cosmology and Astroparticle Physics* 2015.11 (2015), p. 032. arXiv: 1508.06306 [astro-ph.CO].
- [86] Titouan Lazeyras, Christian Wagner, Tobias Baldauf, and Fabian Schmidt. „Precision measurement of the local bias of dark matter halos“. In: *JCAP* 02 (2015), p. 018. arXiv: 1511.01096 [astro-ph.CO].
- [87] Alessandro Manzotti, Marco Peloso, Massimo Pietroni, Matteo Viel, and Francisco Villaescusa-Navarro. „A coarse grained perturbation theory for the Large Scale Structure, with cosmology and time independence in the UV“. In: *JCAP* 09 (2014). eprint: 1407.1342.
- [88] R. E. Smith, J. A. Peacock, A. Jenkins, et al. „Stable clustering, the halo model and nonlinear cosmological power spectra“. In: *Mon.Not.Roy.Astron.Soc.* 341 (2003), p. 1311. arXiv: astro-ph/0207664 [astro-ph.CO].
- [89] Sean M. Carroll, Stefan Leichenauer, and Jason Pollack. „A Consistent Effective Theory of Long-Wavelength Cosmological Perturbations“. In: *Phys. Rev. D* 90, (2013), p. 023518. arXiv: 1310.2920 [astro-ph].
- [90] Ali Akbar Abolhasani, Mehrdad Mirbabayi, and Enrico Pajer. „Systematic Renormalization of the Effective Theory of Large Scale Structure“. In: *Journal of Cosmology and Astroparticle Physics* 2016.05 (2016), p. 063. arXiv: 1509.07886 [hep-th].
- [91] Tobias Baldauf, Lorenzo Mercolli, and Matias Zaldarriaga. „The Effective Field Theory of Large Scale Structure at Two Loops: the apparent scale dependence of the speed of sound“. In: *Phys. Rev. D* 92, (2015), p. 123007. arXiv: 1507.02256 [astro-ph].
- [92] Tobias Baldauf, Emmanuel Schaan, and Matias Zaldarriaga. „On the reach of perturbative descriptions for dark matter displacement fields“. In: *Journal of Cosmology and Astroparticle Physics* 2016.03 (2016), p. 017. arXiv: 1505.07098 [astro-ph].
- [93] Tobias Baldauf, Emmanuel Schaan, and Matias Zaldarriaga. „On the reach of perturbative methods for dark matter density fields“. In: *Journal of Cosmology and Astroparticle Physics* 2016.03 (2016), p. 007. arXiv: 1507.02255 [astro-ph].

- [94]Takahiro Nishimichi, Francis Bernardeau, and Atsushi Taruya. „Response function of the large-scale structure of the universe to the small scale inhomogeneities“. In: (2014). arXiv: 1411.2970 [astro-ph.CO].
- [95]T. Padmanabhan and Suryadeep Ray. „Power transfer in nonlinear gravitational clustering and asymptotic universality“. In: *Mon.Not.Roy.Astron.Soc.Lett.* 372:L53-L57 (2006). eprint: astro-ph/0511596.
- [96]Matthias Bartelmann, Felix Fabis, Daniel Berg, et al. „A microscopic, non-equilibrium, statistical field theory for cosmic structure formation“. In: *New Journal of Physics* 18.4 (2016), p. 043020. arXiv: 1411.0806 [astro-ph].
- [97]C. Pichon and F. Bernardeau. „Vorticity generation in large-scale structure caustics“. In: *Astron. Astrophys.* 343 (1999), p. 663. arXiv: astro-ph/9902142 [astro-ph.CO].
- [98]Stefan Floerchinger, Mathias Garny, Nikolaos Tetradis, and Urs Achim Wiedemann. „Renormalization-group flow of the effective action of cosmological large-scale structures“. In: (2016). arXiv: 1607.03453 [astro-ph.CO].
- [99]Diego Blas, Julien Lesgourgues, and Thomas Tram. „The Cosmic Linear Anisotropy Solving System (CLASS) II: Approximation schemes“. In: *JCAP* 07 (2011), p. 034. eprint: 1104.2933.
- [100]Antony Lewis, Anthony Challinor, and Anthony Lasenby. „Efficient Computation of CMB anisotropies in closed FRW models“. In: *Astrophys.J.* 538 (2000), pp. 473–476. arXiv: astro-ph/9911177 [astro-ph.CO].



# Acknowledgement

First of all, I would like to thank Christof Wetterich for the opportunity of working in his group and his valuable advices. I am thankful to Luca Amendola for agreeing to be the second referee for this thesis. I am indebted to Youness Ayaita for sharing his simulation code and for babysitting me during the first days in Heidelberg.

Furthermore, I wish to thank my collaborator Gerasimos Rigopoulos for fruitful discussions and successful collaboration. I am also thankful to Santiago Casas for many fruitful discussion and his comments on the manuscript. I also like to thank my other collaborators Ewald Puchwein and Marco Baldi. I am grateful to Alessio Spurio Mancini for commenting on the manuscript.

Finally, I am thankful to my office mates Frank Könnig and Henrik Nersisyan for all the fun in the office.



## Colophon

This thesis was typeset with  $\text{\LaTeX}2_{\epsilon}$ . It uses the *Clean Thesis* style developed by Ricardo Langner. The design of the *Clean Thesis* style is inspired by user guide documents from Apple Inc.

Download the *Clean Thesis* style at <http://cleanthesis.der-ric.de/>.



